Toward the Integration of DC Microgrids into a Hybrid AC/DC Paradigm

by

Amr Abdelnaeem Ismail Said

A thesis
presented to the University of Waterloo
in fulfillment of the
thesis requirement for the degree of
Doctor of Philosophy
in
Electrical and Computer Engineering

Waterloo, Ontario, Canada, 2016

AUTHOR'S DECLARATION

I hereby declare that I am the sole author of this thesis. This is a true copy of the thesis, including any required final revisions, as accepted by my examiners.

I understand that my thesis may be made electronically available to the public.

Abstract

The recent penetration of distributed generation (DG) into existing electricity grids and the consequent development of active distribution networks (ADNs) have prompted an exploration of power distribution in a dc microgrid paradigm. Although dc power distribution has been implemented in aircraft, ships, and communication centres, the technology is still at an early stage and must be investigated with respect to technical feasibility when applied to distribution systems. In particular, the operation of a dc microgrid in both grid-connected and islanded modes and its integration into an existing ac infrastructure are subject to significant challenges that impede the practical realization of dc microgrids. On one hand, because the dc voltage profile is coupled with the injected active power at the system buses, it is seriously influenced by the intermittent nature of renewable resources such as solar and wind energy. In islanded operating mode, the presence of system resistance leads to a further trade-off between an appropriate system voltage profile and a precise power management scheme. On the other hand, the development of hybrid ac/dc microgrids introduces a fresh operational philosophy that enhances power sharing among ac and dc subgrids through the coupling of ac and dc steady-state variables.

With these challenges as motivation, the primary goal of this thesis was to develop effective power management schemes and a steady-state analysis tool that can enable the reliable integration of dc microgrids into a smart hybrid ac/dc paradigm. Achieving this objective entailed the completion of three core studies: 1) the introduction of a robust control scheme for mitigating voltage regulation challenges associated with dc distribution systems (DCDSs) that are characterized by a high penetration of distributed and renewable generation, 2) the proposal of a supervisory control strategy for precise DG output power allocation that is based on DG rating and operational costs yet guarantees an appropriate voltage profile for islanded dc microgrids, 3) the development of an accurate and comprehensive power flow algorithm for analyzing the steady-state behaviour of islanded hybrid ac/dc microgrids, and 4) the optimization of hybrid ac/dc microgrids configuration.

As the first research component, a novel multi-agent control scheme has been developed for regulating the voltage profile of DCDSs that incorporate a large number of intermittent energy sources. The proposed control scheme consists of two sequential stages. In the first stage, a distributed state estimation algorithm is implemented to estimate the voltage profile in DCDSs, thus

enhancing the interlinking converter (IC) operation in regulating the system voltages within specified limits. If the IC alone fails to regulate the system voltages, a second control stage is activated and executed through either equal or optimum curtailment strategy of the DG output power. A variety of case studies have been conducted in order to demonstrate the effectiveness, robustness, and convergence characteristics of the control schemes that have been developed.

The second element of this research is a multi-agent supervisory control that has been created in order to provide precise power management in isolated DC microgrids. Two aspects of power management have been considered: 1) equal power sharing, which has been realized via a proposed distributed equal power sharing (DEPS) algorithm, and 2) optimal power dispatch, which has been achieved through a proposed distributed equal incremental cost (DEIC) algorithm. Both algorithms offer the additional advantage of affording the ability to restore the average system voltage to its nominal value. Real-time OPAL-RT simulations have demonstrated the effectiveness of the developed algorithms in a hardware-in-the-loop (HIL) application.

The third part of the research has introduced a sequential power flow algorithm for hybrid ac/dc microgrids operating in islanded mode. In contrast to the conditions in grid-connected systems, variable rather than fixed ac frequencies and dc voltages are utilized for coordinating power between the ac and dc microgrids. The primary challenge is to solve the power flow problem in hybrid microgrids in a manner that includes consideration of both the absence of a slack bus and the coupling between the frequency and dc voltage though ICs. In the proposed algorithm, the ac power flow is solved using the Newton-Raphson (NR) method, thereby updating the ac variables and utilizing them accordingly in a proposed IC model for solving the dc problem. This sequential algorithm is iterated until convergence. The accuracy of the algorithm has been verified through detailed time-domain simulations using PSCAD/EMTDC, and its robustness and computational cost compare favourable with those of conventional algorithms.

The final part highlights the implementation of the developed steady-state models in obtaining an optimum hybrid microgrid configuration. The system configuration could be manipulated by changing the DG droop settings as well as the network topological structure. The contribution of both approaches has been investigated, through an optimum power flow (OPF) formulation, in improving the system loadability as the primary measure of the hybrid microgrid performance.

.

Acknowledgements

First and foremost, I would like to thank God whose guidance lead me this far.

My sincerest gratitude goes to my advisor Professor Ehab El-Saadany for his professional guidance, valuable advice, continual support and encouragement shown throughout the period of this research. My appreciation and thanks are also extended to my PhD committee members: Professor Ramadan El-Shatshat, Professor Mehrdad Kazerani, and Professor Gordon Savage. Thanks are also due to my external examiner, Professor Venkataramana Ajjarapu, for coming from Iowa State University to referee this thesis.

My mother, Mrs. Nadia Tawfik, always receives my deepest thanks, and endless appreciation. My research would not have been possible without her help, constant support and encouragement, and her blessed wishes and prayers.

I wish also to thank my colleagues and friends, Refat Ghuenum, Maher Azzouz, Mostafa Shaaban, and Aboelsood Zidan whose fruitful discussions, advices, and support inspired me during my PhD.

Special thanks go to Professor Hussein Magdy whose support, interest, assistance, and sincere advice during my Master's degree studies at Cairo University had shaped and refined my research character.

Last but not least, I would like to express my sincere gratitude to my colleague Prof. Hatem Zeineldin for his fervent inspiration and strong recommendation and support towards starting my PhD at University of Waterloo.

Dedication

To my beloved mother, Nadia, in recognition of your endless love, support, and encouragement.

Table of Contents

List of Figures

List of Tables

Nomenclature

Acronyms

ACDS	AC distribution system
ADN	Active distribution network
ANM	Active network management
CB	Circuit breaker
CPL	Constant-power load
DCDS	DC distribution system
DEIC	Distributed equal incremental cost
DEPS	Distributed equal power sharing
DG	Distributed generation unit
DLPDS	Distributed Lagrangian primal-dual subgradient
DNO	Distribution network operator
ESS	Energy storage systems
HIL	Hardware-in-the-loop
IC	Interlinking converter
LIB	Limit induced bifurcation
MIMO	Multi-input multi-output
MTDC	Multi-terminal dc system
NR	Newton-Raphson
NTR	Newton trust region
OLTC	On-load tap changer
PCC	Point of common coupling
PEV	Plug-in electric vehicles
PV	Photovoltaic
RCP	Rapid control prototyping
RTS	Real-time simulator
SNB	saddle node bifurcation

Functions & Operators

$A^{\dagger}$	Moore-Penrose or pseudo-inverse of matrix A

$diag(\,)$	Diagonal elements of a matrix
$D_P^j(\,)$	Subgradient of the primal variables as calculated by agent j
$D_\lambda^j(\,)$	Subgradient of the dual variables as calculated by agent j
$Im\{\,\}$	Imaginary part of a complex number
$L_j(\,)$	Lagrangian function of an agent j
$OC_j(\,)$	Operational cost of a DG j
$Pro_P(\,)$	Projection operator for the primal variables
$Pro_\lambda(\,)$	Projection operator for the dual variables
$Re\{\,\}$	Real part of a complex number
$\mathfrak{R}_j(\,)$	Revenue function of a DG j
$\mathfrak{R}_j^{net}(\,)$	Net revenue function of a DG j
σ_n	The n eigenvalue of a matrix
$\eth(k)$	Step size in iteration # k
$\otimes$	Hadamard product operator, a point-to-point matrix multiplication
$\|\ \|$	Cardinality of a set
$\perp$	Complementary contraints

Sets

B	Set of all system buses
$B_{ac,droop}$	Set of buses that contain droop-based DG units in the ac subgrids
$B_{dc,droop}$	Set of buses that contain droop-based DG units in the dc subgrids
G	Set of DG unit buses
L	Set of load buses
$\mathcal{G}$	Weighted indirect graph
$\mathcal{E}$	Non-zero edges of indirect graph
$\mathcal{I}_{ac}$	Set of ac buses
$\mathcal{I}_c$	Set of the ICs within the hybrid microgrid
$\mathcal{I}_{dc}$	Set of dc buses
$\mathcal{N}_u$	Neighboring nodes of node u
$\mathfrak{R}^n$	Set of real numbers
$\mathcal{V}$	Set of vertices

ρ	Set of DG units that operate within their power limits

Parameters

E	Identity matrix
G	Conductance matrix of dc subgrid
J_{AC}	Jacobian matrix for the ac subgrid
J_{DC}	Jacobian matrix for the dc subgrid
$I_{dc,Gi}^{max}$	Maximum output current of a DG unit in a dc subgrid
$I_{dc,i}^{o}$	Constant current load at bus i in a dc subgrid
N_g	Number of DG units in the system
$P_{dc,i}^{o}$	Constant power load at bus i in a dc subgrid
p_u^{min}	Minimum output DG power
p_u^{max}	Maximum output DG power
$P_{ac,G}^{max}$	Maximum active power of an ac DG unit installed in an ac subgrid
$P_{dc,Gi}^{max}$	Maximum output power of a DG unit installed in a dc subgrid
Q_G^{max}	Maximum reactive powers of an ac DG unit
r	DG self-droop gain
r'	DG mutual droop gain
R	Matrix of the DG droop gains
$r_{n-1,n}$	Resistance between buses $n-1$ and n in DCDS
S	Sensitivity matrix
$S_{lim,i}$	Apparent power limit of IC j
ΔT	Total time for performing a complete supervisory control cycle
ΔT_{DG}	DG waiting time to exchange variables after settings update
$V_{ac,max}$	Maximum allowable voltage magnitude in an ac subgrid
$V_{ac,min}$	Minimum allowable voltage magnitude in an ac subgrid
$V_{dc,max}$	Maximum allowable voltage level in a dc subgrid
$V_{dc,min}$	Minimum allowable voltage level in a dc subgrid
v_{per}^{max}	Maximum permissible voltage level on the system
v_{per}^{min}	Minimum permissible voltage level on the system
v^{nom}	Nominal voltage of the dc system

V^*	Vector of DG voltage reference value in a system
$V_{ac,i}^*$	No-load reference values of the DG output voltage in ac subgrids
$V_{dc,I}^*$	DG no-load reference voltages for I/V droop characteristics in dc subgrids
$V_{dc,P}^*$	DG no-load reference voltages for P/V droop characteristics in dc subgrids
Y	Impedance matrix of the system
Y_{ij}	Y-bus admittance matrix magnitude
Y'	Reduced bus admittance matrix
1_{N_g}	Column vector of length N_g with all elements being ones
$\propto$	Active and reactive power exponent in the exponential load model
β	Reactive power exponent in the exponential load model
e	Square matrix with all elements of ones
ϑ_I	Reciprocals of the droop gain of the DG output current in a dc subgrid
ϑ_P	Reciprocals of the droop gain of the DG output power in a dc subgrid
ω_o	Nominal system frequency
ω_{max}	Maximum value for the system permissible frequency
ω_{min}	Minimum value for the system permissible frequency
ω^*	No-load DG reference frequency
θ_{ij}	Y-bus admittance matrix angle
Θ	Design parameter that guarantees stability of the supervisory control loop
Θ_c	Critical value of Θ above which the supervisory control loop is unstable
$\mathcal{W}$	Adjacency matrix of weighted graph

Variables

I	Vector of injected currents at the system buses
$I_{dc,Gi}$	Output DG current in a dc subgrid
i_j^g	Output current of DG j
I^g	Vector of output DG current

I_g^{ref}	Vector of reference DG currents
Δi_g	Change in the DG current
ΔI_g	Vector of change in the output DG currents
ΔI_g^{req}	Vector of required change in the DG output current
I^l	Vector of current injection at load buses of the dc system
Δi_u^{req}	Required change in the output DG current
LF	Loading factor
$P_{ac,Gi}$	Output active power of the DG in ac subgrids
$P_{ac,i}$	Injected power in an ac subgrid
$P_{ac,i}^o$	Nominal values for the active power in the exponential load model
$P_{ac,Loss}$	Losses in an AC subgrid
$P_{c,ac,j}$	Active power injected through IC j at the ac-side
$P_{c,dc,j}$	Active power injected through IC j at the dc-side
$P_{c,loss,j}$	Active power loss of IC j
$P_{c,tot}$	Total power transfer through ICs from AC subgrids to dc subgrids
$P_{dc,Gi}$	Output DG power in a dc subgrid
$P_{dc,i}$	Injected power in a dc subgrid
P_{loss}	System total loss
$p_{n-1,n}$	Active power flowing between buses n-1 and n
Δp_n	Change of active power injection at bus n
$\Delta\, p_u^{req}$	Required change in the output DG power
Q_i	Reactive powers injected at ac bus i
Q_i^o	Nominal values for the reactive power in the exponential load model
$Q_{c,j}$	Reactive power through IC j
Q_{Gi}	Output reactive power of the DG in an ac subgrid
$Q_{lim,j}$	Reactive power limit of IC j
$sw_{(i,j)}$	switch state between buses i and j
V	Vector of voltages at the dc system buses
v_j^*	Voltage reference of DG j

ΔV^*	Vector of change in the DC no-load references
$V_{ac,i}$	AC voltage magnitude at bus i
$V_{dc,i}$	Voltage level at bus i in a dc subgrid
V^l	Vector of voltages at load buses of the dc system
v_j^g	Output voltage of DG j
V^g	Vector of output DG voltages
ΔV_g	Vector of change in the output DG voltages
Δv^{req}	Required change in the output DG voltage
v_{max}	Global maximum voltages over the DCDS
v_{min}	Global minimum voltages over the DCDS
$v_{(n)new}$	Voltage of bus n after change in the power injection
$v_{(n)old}$	Voltage of bus n before change in the power injection
Δv^{req}	Required change in the average system voltage
v^{sys}	Average system voltage
δ_i	AC voltage angel at bus i
λ	Vector of Lagrangian multipliers.
λ_{avg}	Average Lagrangian multiplier of a set of agents
μ_i	Reciprocal of the DG droop active power gains in ac subgrids
η_i	Reciprocal of the DG droop reactive power gains in ac subgrids
ω	Frequency in an ac subgrid
$\Delta\omega$	Deviation of the frequency
$\varphi,\ \varkappa,\ \Gamma$ and Ψ	General variables that are exchanged within the graph
$\overline{\varphi}$	Vectors of variables that are exchanged within the graph

Chapter 1
Introduction

Environmental concerns related to global warming have increased significantly over the past few decades. At the same time, worries about energy shortages have stimulated interest of researchers in discovering alternative sources of energy. In response to these developments, countries around the world are spending billions of dollars to increase the penetration of renewable energy sources. In the Canadian province of Ontario, for example, the capacity of the numerous wind farms that have been built totals 1.7 GW, and that of biomass installations has reached 122 MW. By 2015, 3 GW of wind energy, 280 MW of solar energy, and 253 MW of biomass energy were available, and a 2.4 GW embedded mix of power from renewable sources was in service at the distribution level in that same year.

Interestingly, photovoltaic (PV) arrays and wind turbines are more compatible with dc than with ac systems. In [1], Wu and et al. contrasted the integration of a PV array into ac versus dc systems in terms of the number of power conversion stages required and the overall efficiency. They demonstrated that just two conversion stages are required for the array to feed a nonlinear load via a dc system compared to five stages if an ac system is utilized. This reduction in the number of conversion stages significantly increases power conversion efficiency: approaching 98 % in dc systems compared to 86 % in ac systems. With respect to biomass distributed generation (DG), a new technology has been developed based on the conversion of biomass fuel into hydrogen gas for fuel cell operation [2]. The purpose of the conversion is to increase the efficiency of the biomass generation and to reduce the NOx emissions traditionally associated with biomass sources. Figure 1.1 provides a quick comparison of the integration of renewable sources into ac and dc systems.

Along with renewable DG units, electronic loads have also become an integral feature of modern life. New high-efficiency and high-quality dc lighting systems have been invented, and the operation of major loads such as modern elevator motors is based on variable speed drives [3]. Another key load in future electric distribution systems comes from plug-in electric vehicle (PEV) technology, and other evolving innovations, such as solid-state transformers, will also increase the drive toward the implementation of dc systems [4]. Additional considerations include the following beneficial characteristics of dc distribution systems:

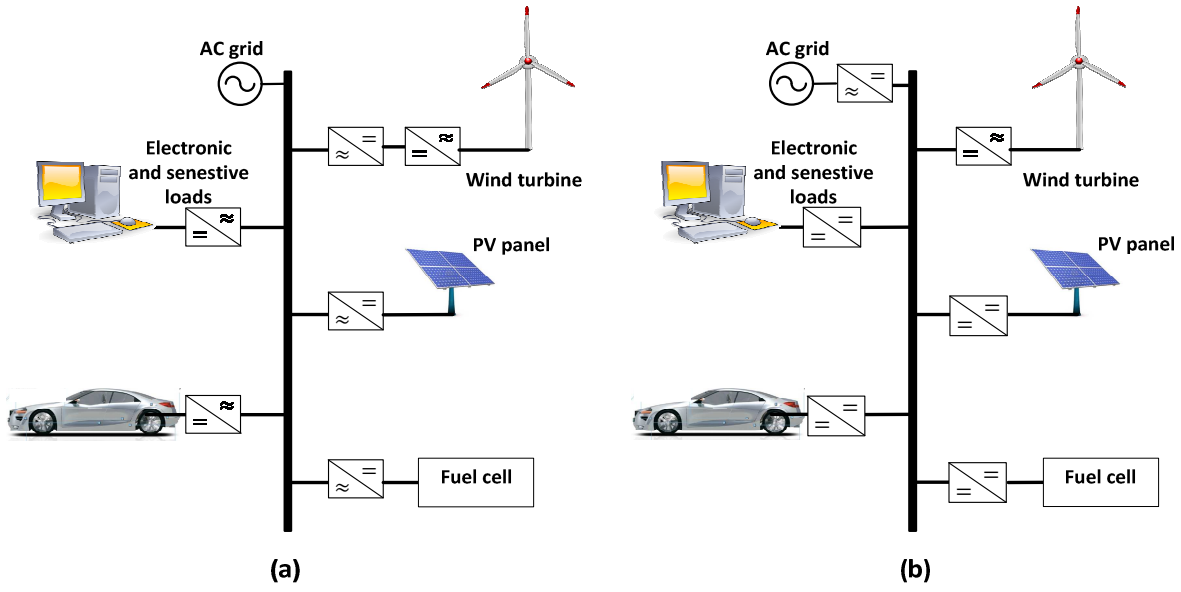

Figure 1.1: Integration of renewable DG units into power systems: (a) AC (b) DC

1. Higher overall system efficiency
2. Easier expansion of power capacity
3. Less interference with ac grids
4. Absence of issues related to frequency stability and reactive power
5. Lack of the skin effect and losses associated with ac systems

Given these clear advantages, dc distribution systems have become an increasingly common research focus. A particular area of interest is the philosophy governing the operation of isolated dc systems and the integration of dc and ac microgrids in order to configure a new hybrid ac/dc paradigm. Figure 1.2 illustrates a simple hybrid ac/dc paradigm in a nanoscale grid, as reported in the literature.

1.1 Motivation

The operation of a dc distribution system is based on a totally fresh concept in distribution systems. In contrast to ac systems, in dc systems, the voltage and power at different dc system buses are the only

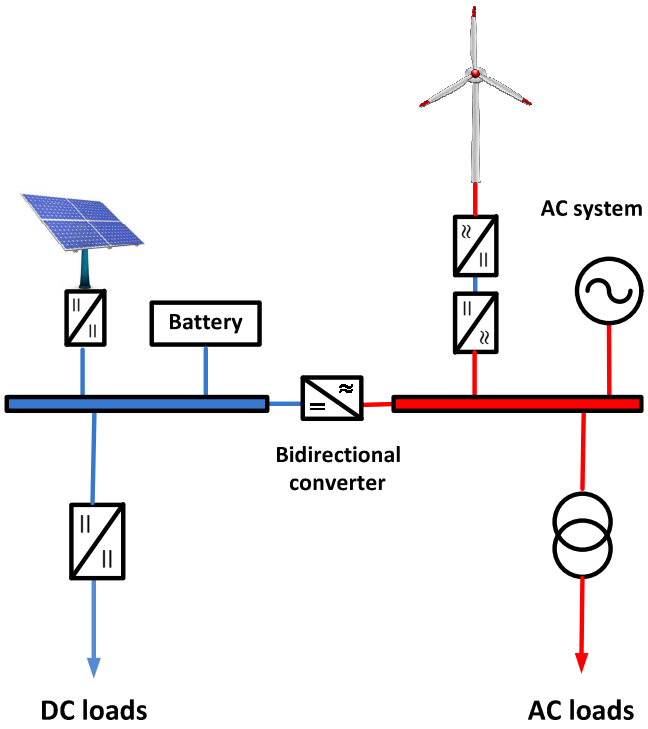

Figure 1.2: AC/DC hybrid nanogrid

system variables that are also coupled. The presence of a high level of link resistance in dc distribution systems hinders accurate decentralized power management in general and efficient DG power sharing and economic dispatching in particular. The literature includes a variety of proposed control schemes designed to handle power management in dc distribution systems. However, most of the schemes suggested are based on centralized approaches that entail a significant communication infrastructure, thus reducing overall system reliability. A few energy management studies have been conducted based on distributed schemes, but they are suitable only for small-scale systems.

The evolving dc network will also be integrable with traditional ac networks through interlinking converters (ICs), thereby forming a new hybrid distribution paradigm. If the connection with the main substation is lost, the hybrid distribution system forms an islanded microgrid that can partially or totally supply the local loads in the ac and dc subgrids. The operational concept of this newly configured paradigm can be better understood if the hybrid system is subdivided into ac and dc subgrids connected via ICs. The DG units installed in ac subgrids implement P/f and Q/V droop characteristics that enhance load sharing. Likewise, the DG units apply either P/V or I/V droop characteristics that enable appropriate power sharing within the dc subgrid. At the same time, the ICs

manage overall load sharing between the ac and dc subgrids by relating the ac frequency and dc voltage. While consequently complex, analysis of islanded hybrid ac/dc microgrids is nonetheless important due to 1) the absence of a slack bus, 2) the frequency variations that occur in the ac subgrid, and 3) the correlation between the frequency and the dc voltage. The practical implementation of this operational philosophy in large-scale hybrid microgrids must be preceded by several initial steady-state and dynamic studies that could be performed through an inclusive and accurate steady-state analysis tool. Recently published power flow studies have targeted only purely ac microgrids, with the nontraditional operational aspects of integrated dc subgrids remaining unaddressed.

For these reasons and to overcome the challenges mentioned above, the facilitation of the widespread construction of a dc and hybrid ac/dc microgrid concept under a smart grid paradigm requires robust control schemes and analysis tools. Any approaches proposed should be capable of performing the following functions:

1. Providing a reliable distributed supervisory control environment that manages the DG output power in large-scale dc microgrids in both grid-connected and islanded operating modes
2. Accurately defining the steady-state variables for hybrid ac/dc microgrids, including consideration of a special operational philosophy for individual subgrids as well as the nature of the coupling between the subgrids' variables

1.2 Research Objectives

The broad goal of the research conducted for this thesis was to incorporate the concept of dc grids into the operational perspectives of active distribution networks (ADNs). However, several factors required addressing prior to the realization of this approach. On one hand, dc microgrids may follow different paradigms (standalone dc microgrid or hybrid ac/dc microgid) with different modes of operation (grid-connected or islanded), each requiring consideration of specific objectives and constraints. For example, in islanded dc systems, equal power sharing is the stated main goal, while for a dc distribution system connected to a stiff grid, the primary target is to maximize DG revenue without violating system constraints. On the other hand, the interaction between the ac and dc subgrids in an islanded hybrid paradigm introduces a fresh operational scheme that involves thorough steady-state and dynamic analysis prior to the practical implementation of such systems. With respect to addressing these challenges, the main objectives of this research can be summarized as follows:

1. Developing a distributed algorithm for mitigating any voltage regulation problems that may arise in the case of a large-scale dc microgrid connected to a stiff grid: The algorithm supports the main IC decision in order to prevent any voltage violations at different system buses. If the IC fails to regulate the voltage level at all system buses, the output DG power should be optimally curtailed as an additional control action to support the IC functionality.
2. Developing a distributed supervisory control scheme that enhances the performance of isolated dc microgrids: The creation of the proposed scheme required consideration of both the achievement of precise DG power management and the enhancement of the overall system voltage profile through the operation of the DG units around the nominal voltage value.
3. Developing an appropriate load flow algorithm that reflects the accurate steady-state system behaviour of islanded hybrid ac/dc microgrids: The proposed algorithm must comprise an extensive range of different operational modes not only for the DG units, but also for the ICs.
4. Investigating the optimum system configuration that enhances the system performance: in the light of special operational characteristics of the hybrid ac/dc microgrids, the optimum system configuration could be defined according to several operational criteria among which system loadability is the most salient.

1.3 Thesis Organization

The remainder of this thesis is structured as follows:

Chapter 2 provides the required background and critical survey of operational studies previously conducted with respect to microgrids in general and dc microgrids in particular.

Chapter 3 introduces a sequential multi-agent control scheme for mitigating voltage regulation problems associated with dc distribution systems that include a high penetration of dispatchable and renewable DG units. In the first stage, the IC adjusts the lower and upper system voltage levels around unity, while in the second stage, the DG units react if the ac/dc converter alone fails to regulate the system voltages between permissible limits.

Chapter 4 explains the developed multi-agent supervisory control strategy that provides precise power management in isolated dc microgrids. Two distributed power management algorithms have been created to enable consideration of both equal power sharing between the DG units

and their optimal power dispatch. As a side-effect benefit, the developed algorithms also provide the ability to restore the average system voltage to its nominal value.

Chapter 5 describes the development of a sequential power flow algorithm for hybrid ac/dc microgrids operating in islanded mode. The algorithm incorporates the operational characteristics of the ac and dc subgrids as well as the scheme for exchanging power between the subgrids. To obtain an efficient solution with a low computational cost, the Newton-Raphson method is implemented sequentially for the ac and dc subgrids, thus offering a significant reduction in problem size compared to that provided by a unified algorithm.

Chapter 6 provides an optimum system configuration analysis to enhance the system capability in serving the maximum possible demand. The analysis is conducted through optimal power flow (OPF) formulation that considers manipulating the DG droop settings as well as the system topological structure.

Chapter 7 sets out the conclusions and contributions of the research presented in this thesis as well as suggestions for future work.

Chapter 2
Background and Literature Review

2.1 Introduction

In chapter 1, the motivations of the research work have been highlighted and the research objectives have been introduced. This chapter states the essential knowledge and critical survey pertaining to the research objectives. First a general background is introduced to provide a better understanding of the operational schemes of dc microgrids and their integration within the hybrid ac/dc paradigm. Since this work focuses on intelligent distributed control, the implementation of multi-agent technology is summarized and preceded by main communication infrastructures in power systems. Thereafter, a functional survey is presented to address the main operational studies in active distribution systems in general and dc distribution systems in specific. This survey could be divided into two folds. The first part tackles the control schemes followed to achieve an appropriate voltage quality in distribution systems (in connected or isolated modes of operation). The second part outlines power management and coordination of power system components within dc and ac/dc hybrid microgrids.

In contrast to ac active distribution networks, which have roots in the traditional ac distribution system, the dc distribution systems have been implemented in limited applications. In other words, although dc power distribution systems are currently being considered for datacom centers in Japan and Europe [5], [6] and are also being contemplated for ship and aircraft power systems [7], dc distribution has not been implemented in common distribution networks. Therefore, practical problems related to dc distribution have not yet shown up on large scale systems. Accordingly, in addition to dc distribution research, this survey will review some common problems in multi-terminal dc (MTDC) and ac active distribution networks that can be mirrored in early dc distribution systems.

2.2 Hybrid AC/DC Microgrid Philosophy of Operation and Communication Schemes

The most generic paradigm in which the dc microgrid may exist is within a hybrid ac/dc network as illustrated in Figure 2.1. However, the switching action of the system circuit breakers, i.e., CB1 and

CB2 presented in the figure, will yield different operational paradigms for the dc subsystem, and thus, different operational schemes for the DG units and the interlinking ac/dc converter will be applied. These operational paradigms could be vividly summarized by manipulating the presented circuit breakers as follows

1) Gird-connected dc microgrid, CB1 is on and CB2 is on: In this mode of operation, the IC provides a slack bus for the dc subgrid, since the ac system is stiff enough to accommodate any power mismatch between the load and generation within the dc microgrid. Accordingly, the DG units may operate as constant power resources that inject their maximum output power since any power surplus or deficiency will be transferred to the stiff main grid through the IC. In this operation, the IC is considered a voltage forming element that settles the system voltage at the point of common coupling. However, the power injection from a DG unit still affects the voltage profile of its own feeder.

2) Islanded dc microgrid, CB2 is off, In this scenario the dc microgrid represents a standalone entity that could exchange power with neither the main substation nor the ac subgrid. Given the absence of a major generation unit that could replace the role of a stiff grid bus, the DG units have to collaborate in achieving two major functions: 1) attaining a perfect match between the generation and loads, 2) forming the dc subgrid voltage.

3) Islanded hybrid ac/dc microgrid, CB1 is off and CB2 is on: In this scenario both the ac and subgrids are connected together through the IC with the absence of a main stiff grid. Depending on the relative capacity of each subgrid, the IC could perform one of different objectives. If any of the subgrids is large enough (considerably stiffer), the IC could operate as a stiff bus for the

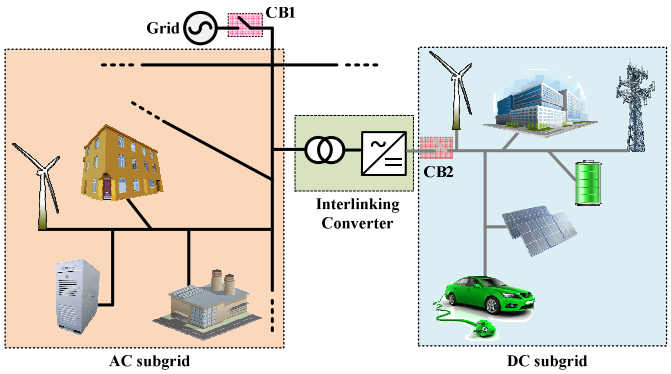

Figure 2.1: Schematic diagram of a hybrid microgrid

weaker subgrid. Thus, any power mismatch between the load and generation in the weaker subgrid could be handled by the stiffer subgrid. However, if neither of the subgrids connected to the IC is relatively large, the IC role will be restricted to facilitate active power exchange between the two subgrids. In this case, the subgrid ac voltage and frequency and dc voltage are locally formed by the DG units installed in each subgrid.

In the presented analysis, capacities of DG units are assumed relatively small, i.e., no large DG unit could serve as a slack for the entire system. Thus, in order to maintain the microgrid power adequacy, three control topologies for the DG units and the IC could be applied: centralized, distributed, and decentralized. The centralized layout, as its name implies, relies on a central supervisory control that could send the set points for the DG output power as well as the power transfer through the IC. In contrast, the distributed control refers to a supervisory control scheme that is distributed among the system components. For instance, a set of DG units could globally exchange some information regarding their total output power and, accordingly, each DG could locally calculate the appropriate change in its power generation value to achieve a predefined power management scheme. Compared with the centralized approach [8], [9], the distributed control is 1) more economical, with low communication and computational costs, and 2) more efficient in use of local information [10]. These advantages could be considered the main reasons that distributed communication is promoted as the ideal environment in realizing the mulit-agent concept, discussed in the following chapter

On the other hand, the decentralized approach is implemented without either supervisory control or communication layout. In this control strategy, DG units and ICs depend on the local system variables to adjust the output power and power transfer, respectively. For instance, the output active power is adjusted based on the frequency and local voltage droop scheme in the ac and dc subgrids, respectively. It is noteworthy that the decentralized control could be implemented as a primary control stage within a hierarchal control scheme that adopts either a centralized or distributed control on a secondary control stage. This hierarchal control alleviates the high bandwidth communication requirements since the system power adequacy is always maintained through the decentralized control, while advanced control objectives such as power dispatching or sharing are maintained through the secondary stage.

2.3 Multi-agent Technology in Power System Studies

Multi-agent technology allows for the rapid and detailed creation of a system model and constitutes a robust framework for distributed control. Yet, due to its emergent nature, there are several research issues that have not been addressed in the application of this technology in ADNs. Important among these are: 1) lack of a consensus definition in ADNs regarding what an intelligent agent is; 2) no unified organization paradigm for the multi-agent system in ADNs; 3) no solid mathematical approaches to determine the optimal coordination and communication protocols among control agents; and 4) lack of testing around issues related to effectiveness, robustness, stability, and convergence characteristics for multi-agent systems in ADNs.

In order to carry out research around multi-agent techniques, we have to differentiate between two frameworks for multi-agent decision-making. The first depends on heuristic techniques, where each agent chooses to update its state based on if-then conditions. This kind of multi-agent framework is widely used in the literature in solving a variety of power system problems, such as voltage regulation [11]–[13], self-healing [14], real-time operation [15], etc. The second framework depends on mathematical formulas that guarantee rates of convergence and solution quality, i.e., how far it is from the optimal solution.

This research extensively applies mathematical multi-agent approaches in order to achieve power management and voltage control for dc microgrids in both grid-connected and islanded modes of operation. Accordingly, the reminder of this section summarizes the communication layout and mathematical techniques employed to develop the multi-agent algorithms needed for the presented work.

2.3.1 Communication Layout

As demonstrated in Figure 2.2, the data exchange among the agents can be modeled as a weighted graph: $\mathcal{G} = \{\mathcal{V}, \mathcal{E}, \mathcal{W}\}$, in which $\mathcal{V} = \{1,2,\dots,n\}$ is a set of vertices; $\mathcal{W} := [\mathcal{W}_u^t]$ is the adjacency matrix with $\mathcal{W}_u^t \geq 0$ representing a weight of edge (u,t); and $\mathcal{E} \in \mathcal{V} \times \mathcal{V} \backslash diag(\mathcal{V})$ is a set of non-zero edges. In other words, $(u,t) \in \mathcal{E}$ if the weight $\mathcal{W}_u^t > 0$. In alignment with the literature, self-loops are not counted in $\mathcal{E}$. The neighboring nodes of node u are ones that can send and receive information to/from node u, denoted $\mathcal{N}_u = \{t \in \mathcal{V}: (t,u) \in \mathcal{E}, and\ t \neq u\}$. In this work, standard assumptions regarding network communication graphs have been adopted [16], [17]:

Assumption 1(Non-degeneracy):

- There is an $\alpha > 0$, such that $\mathcal{W}_{\mathrm{i}}^{\mathrm{i}} \geq \alpha$.
- $\forall\, i, j \in \mathcal{V}$, $\mathcal{W}_j^i \geq 0$

Assumption 2 (Strong connectivity): There exists a path that connects any two vertices $u, t \in \mathcal{V}, u \neq t$.

Assumption 3 (Doubly stochastic adjacency matrix): There is balanced communication defined by

$$\mathcal{W}_u^t = \begin{cases} \dfrac{1}{max(|\mathcal{N}_u|, |\mathcal{N}_t|) + 1} & if \quad t \in \mathcal{N}_u \\ 1 - \displaystyle\sum_{t \in \mathcal{N}_u} \mathcal{W}_u^t & if \quad t = u \\ 0 & otherwise \end{cases} \tag{2.1}$$

The graph model can be operated in two modes: Gossip and average consensus. In Gossip mode, any agents can broadcast its own information to others at a maximum of n-1 iteration. This mode is suitable if a certain agent wants to inform others about its state, for instance, DG unit broadcasts a voltage violation at its bus. Meanwhile the average consensus concept is applied if a set of agents pursue unanimous agreement around a system state as explained in details in the next subsection.

2.3.2 Average Consensus Theory

The main objective of the average consensus theory is sharing an average value of a certain variable φ among agents, for example, φ can represent the average system voltage. Each agent, a DG for instance, would have an initial value $\varphi[0]$ that represents its own average estimation at the beginning of the data exchange. For an agent to update its estimation of the average value, it must exchange information about its estimated average value with its neighbors, as follows:

$$\varphi_u[1] = \sum_{t \in \{\mathcal{N}_u\} \cup \{u\}} \mathcal{W}_t^u \;\; \varphi_t[0] \tag{2.2}$$

For simplicity, a vector $\overline{\varphi}[\mathrm{k}] = [\varphi_1[\mathrm{k}]\, \varphi_2[\mathrm{k}] \ldots \varphi_{\mathrm{N_g}}[\mathrm{k}]]^{\mathrm{T}}$ is defined to gather the average values estimated by all of the agents. Thus (2.2) can be generalized at any iteration $\mathrm{k} + 1$ in a compact form

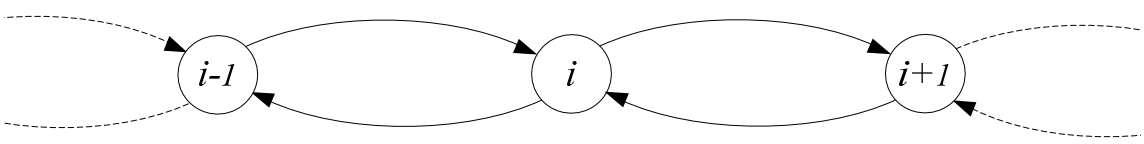

Figure 2.2: Exchange of information graph

as

$$\overline{\varphi}[k+1] = \mathcal{W}\,\overline{\varphi}[k] \tag{2.3}$$

, The relation between the initial vector $\overline{\varphi}[0]$ and $\overline{\varphi}[m]$ after *m* iterations can then be given as

$$\overline{\varphi}[m] = \mathcal{W}^m\,\overline{\varphi}[0] \tag{2.4}$$

Because $\mathcal{W}$ is an irreducible and doubly stochastic matrix, as defined according to Assumptions I and II, respectively, $\lim_{\mathrm{m}\to\infty} \mathcal{W}^{\mathrm{m}}$ converges to a rank-one deterministic matrix $\frac{1}{N_g} e$, where e is a square matric with all elements are ones. Equivalently, $|\sigma_2(\lim_{\mathrm{m}\to\infty} \mathcal{W}^{\mathrm{m}})| \to 0$, where σ_2 is the second largest eigenvalue of a matrix. $\mathcal{W}^m$ also converges at a geometric rate dependent on $\sigma_2(\mathcal{W})$ [18]. The more connected the graph, the smaller the $\sigma_2(\mathcal{W})$ value and the faster the convergence [19]. This interpretation explains how each DG can acquire the average value of $\overline{\varphi}[0]$ after a sufficient number of iterations.

2.3.3 Distributed Lagrangian Primal-Dual Subgradient Algorithm

Distributed optimization is a relatively new field that was developed to divide cooperative optimization problems between several agents. The work proposed by Nedic´ et al. [20] gave a mathematical formula for solving convex problems in a distributed manner. That work was extended to include agents' private constraints by the authors in [21]. Further, Zhu and Martínez developed a novel multi-agent distributed optimization dedicated to convex problems with strong duality under global equality and inequality constraints [17]. Yet, little research in power systems has implemented these distributed optimization approaches [22], [23].

In our proposed work, a multi-agent Distributed Lagrangian Primal-Dual Subgradient (DLPDS) algorithm is a key technique in coordinating different DGs operations under global systems constraints (voltage and cables current carrying capacity limits). A brief explanation of the DLPDS algorithm can be summarized as follows. Any convex optimization could be defined as an objective function, global constraints, and private constraints as defined in (2.5), (2.6), and (2.7), respectively.

$$min \sum_{u} f_u(P) \tag{2.5}$$

Subject to:

$$g(P) \leq 0 \tag{2.6}$$

$$P_{min} \leq P \leq P_{max} \tag{2.7}$$

where P is a vector of the problem variables. Considering only the global constraints, the equivalent Lagrangian equation could be represented as

$$L(P,\lambda) = \sum_{u} f_u(P) + \lambda^T g(P) \tag{2.8}$$

$$\lambda_u \in [0,\infty) \tag{2.9}$$

where λ is a vector of Lagrangian multipliers. Then, each agent will be responsible to solve its own optimization function (2.10), while taking into consideration its private constraints (2.11).

$$L_u(P,\lambda) = OC_u(p_u^u) + \lambda_u^T g(P^u) \tag{2.10}$$

$$P \in \cap_u [P_{min}^u, P_{max}^u] \tag{2.11}$$

Then, Agents exchange information with each other based on (2.12)-(2.15)

$$x_P^u(k) = \sum_{t \in \{\mathcal{N}_u\} \cup \{u\}} \mathcal{W}_t^u \; P^t(k) \tag{2.12}$$

$$x_\lambda^u(k) = \sum_{t \in \{\mathcal{N}_u\} \cup \{u\}} \mathcal{W}_t^u \; \lambda^t(k) \tag{2.13}$$

$$P^u(k+1) = Pro_{P_u}\left[x_P^u(k) - \eth(k)\frac{\partial L_u(P, x_\lambda^u)}{\partial P}\right] \tag{2.14}$$

$$\lambda^u(k+1) = Pro_{P_u}\left[x_\lambda^u(k) - \eth(k)\frac{\partial L_u(x_P^u, \lambda)}{\partial \lambda}\right] \tag{2.15}$$

where Pro_{P_u} (and Pro_{λ_u}) is the projection of the primal (and dual) variables based on each agent's private constraints, and $\eth(k) = \frac{1}{k+1}$.

It is worth noting that DLPDS is dedicated to convex problems with strong duality. In our analysis, DLPDS will be utilized for quadratic objective function with linear constraints, as provided in (2.16) and (2.17). Quadratic problems should be tested in order to have a sense in tuning the algorithm:

$$min \frac{1}{2} P^T A P + B_O{}^T P + C_O \tag{2.16}$$

Subject to:

$$B_i{}^T P + C_i \leq 0 \tag{2.17}$$

Lagrangian equation:

$$\mathrm{L}(\mathrm{P},\lambda) = \frac{1}{2}P^T AP + B(\lambda)^T P + C(\lambda) \tag{2.18}$$

$$B(\lambda) = B_O + \sum_{i=1}^{m} \lambda_i B_i \tag{2.19}$$

$$C(\lambda) = C_O + \sum_{i=1}^{m} \lambda_i C_i \tag{2.20}$$

The dual equation takes the form:

$$g(\lambda) = \inf_P L(P,\lambda) = -\frac{1}{2}B(\lambda)^T A^{\dagger} B(\lambda) + C(\lambda) \tag{2.21}$$

where ($A^{\dagger}$) is Moore-Penrose or pseudo-inverse of matrix A.

2.4 Voltage Regulation in ADNs

2.4.1 Voltage Regulation in ADNs Connected to a Stiff System

Voltage regulation is one of the major concerns regarding the appropriate operation of distribution systems. In its basic form, voltage regulation schemes in ac distribution systems tend to adjust the settings of traditional voltage control devices (i.e., an on-load tap changer [OLTC] on the head of a group of feeders, line voltage regulators, and shunt capacitors) in order to regulate the bus voltages to their specified acceptable limits [24], [25]. With the high degree of complexity that accompanies ADN structures, conventional voltage regulation schemes are expected to face numerous challenges. Important among these are significant changes in the voltage profile of distribution feeders, operational interference between DG units and traditional voltage control devices, and excessive wear and tear of traditional voltage control devices [26].

Recently, inverter-based DGs have been proposed to supply reactive power in addition to active power to cooperate in the mitigation of voltage rise problems [10]. In restrictions regarding the operation of DG units under the unity power factor, active power curtailment is the appropriate solution [27] [28]. In general, due to the intermittency of renewable DGs and the uncertainty of loads,

the concept of active network management (ANM) has emerged [28]. In contrast to conventional DG control schemes, ANM is a real-time monitoring and control strategy that can be adopted to facilitate increased DG access and connections while avoiding high network reinforcement costs. In [29], the ANM of network power flows had the potential reported to increase energy sourced from renewable generation threefold, compared to that of being conservative with throttling planning constraints. In [30], the authors differentiate between two main categories of DGs – firm and non-firm. Firm DGs are allowed to inject their active power all the time, whereas non-firm units are only allowed to do so if the system's operation constraints are not violated.

In the case of dc distribution systems operating in grid-connected mode, the injected/consumed power at different buses and the voltage at the point of common coupling with the main ac grid are the only factors shaping the voltage profile throughout the entire system. This inflexibility imposes restrictions on renewable power injection to meet the voltage regulation criteria (i.e., $\pm$ 5 % tolerance [1]). In [31], a multilevel voltage criteria has been proposed in order to facilitate the operation of the ac/dc main IC and to help DG units and energy storage systems (ESSs) determine their suitable output power.

2.4.2 Voltage Regulation in Islanded ADNs

Unlike ac distribution systems operating in grid-connected mode where traditional voltage regulators can be used to correct any voltage constraints violations, such devices will not be available to achieve the required functionality in the case of islanded mode of operation. Hence, the voltage profile relies on DGs' reactive power and VAR compensators, if any exist. As such, numerous centralized and decentralized control schemes have been proposed in the literature to mitigate the challenges of voltage regulation in ADNs [10], [32]. Given the distributed nature of ADNs, multi-agent distributed systems have been mentioned recently as a potential technology for voltage regulation in such systems [11], [33].

The problem of voltage regulation in dc isolated distribution systems occurs in different aspects. In general, voltage regulation in isolated dc distribution (and transmission) systems is directly related to current sharing [34] (or power sharing [35]). In isolated dc distribution systems, different DG units operate based on droop V/I characteristics, as illustrated in Figure 2.3(a), which is modeled by a constant voltage source in series with a resistance, as illustrated in Figure 2.3. The droop variables, reference voltage, and slope are the factors that define current sharing among the DGs. Perfect current

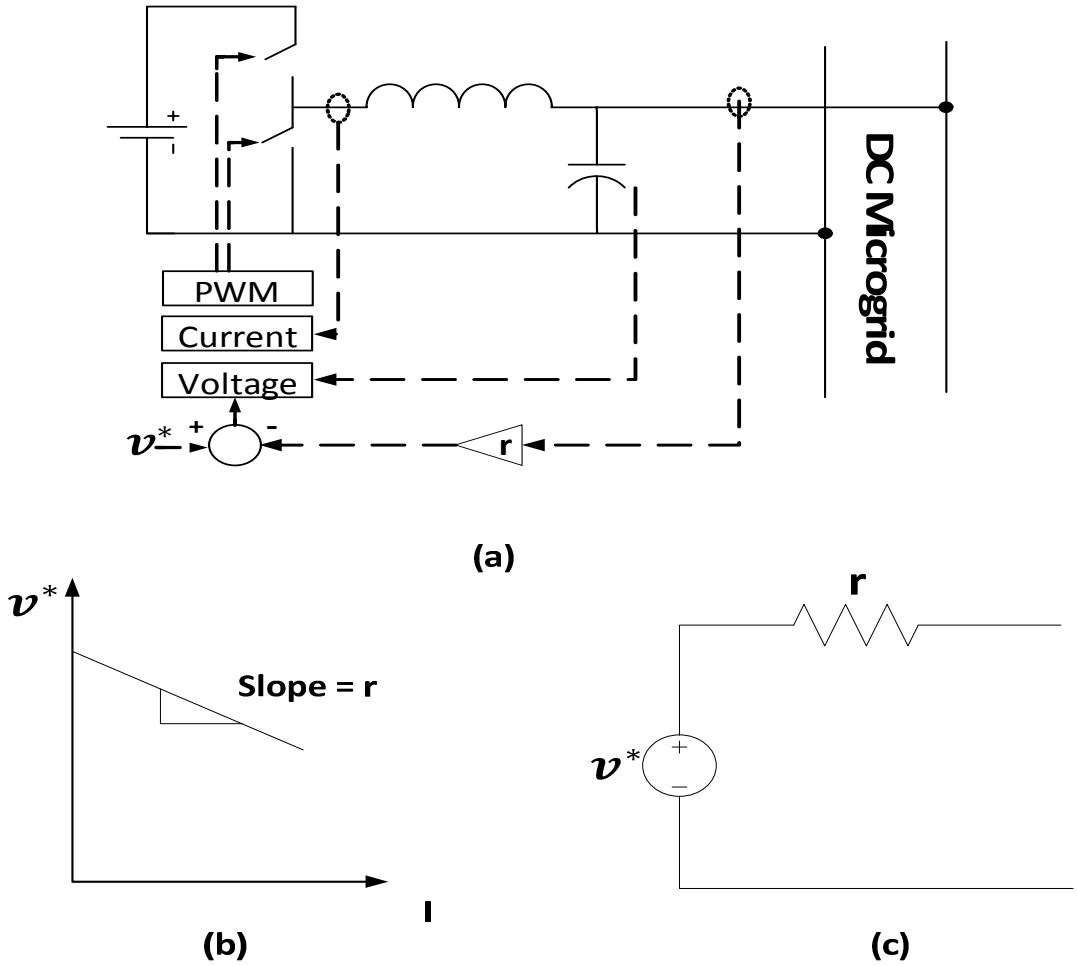

Figure 2.3: V/I droop characteristics of a DG in dc systems: (a) actual circuit; (b) characteristic equation; (c) circuit model

sharing can be obtained in autonomous dc microgrids if network link resistance is negligible. However, as this is not commonly the case, current sharing will be affected in the presence of high system resistance [34], [35]. High DG droop slope is a solution to overcome existing system high resistance. However, based on the loading conditions, this option will lead to high voltage variation. In contrast, low droop slope results in a good voltage profile over the system with poor current sharing among the DGs. Figure 2.4 gives a comparison between low and high droop slope settings for DGs in the presence of reference voltage mismatch between DG units (a) or high system resistance (b). A comprehensive discussion regarding the trade-off between sharing and voltage profile was reported in [26].

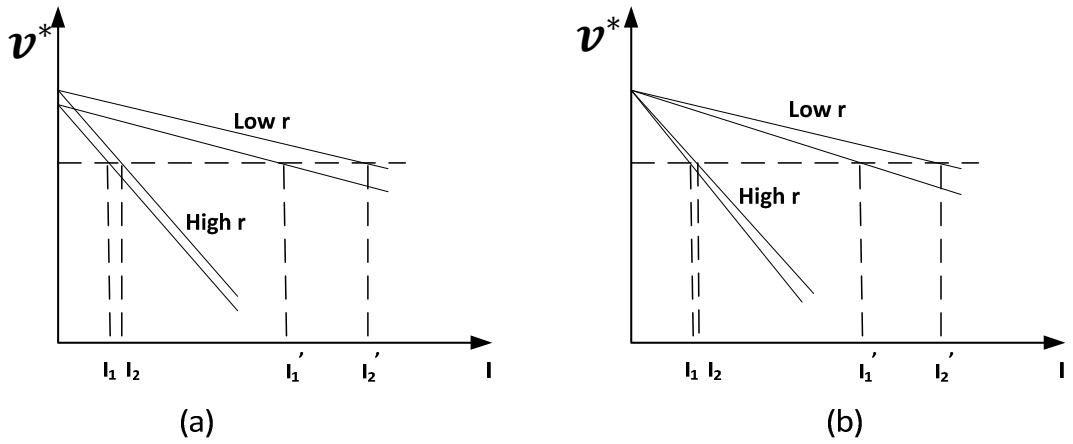

Figure 2.4: Comparison between low and high droop gains: (a) mismatch in DGs' reference voltage; (b) presence of high system resistance

In order to guarantee perfect current sharing and an acceptable voltage profile, supervisory control is required to adapt the reference voltage for different DG units, based on loading conditions. An initial design for a centralized supervisory controller was proposed in [32], while a distributed supervisory control via multi-agent protocol was proposed in [37]. According to the latter approach, the authors proposed implementing a common bus communication topology to provide all system DG units with full observability. In other words, all of the DGs in the system would provide their own instantaneous current on a common bus, so that each DG could aggregate the total DG current and update its reference voltage based on the total system loading current, as illustrated in Figure 2.5. Analytically, the steady state performance of the mentioned supervisory controller performance can be summarized as follows.

The DG output voltage is a function of its own reference voltage and the output current of all the DG units communicating with it. Thus the voltage at the terminal of DG units could be defined as

$$\begin{bmatrix} v_1^g \\ \vdots \\ v_j^g \\ \vdots \\ v_{Ng}^g \end{bmatrix} = \begin{bmatrix} v_1^* \\ \vdots \\ v_j^* \\ \vdots \\ v_{Ng}^* \end{bmatrix} - \begin{bmatrix} r_{11} & \cdots & -r_{1j}{}' & \cdots & -r_{1n}{}' \\ \vdots & \ddots & \vdots & \ddots & \vdots \\ -r_{j1}{}' & \cdots & r_{jj} & \cdots & -r_{jn}{}' \\ \vdots & \ddots & \vdots & \ddots & \vdots \\ -r_{n1}{}' & \cdots & -r_{nj}{}' & \cdots & r_{nn} \end{bmatrix} \begin{bmatrix} i_1^g \\ \vdots \\ i_j^g \\ \vdots \\ i_{Ng}^g \end{bmatrix} \tag{2.22}$$

Where v_j^g, i_j^g and v_j^* are the output voltage and current, and voltage reference of DG j; r and r' are the self-droop and mutual droop gains, respectively. In compact form, (2.22) can be presented as

$$V^g = V^* - R\, I^g \tag{2.23}$$

The representation shown in (2.23) comprises both V^g and I^g as variables which is not recommended in solving load flow algorithms. Thus the (2.23) can be modified in the following steps.

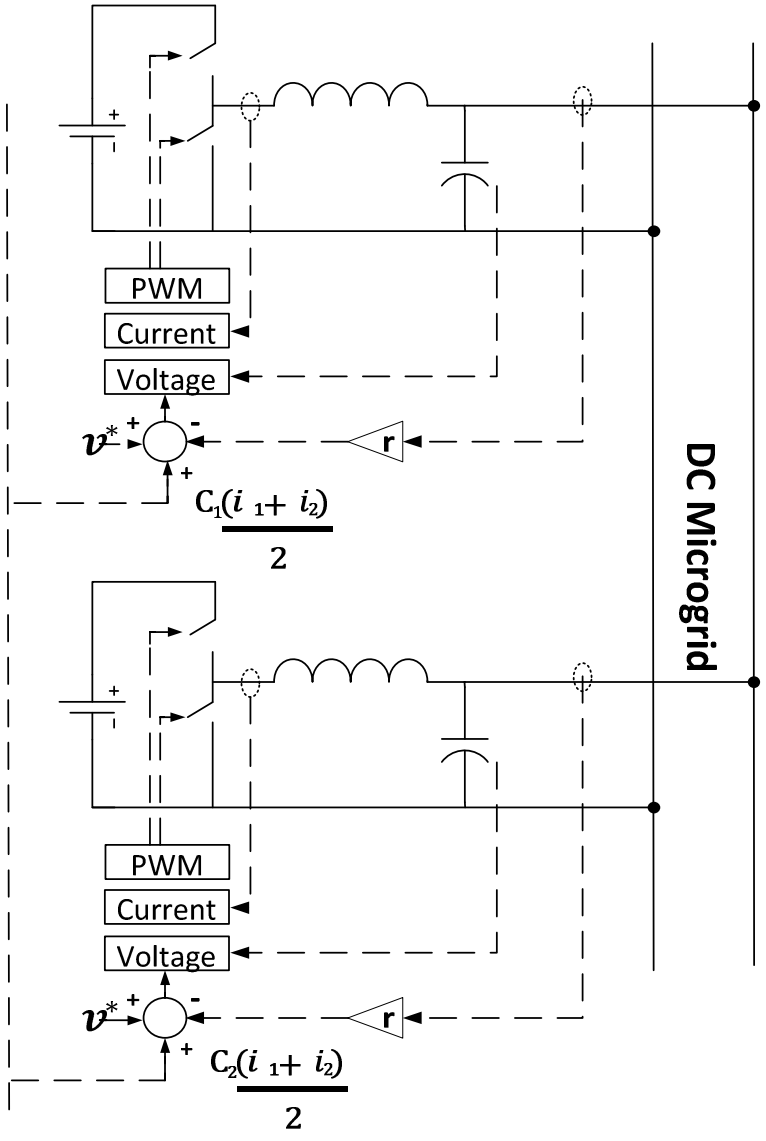

Figure 2.5: DGs under exchanging loading current

The system current voltage relation via admittance matrix:

$$I = Y\,V \tag{2.24}$$

Where, Partitioning (2.24) into DG buses (G) and load buses (L), leads to:

$$\begin{bmatrix} I^g \\ I^l \end{bmatrix} = \begin{bmatrix} Y^{gg} & Y^{gl} \\ Y^{lg} & Y^{ll} \end{bmatrix} \begin{bmatrix} V^g \\ V^l \end{bmatrix} \tag{2.25}$$

Substituting from (2.25) into (2.23) yields

$$V^g = V^* - R\left(Y^{gg}\,V^g + Y^{gl}\,V^l\right) \tag{2.26}$$

Simplifying (2.26) leads to:

$$V^g = (E + R_D\,Y^{gg})^{-1}\,(V^* - R_D\;Y^{gl}\,V^l) \tag{2.27}$$

where E is the identity matrix. Accordingly, it was found that in order to obtain perfect current sharing among the DGs, the droop parameters must be set at very high values, which means very unstable operation of all systems. In [36], the researchers modified the work proposed in [34] by adding an integrating term in the DG supervisory voltage and current control loops to provide a viable solution for the voltage regulation problem. However, the aforementioned control structure relies on common communication bus technology. As reported by [36], scenarios involving large numbers of DG units will be subject to significant delay while the updated data is written to the common bus, with the consequent possibility of instability problems triggered by asynchronous read/write actions. In addition, the failure of any point at the bus will ruin the whole control scheme. Restrictions on its length and the number of agents connected also limit the use of a common communication bus [37]. Moreover, the control algorithms provided in [34], [36] did not consider the operational costs of the DG units.

2.5 Power Management Studies in Islanded DC and AC/DC Hybrid Microgrids

Isolated dc microgrids introduce a new operational concept in the smart grid paradigm. The coordination between its main components (variable loads, generation and storage system) is the main theme in many of the recent publications. In [38], the authors provided a decentralized power management scheme for a stand-alone dc microgrid, including a storage system, DG units, and variable loads. The main concern in that work is the change in battery charging and discharging criteria based on the system state (voltage level), which is defined based on the mismatch between loading and generation conditions. In [39], the authors divided the operating voltage region into levels

according to which renewable DG units could locally determine the appropriate operational mode: maximum power tracing or droop control.

In [40], the authors proposed a supervisory technique in order to coordinate charging among different batteries operating at a common dc bus. The coordination algorithm depends on the state of charge of each battery and the available power sources in the common dc bus. Based on that information, the droop characteristics of each battery are adjusted to keep either all of the batteries at the same state of charge or to charge according to a predefined rate. In [41], a solid state transformer hierarchical control for the dc side is illustrated. The control hierarchy is composed of three main stages: primary, secondary and tertiary. Each stage operates within a certain time frame (seconds in primary, hours in tertiary) and according to pre-specified conditions. To be more specific, tertiary control operates in the connected mode to regulate power flow to and from the main grid, whereas the secondary control is active in islanded mode (i.e., when the system is disconnected from the main grid). In [42], the authors proposed connecting multiple ac buses to a common dc bipolar system to increase the system reliability and to reduce buses peaks and charging losses. The former two advantages can be inferred directly from the meshed configuration introduced in that approach. The reduction in charging losses was explained via the conversion stages required for charging vehicles via ac or dc infrastructure. In more detail, the current charging system utilizes the common ac system to provide dc voltage (via SCRs) which is converted to 6600Vac through IGBTs. Application of SCR in the middle stage imposes additional losses at the start of charging processes. Such extra losses can be avoided in the presence of dc infrastructure. In [43], the authors proposed an observer-based approach to capture sudden load changes, deviating the system voltage level and accordingly tripping the protection system, in hybrid ac/dc microgrids. The authors equipped the ac/dc converter control loop with an observer-based mechanism which enhances the dc voltage performance using local measurements of both the dc voltage side and the ac/dc active power transfer. These measurements are utilized as local feed-forward signals that indicate any changes in the loading condition.

In [44], the authors proposed detailed control algorithms that handle power management in ac/dc hybrid microgrids. The main focus was on manipulating energy management among ac and dc loads, battery systems, and renewable sources. Accordingly, the authors based their work on a centralized controller with rapid communication, which implies a higher failure risk as the system is fully dependent on communication among DG units, to implement the coordination algorithm. In [45], the authors introduced the droop-based co-ordination for DG units installed in hybrid ac/dc microgrids.

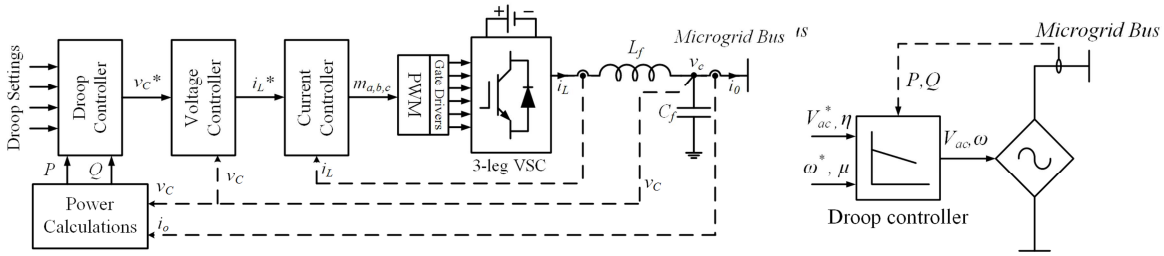

(a) (b)

Figure 2.6: DG in ac microgrids: (a) Power circuit and control structure, (b) simplified model

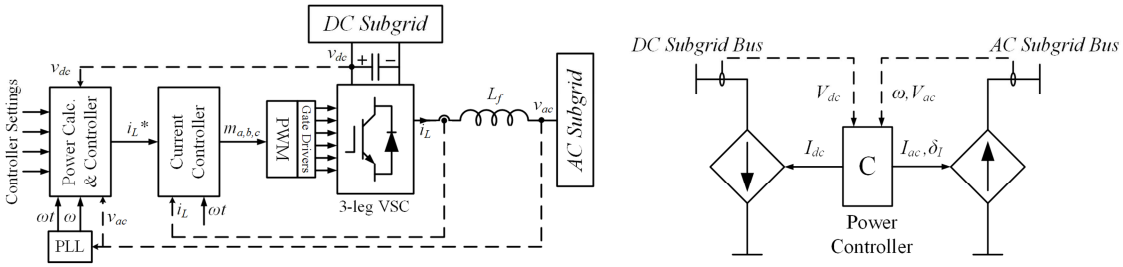

(a) (b)

Figure 2.7: IC in hybrid ac/dc microgrids: (a) Power circuit and control structure, (b) simplified model

According to this control scheme, all dispatchable DGs implement droop characteristics, non-dispatchable units apply their maximum output power, and ICs transfer constant power between the ac and dc subgrids. In dc subgrids, the droop characteristics are realized as discussed before for islanded dc microgrids, section 2.4. In ac subgrids, the droop characteristics are applied through adapting the DG frequency and voltage based on the output active and reactive powers, respectively:

$$P_{ac,Gi} = \mu_i(\omega_i^* - \omega) \tag{2.28}$$

$$Q_{Gi} = \eta_i(V_{ac,i}^* - V_{ac,i}) \tag{2.29}$$

where ω^* and v_{ac}^* are the no-load reference values for the DG output frequency and voltage, and μ_i and η_i are the reciprocals of the DG droop gains. Figure 2.6 (a) demonstrate the structure and control loops of an ac DG unit operating in droop-control mode. The simplified representation of droop-controlled DGs is illustrated in Figure 2.6 (b).

In general, the operational philosophy of hybrid ac/dc systems considers the capacity difference between the ac and dc subgrids [44], [45]. In [14], the authors viewed the dc system as a stiff system because it contains a battery storage system and thus the ac/dc converter operated to provide a fixed voltage slack terminal for the ac subgrid. In [45], the opposite situation was considered, where the ac system was viewed as a stiff system (it contains several dispatchable units) that provides a slack bus to the dc subgrid via the IC. In contrast with both assumptions, the authors in [46]–[48] proposed an IC operational criterion that relates the ac frequency to the dc voltage if there is no considerable difference between the capacities of the ac and dc subgrids. For higher system security, such islanded microgrids are characterized by droop control schemes that enable overall load sharing among the installed DGs as illustrated earlier [32]. To maintain a power balance between the ac and dc subgrids, the IC compares the deviation in frequency of the ac system and the deviation in voltage of the dc system to determine the higher loaded system and thus the power flow direction between the two systems. As shown in Figure 2.7(a), the ICs typically implement CC-VSCs, allowing for power exchange between ac and dc subgrids. The ac frequency and dc voltage are locally measured at the IC terminals. The local measurements are processed by the power controller to set the active power references. Figure 2.7(b) presents a simplified model, implying that the IC is realized as a load for one subgrid while being seen as a supply for another. This control strategy represnts a strong alternative that enables proper coordination between the subgrids; However, it introduces a new concept of coupling the ac frequency and dc voltage in the hybrid ac/dc paradigm.

2.6 Steady-State Analysis of ADNs

A practical implementation of the hybrid ac/dc microgrid paradigm could not be realized without performing a series of operational and planning studies by distribution utilities. These studies include, but are not limited to:

1- Optimal sizing and allocation for the system distributed energy resources (DER)

2- System reconfiguration and power restoration

3- Volt/Var planning and control

4- Economic dispatch and power management of the installed DER

5- Dynamic stability analysis

6- Protection design and Contingency analysis

In order to provide a scalable and thorough study of all the aforementioned topics, a comprehensive and generic power flow tool should be developed beforehand. Although several recent studies have been conducted to materialize the concept of ac/dc microgrids through time-domain simulations, the presented studies are still limited to a small number of buses analyzed for a very narrow operational time horizon. In general, time-domain simulations (e.g. PSCAD/EMTP or SIMULINK) consider a set of algebraic and differential equations that model the system dynamic behavior. This complex representation hinders the capability of time-domain SW in simulating large-scale systems for long time horizon. Alternatively, the steady-state system variables could be obtained through a power flow algorithm that accurately models and efficiently solves the system algebraic equations, accordingly more suitable for running extended system studies within a reasonable time frame.

Only a handful of recent research studies tackled the subject of power flow analysis in islanded ac microgrids or in MTDC networks. In [49], the authors proposed a power flow algorithm that incorporates the system frequency of islanded ac microgrids, utilizing the Newton-trust region (NTR) method. The authors of [50] employed particle swarm optimization to solve the optimal power flow of islanded ac microgrids. A power flow approach applicable for droop-based dc buses was developed in [51]. In [52], an ac/dc power flow algorithm was proposed for multi-terminal dc systems (MTDC), taking into consideration the converters' losses. However, this approach is not applicable to hybrid microgrids, because there is no slack bus in the system. The steady-state models of the droop-based DGs were highlighted for the ac and dc microgrids in [53], without providing a proper model for the IC that considers coupling between the subgrids. In addition, the authors did not propose a systematic steady-state methodology in that work.

2.7 Discussion

Throughout the literature review provided in this chapter, it is obvious that while sufficient work has been done with respect to power management in dc and ac/dc distribution systems to meet system adequacy or to regulate the system voltage, most of the provided schemes are based on centralized techniques. In contrast to studies in ac systems, the operational problem of voltage regulation in dc systems was tackled only in an isolated dc system context. The centralized approaches in the literature contradict with the plug and play, and reliability concepts of smart grid paradigm. A few studies are provided based on distributed control manner, albeit the significant deficiencies in terms of accuracy and generality. Via the recent mathematical distributed optimization, introduced in this

chapter, a more advanced and robust distributed power management schemes can be developed. Moreover, deeper studies into voltage regulation in connected mode are lacking. Such studies will be significant to cope with the large scale medium voltage dc systems introduced by ABB research laboratories.

Obvious limitations on steady state studies are noticed in ac/dc hybrid system studies. The main reason for this is the absence of an inclusive load flow tool that is adequate for the system nature and different operation philosophy. Developing such a tool will open the door wide for further steady-state analysis such as system loadability, reconfiguration, and restoration studies.

Chapter 3
A Novel Multi-agent Control Scheme for Voltage Regulation in DC Distribution Systems

3.1 Introduction

In chapter 2, it was demonstrated that one of the most salient studies in microgrids is power management, which is directly related to DG voltage regulation in dc systems. In dc microgrids operating in grid-connected mode, the DG units are allowed to inject their maximum output power since the main grid could manipulate any difference between the microgrid generation and load. However, unlike ac networks, the dc voltage is coupled with the DG active power injection, and thus, high penetration of DG resources may deteriorate the system voltage profile [54], [55].

In this chapter, issues around voltage regulation in large-scale dc distribution systems (DCDSs) with high penetration of DG units are addressed. A multi-agent distributed control scheme, based on two-way communication between DG units and the system's main ac/dc interfacing converter, is proposed. The proposed control scheme aims to mitigate the challenges of voltage regulation in DCDS and facilitate seamless integration for high DG penetration. Two sequential stages are carried out in the proposed distributed control scheme. The first stage is designed to provide the ac/dc converter with the capability of optimally adjusting its output voltage, taking into consideration the distribution of the voltage profile in the downstream dc network. If the ac/dc fails to regulate the system voltages appropriately, the second stage is activated to enable DG units to share in the voltage regulation process.

To that end, two power management multi-agent based strategies are proposed. The first strategy is based on equal power curtailment, where all DG units participating in the voltage violation problem are subjected to equal curtailment ratios according to their capacities. The curtailment ratio is calculated via an average consensus-based algorithm. This strategy is classified as a non-cooperative strategy and can be adopted for a set of DG units owned by different entities within the same DCDS [27], [28]. The second strategy is based on maximizing overall DG operation revenue. Here, the DG units cooperate together to allocate the output power combination that achieves the maximum net

revenue for the DCDS, without violating the system voltage limits. This strategy can be adopted for a set of DG units that are owned by the same entity, e.g., a local distribution company [22], [56]. The problem is formulated mathematically as a convex optimization problem under global constraints, and a DLPDS algorithm is proposed to solve it in a multi-agent environment [17].

The rest of the chapter is organized as follows: In section 3.2, the estimation of the voltage profile due to changes in the injected DG power is addressed for DCDSs. Detailed model and mathematical formulations regarding the first and second stages of the proposed voltage control scheme are illustrated in sections 3.2 and 3.4, respectively. To verify the effectiveness of the proposed multi-agent technique, several case studies are provided in section 3.5, and the main findings of this work are discussed in section 3.6.

3.2 Voltage Profile Estimation in DCDS

The main objective of the DCDS is to enhance the performance of dc loads while increasing the DG penetration. Figure 3.1 shows a proposed structure of future DCDS. As shown in the figure, an ac/dc bidirectional converter is connected in the main substation to interface the ac grid with the dc distribution network. The ac/dc bidirectional converter is the main device responsible for voltage regulation in the downstream feeders. Nonetheless, the integration of high DG penetrations in DCDS can significantly change the system voltage profile and interfere with the operation of the ac/dc bidirectional converter due to: 1) many of the DG units being characterized by high degree of uncertainty, such as PV and wind; and 2) a large number of small-sized DG units being required to be controlled. Estimations of voltage profile changes due to changes in the injected power can be analyzed based on the following discussion.

3.2.1 Voltage Profile Estimation in Radial DCDS

To avoid confusion, all of the following calculations are considered on a per unit (p.u.) basis. Figure 3.2 illustrates a typical diagram of a DCDS radial distribution feeder. Without the installation of DG units, the direction of power flow is unidirectional from the upstream ac network towards the downstream dc network. However, when DG resources are installed, a bidirectional power flow is expected. As depicted in the figure, the injection of power Δp_n at bus# n will reduce the power flow through the bidirectional converter at the point of ac/dc coupling by the same amount of power Δp_n, neglecting the change of system losses. Similarly, the branch power flow between any two upstream

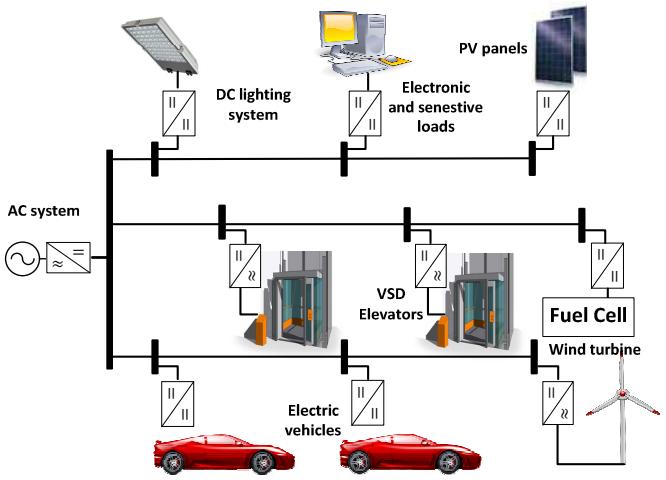

Figure 3.1: Proposed dc distribution system

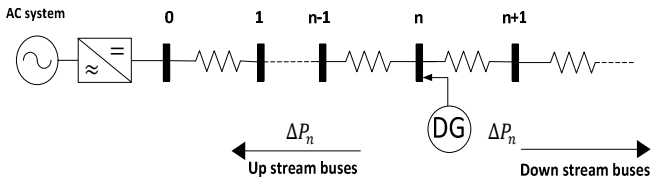

Figure 3.2: Radial dc distribution feeder

buses will be reduced with the same amount of Δp_n. On the other hand, there will be no change in the branch power flow between the buses downstream bus# n.

Consider the initial voltage difference between bus# n and its upstream bus# n-1 pre-injecting Δp_n as

$$v_{(n-1)old} - v_{(n)old} = \frac{p_{n-1,n}\, r_{n-1,n}}{v_{(n-1)old}} \approx p_{n-1,n}\, r_{n-1,n} \tag{3.1}$$

where $p_{n-1,n}$ is the power flowing between buses n-1 and n, and $r_{n-1,n}$ is the resistance between the two buses. The assumption provided in (3.1) is acceptable, since the p.u. voltage at any of the system buses is always $\pm 5\%$ around the unity. In the light of the above observation, changes in the voltage profile of a feeder after injecting Δp_n at bus# n can be given as:

$$v_{(n-1)new} - v_{(n)new} = (p_{n-1,n} - \Delta p_n) r_{n-1,n} \tag{3.2}$$

Subtracting (3.2) from (3.1) gives:

$$v_{(n)new} - v_{(n)old} = v_{(n-1)new} - v_{(n-1)old} + \Delta p_n \, r_{n-1,n} \tag{3.3}$$

Similarly, changes in the voltage at bus n-1 can be derived as follows:

$$v_{(n-1)new} - v_{(n-1)old} = v_{(n-2)new} - v_{(n-2)old} + \Delta p_n \, r_{n-2,n-1} \tag{3.4}$$

Using a backward sweep, the same sequence of equations can be recursively obtained until reaching the stiff bus named as bus# 0, as follows:

$$v_{(1)new} - v_{(1)old} = v_{(0)new} - v_{(0)old} + \Delta p_n \, r_{0,1} \tag{3.5}$$

Taking into consideration that bus# 0 is the interfacing bus with the ac system (which is a stiff [i.e., voltage-controlled] bus), (3.5) would be

$$v_{(1)new} - v_{(1)old} = \Delta p_n \, r_{0,1} \tag{3.6}$$

Applying (3.6) recursively in (3.3), yields

$$v_{(2)new} - v_{(2)old} = \Delta p_n \, r_{0,1} + \Delta p_n \, r_{1,2} \tag{3.7}$$

From (3.6) and (3.7), one can obtain the voltage change at any bus# i≤ n, as follows:

$$v_{(i)new} - v_{(i)old} = \Delta p_n \, r_{0,1} + \Delta p_n \, r_{1,2} + \Delta p_n \, r_{2,3} + \cdots + \Delta p_n \, r_{n-1,n} \tag{3.8}$$

Thus, the change in a voltage magnitude at any upstream bus with Δp_n change at bus n can be formulated in a compact form as

$$v_{(i)new} = v_{(i)old} + \Delta p_n \sum_{h=1}^{h=i} r_{h-1,h} \tag{3.9}$$

On the other hand, the change in voltage magnitude in downstream buses will be the same as the change in voltage magnitude of bus n, as no change in power flow occurred. Hence, the change in voltage magnitude at any arbitrary bus i due to Δp_n at bus n in a dc radial distribution feeder can be formulated as

$$\Delta \, v_{(i)} = R_{i,n} \Delta p_n \tag{3.10}$$

where

$$R_{i,n} = \sum_{h=1}^{min(i,n)} r_{h-1,h} \tag{3.11}$$

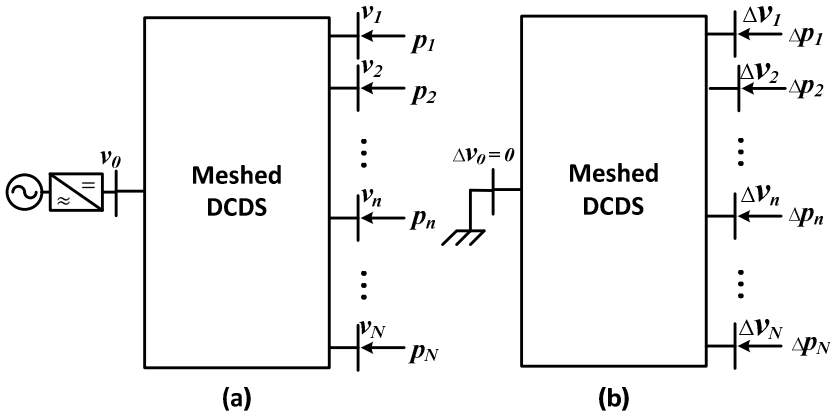

Figure 3.3: Meshed DCDS representation: (a) initial condition, and (b) incremental power flow

3.2.2 Voltage Profile Estimation in Meshed DCDS

In meshed dc networks, changes in the system voltage profile due to changes in power injection cannot follow the aforementioned analysis, since the injected power flows to the slack bus through different routes. Instead, all of the DCDS should be studied as a single system, shown in Figure 3.3(a), which can be mathematically represented via a state space model:

$$P = V \otimes YV \tag{3.12}$$

where

$$P = [p_0 \quad p_1 \quad \dots \quad p_N]^T \tag{3.13}$$

$$V = [v_0 \quad v_1 \quad \dots \quad v_N]^T \tag{3.14}$$

Y is the bus admittance matrix of the system. $\otimes$ is Hadamard product operator, i.e., a point-to-point matrix multiplication. In incremental form, the power flow equation can be represented using the Jacobin representation:

$$\Delta P = J_{dc}\, \Delta V \tag{3.15}$$

with:

$$J_{dc} = \begin{bmatrix} \sum_{\substack{h=0 \\ h\neq 0}}^{N} y_{0,h}(2\,v_0 - v_h) & -y_{0,1}v_0 & \dots & -y_{0,N}v_0 \\ -y_{1,0}v_1 & \sum_{\substack{h=0 \\ ,h\neq 1}}^{N} y_{1,h}(2\,v_1 - v_h) & \dots & -y_{1,N}v_1 \\ \vdots & \vdots & \ddots & \vdots \\ -y_{N,0}v_N & -y_{N,1}v_N & \dots & \sum_{\substack{h=0 \\ h\neq N}}^{N} y_{N,h}(2\,v_N - v_h) \end{bmatrix} \quad (3.16)$$

The terms of the Jacobian matrix ($J_{dc} = \frac{\partial P}{\partial V}$) are not constants and depend on the system voltages. However, since the system voltage profile is kept around unity, changes in the Jacobian matrix will be negligible [10]. Considering a flat voltage profile around 1 p.u., the Jacobian matrix can be approximated by the bus admittance matrix in p.u. values, i.e. $J_{dc} \approx Y$. This result was implicitly discussed in [35] and lines up with our previous assumption in (3.1). Since bus zero is a stiff bus in the system, its voltage is constant disregarding any change in the injected power, i.e. $\Delta v_{(0)} = 0$. The first column and row vectors in (3.12) can therefore be eliminated by reconsidering the configuration in Figure 3.3 (b):

$$\Delta P' = Y' \Delta V' \quad (3.17)$$

with:

$$\Delta P' = [\Delta p_1 \quad \Delta p_2 \quad \dots \quad \Delta p_N]^T \quad (3.18)$$

$$\Delta V' = [\Delta v_1 \quad \Delta v_2 \quad \dots \quad \Delta v_N]^T \quad (3.16)$$

where Y' is the reduced bus admittance matrix for the system in Figure 3.3 (b).Thus, the estimation of voltage profile change due to changes in the injected power can be inferred as

$$\Delta V' = R \Delta P' \quad (3.20)$$

where $R = Y'^{-1}$ is the bus resistance matrix for the system. In general, the admittance matrix for distribution systems is sparse, so obtaining R via its inversion is not recommended. Instead, the R matrix for DCDS can be directly formulated via the typical methodology of the impedance matrix in ACDS [57]. It is noteworthy that (3.20) is valid also for radial DCDS. However, the entries of the matrix R will exactly match the ones obtained previously in (3.10).

3.3 First Stage of the Proposed Voltage Control Scheme

Appropriate decisions in control agents cannot be taken without proper knowledge of the current state of the network. Hence, real-time measurements and communication links must be provided for proper state estimation and decision making. In this work, a distributed multi-agent control schemes with two-way communication is proposed to mitigate the voltage regulation challenges in DCDS. Three categories of control agents with different functionalities are considered in the proposed control scheme: an ac/dc converter control agent, DG control agents, and end-feeders control agents (for radial systems only). The communication network is divided into sub-networks, where each gathers a group of DG units that have mutual power/voltage effect. For example, a group of DG units may share the same feeder in a radial system, or a group of DG units may have a highly mutual power/voltage effect (based on the decomposition concept introduced in [27]) in meshed systems. The proposed control scheme consists of two sequential stages. In this section, the first stage of the proposed control scheme is presented.

First, the end-feeders and DG control agents operate cooperatively to estimate the voltage profile along the feeder(s). The cooperation aims to provide the ac/dc converter control agent with the current state of the minimum and maximum voltages in each feeder, which is considered as adequate knowledge for appropriate ac/dc converter decision-making. To that end, the end-feeder control agent measures its own voltage and current and supplies these values to its upstream DG control agent. The DG control agents exchange information with other neighboring DG units regarding the DG voltages and their contribution in the feeder global minimum calculation.

In order to estimate the global minimum of a certain feeder, the feeder is divided into a set of segments, where two DG units bound each segment. Each DG can estimate the minimum voltage of the segment between itself and the downstream DG, based on the two DG voltages and DG currents flowing into the segment [33]. The DG compares the calculated minimum voltage of the segment and the received minimum voltage over all the downstream segments, and then it can update the global minimum and send it to its upstream DG. The ac/dc converter control agent measures its local voltage and receives different maximum and minimum voltages points from the different feeders. It then determines the global minimum and maximum voltage in the system overall and takes corrective action to regulate the system voltage, as follows:

$$v_{(0)new} = v_{(0)old} + \left(v^{nom} - \frac{v_{max} + v_{min}}{2}\right) \tag{3.21}$$

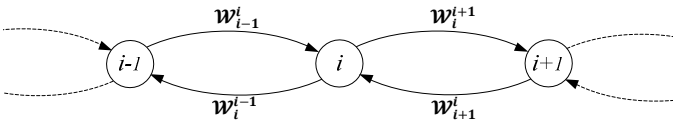

Figure 3.4: Proposed communication network (graph).

where $v_{(0)new}, v_{(0)old}$ are the new and old output voltages of the ac/dc converter, and v_{max}, v_{min} are the global maximum and minimum voltages over the distribution network.

3.4 Second Stage of the Proposed Voltage Control Scheme

The distributed state estimation scheme described in the previous section provides the ac/dc converter with appropriate information to regulate the voltage on its own, without contributing actions from the DG units. Yet, in some operating conditions, the ac/dc converter control agent might face the problem of an infeasible solution (i.e., a problem in which the difference between the actual system maximum and minimum voltages exceeds the difference between the specified system maximum and minimum voltages). In such operating conditions, the ac/dc converter control agent fails to regulate the voltage properly and it thus has to work as initiator and send a request message for all DG control agents to activate the second stage of the proposed algorithm. Since DG units cause an over voltages in their feeders, the participation of DG units will be through active power curtailment when stage two is activated. The option of power curtailment seems to be very appealing, and hence it has the potential to significantly increase the energy sourced from renewable generation, compared to keeping conservative with throttling planning constraints [29], [58]. In addition, curtailment can be simply implemented for both dispatchable and non-dispatchable (i.e., renewable) DG units via minor changes in the DG converter control logic [28], [59]. In this work, it is assumed that all installed DG control units have active power curtailment functionality.

In this section, a distributed multi-agent voltage control scheme is proposed for DG control agents in order to assist the ac/dc converter control agent if the latter cannot solely keep the voltage at all system buses within their specified limits. Details of the proposed control scheme are explained in the following subsections.

3.4.1 Problem Formulation

Under the smart-grid context, DG units will be actively sharing voltage control. Various strategies incorporating DG active power control have been proposed for ACDS [28], [30]. Nevertheless, careful consideration should be given to the participation of DG units in the voltage regulation of DCDS. In the following subsections, two multi-agent schemes for power management are discussed in order to maintain the system voltage within the permissible limits in DCDS. The first scheme is the equal power curtailment, which is realized via an average consensus-based algorithm. The second scheme is the maximum revenue, according to which the DG units cooperatively allocate the combination of their output power that results in the maximum net revenue for the dc network without violating the system voltage bounds. This algorithm is implemented through a distributed Lagrangian primal-dual subgradient, which is an efficient algorithm for obtaining the global optimal solution in a multi-agent framework for such a convex problem.

3.4.1.1 Equal Power Curtailment Scheme

In this section, a consensus-based algorithm is proposed to enable different DG units to work under the same curtailment ratio in the presence of a voltage violation that cannot be mitigated using the ac/dc converter control agent. In order to enable each DG unit to locally estimate the curtailment ratio of all units, two auxiliary variables have to be exchanged between the DG units in the neighborhood through a communication network presented in Figure 3.4: Γ_j, representing the average output power, and Γ_j, representing the average maximum power as estimated by DG j. The data propagation among the DG agents can be detected by assuming the initial values of the auxiliary variables, as follows:

$$\Gamma_j[0] = p_j \tag{3.22a}$$

$$\Psi_j[0] = p_j^{max} \tag{3.22b}$$

where p_j is the DG output power in the current state and p_j^{max} is the DG capacity. Each DG then updates its Γ_j, Ψ_j based on the exchanged information with its neighbor DG units as:

$$\Gamma_j[1] = \sum_{i \in \{\mathcal{N}_j^-\} \cup \{j\}} \mathcal{W}_i^j \ \Gamma_i[0] \tag{3.23a}$$

$$\Psi_j[1] = \sum_{i \in \{\mathcal{N}_j^-\} \cup \{j\}} \mathcal{W}_i^j \ \Psi_i[0] \tag{3.23b}$$

In order to the illustrate the change of Γ_j, Ψ_j through several iterations, vectors Γ and Ψ are defined to aggregate all DG units in a strong connected graph assumed as illustrated in section 2.3.2:

$$\Gamma[1] = [\Gamma_1[1]\, \Gamma_2[1] \dots\, \Gamma_{Ng}[1]]^T \tag{3.24a}$$

$$\Psi[1] = [\Psi_1[1]\, \Psi_2[1] \dots\, \Psi_{Ng}[1]]^T \tag{3.24b}$$

Thus, (18) can be rewritten in a compact form as:

$$\Gamma[1] = \mathcal{W}\, \Gamma[0] \tag{3.25a}$$

$$\Psi[1] = \mathcal{W}\, \Psi[0] \tag{3.25b}$$

After k iterations, $\Gamma[k], \Psi[k]$ can be represented in terms of the initial vectors $\Gamma[0], \Psi[0]$, respectively, as

$$\Gamma[k] = \mathcal{W}^k\, \Gamma[0] \tag{3.26a}$$

$$\Psi[k] = \mathcal{W}^k\, \Psi[0] \tag{3.26b}$$

From section 2.3.2 , we could recall that $lim_{k\to\infty}\, \mathcal{W}^k$ converges to a rank-one deterministic matrix $(\frac{1}{N_g}\, e)$, where N_g is the number of operating DG units and e is an $N_g \times N_g$ matrix with all elements being ones, thus $\lim_{k\to\infty} \Gamma[k]$ and $\lim_{k\to\infty} \Psi[k]$ converges to the average DG output power and capacity, respectively. Let us define Λ_j as a function of Γ_j, Ψ_j, as follows:

$$\Lambda_j[k] \;=\; \frac{\Gamma_j[k]}{\Psi_j[k]}\, \Psi_j[0] \tag{3.27}$$

If the number of iterations k is very large, the following relation can be inferred

$$\lim_{k\to\infty} \Lambda_j[k] \;=\; \frac{\sum_{i=1}^{N_g} p_i}{\sum_{i=1}^{N_g} p_i^{max}}\, p_j^{max} \tag{3.28}$$

Hence, Λ_j represents the locally estimated DG output power of the DG j to match an overall curtailment ratio with the other DG units. In order to consider the equal curtailment sharing and the system voltage limits, the following algorithm could be adopted by each DG agent at arbitrary iteration k:

1. Starting with the auxiliary variables as stated in (3.22).
2. Updating the auxiliary variables:

$$\Gamma_j[k] = \sum_{i \in \{\mathcal{N}_j^- \} \cup \{j\}} \mathcal{W}_i^j \ \Gamma_i[k] \tag{3.31}$$

$$\Psi_j[k] = \sum_{i \in \{\mathcal{N}_j^- \} \cup \{j\}} \mathcal{W}_i^j \ \Psi_i[k] \tag{3.32}$$

3. Calculating the estimated output power to satisfy the equal curtailment condition:

$$\Lambda_j[k] \ = \frac{\Gamma_j[k]}{\Psi_j[k]} \ p_j^{max} \tag{3.33}$$

4. Updating the DG output power, as follows:

$$p_j[k+1] = \ \Lambda_j[k] + \frac{1}{N_g \ R_{n,j}} \left(v_{per}^{max} - \ v_n[k] \right) \tag{3.34}$$

where v_{per}^{max} is the upper limit of permissible voltage level, $v_n[k]$ is the highest DG voltage within a sub-network, $R_{n,j}$ is the sensitivity constant that relates the change in DG power at bus j with change of voltages at bus n, as discussed in (3.10), (3.20). According to (3.34), each DG modifies its output power based on two main terms. The first term ($\Lambda_j[k]$) is to keep all DG units operating under the same curtailment ratio, whereas the second term, $\frac{1}{N_g \, R_{n,j}} \left(v_{per}^{max} - \ v_n[k] \right)$, is an excitation term by which the DG units update their output powers to maintain the DG voltages not violating v_{per}^{max}. The iterative application of the aforementioned sequence, i.e., (3.31)-(3.34), results in an equilibrium point defined by $\Lambda_j = \ p_j$ and $v_n \ = v_{per}^{max}$. Thus, all DG units will keep operating at the same curtailment ratio without any voltage violation.

3.4.1.2 Maximizing Revenue Scheme

In this strategy, a group of DG units within a sub-network cooperates together in order to determine their optimal powers for achieving maximum revenue without violating the voltage limits at any of the DG buses. The net revenue ($\mathfrak{R}^{net}$) of a DG j can be defined in terms of the revenue ($\mathfrak{R}$) and the operating cost (OC), as follows:

$$\mathfrak{R}_j^{net}(p_j) = \mathfrak{R}_j(p_j) - OC_j(p_j) \tag{3.35}$$

Thus, the optimization problem can be formulated as

$$max \sum_{j \in G} NR_j(p_j) \tag{3.36}$$

subjected to:

$$p_j^{min} \leq p_j \leq p_j^{max} \qquad \forall\, j \in G \tag{3.37}$$

$$v_{per}^{min} \leq v_j \leq v_{per}^{max} \qquad \forall\, j \in G \tag{3.38}$$

Since the functionality of the ac/dc converter is to keep the maximum and minimum voltages of the system even around the reference value, it will be sufficient to check that the DG voltages (the maximum voltage points) are not exceeding the maximum limit. Further, the change in DG voltage is a function in the DG output power, and thus (3.38) can be replaced with:

$$\sum_{i \in G} R_{j,i}\, \Delta p_i \leq v_{per}^{max} - v_j \qquad \forall\, j \in G \tag{3.39}$$

In general, the $\mathfrak{N}^{net}$ of DG operation can be simplified into quadratic and linear equations for dispatchable and renewable DG units, respectively [60]. The aforementioned maximization problem, defined by (3.35)-(3.39), consists of a quadratic objective function with negative quadratic coefficients and affine inequalities; it can be classified as a convex optimization problem [61]. This convex problem is, in the present work, converted into a standard distributed multi-agent optimization problem using a DLPDS algorithm [17]. Each DG unit will be responsible for solving its optimization problem in order to maximize its revenue, based on its private and global constraints defined in (3.37), (3.39), respectively. According to DLPDS, the DG Lagrangian function will include the DG objective and the global constraints only, as follows:

$$L_j(P, \lambda) = -NR_j(p_j) + \lambda^{j^T} g(P_j) \tag{3.40}$$

where λ is a vector of a Lagrangian multiplier, and g(P) is a vector corresponding to the global constraints as stated in (3.39). In order to obtain the global optimal solution, the following algorithm could be adopted by each DG agent at arbitrary iteration k. First, each DG agent exchanges the primal and dual variables (P, μ) with its neighbors:$\boldsymbol{\lambda}$

$$v_P^j(k) = \sum_{i \in \left\{\mathcal{N}_j^-\right\} \cup \{j\}} \mathcal{W}_i^j P^i(k) \tag{3.41}$$

$$v_{\lambda}^{j}(k) = \sum_{i \in \{\mathcal{N}_j^-\} \cup \{j\}} \mathcal{W}_i^j \, \lambda^i(k) \tag{3.42}$$

Then, the gradient of the change in primal and dual variables can be calculated as

$$D_P^j(k) = \frac{\partial L_j\left(P, v_{\lambda}^{j}\right)}{\partial P} \tag{3.43}$$

$$D_{\lambda}^{j}(k) = \frac{\partial L_j\left(v_P^j, \lambda\right)}{\partial \lambda} \tag{3.44}$$

Finally, each DG agent updates its primal and dual parameters, as follows:

$$P_j(k+1) = Pro_{P_j}\left[v_p^j(k) - \eth(k) D_P^j(k)\right] \tag{3.45}$$

$$\lambda_j(k+1) = Pro_{\lambda_j}\left[v_{\lambda}^{j}(k) + \eth(k) D_{\lambda}^{j}(k)\right] \tag{3.46}$$

where $\mathrm{Pro_P}$, Pro_{λ} are the projection operators of the DG output powers and Lagrangian multipliers, respectively. $\eth(\mathrm{k})$ is a diminishing step-size that satisfies $\eth(\mathrm{k}) > 0$ for any step k, $\sum_{\mathrm{k}=1}^{+\infty} \eth(\mathrm{k}) = +\infty$, and $\sum_{\mathrm{k}=1}^{+\infty} \eth(\mathrm{k})^2 < +\infty$. In order to meet this condition, the step-size can be assigned as $\eth(\mathrm{k}) = \frac{1}{\mathrm{k}}$ [62]. In (3.45), each DG agent projects the output of the optimization iteration onto its private constraints of the power generation limits (3.37), which is not considered in the agent Lagriangian function (3.40). Similarly in (3.46), the DG agents project the dual parameters onto the nonnegative real numbers, i.e., $\lambda^{\mathrm{j}} \geq 0$, which is the default domain of the dual parameters.

The overall exchange of data is demonstrated in Figure 3.5 that presents DG2 placed with two other DG units (DG1 upstream and DG3 downstream) in a single feeder. As depicted, DG2 exchanges the voltage values of the DG buses with the other DG units. DG2 also receives the upstream current at DG3 in order to estimate the local minimum voltage value between DG2 and DG3. Thus, DG2 compares the estimated local minimum with the received downstream global minimum and updates the latter if required. In addition, different DG units would have to exchange the auxiliary variables, i.e., (Γ , Ψ) or (P, λ), required to carry out the DG power management control schemes if necessary.

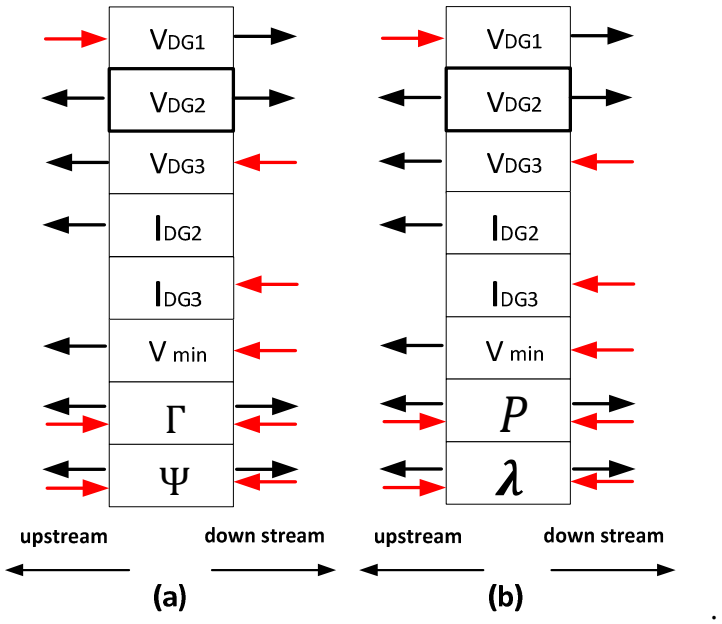

Figure 3.5: The data flow between DG2 and its neighbors for different control strategies: (a) the equal curtailment, and (b) the maximizing revenue

3.5 Simulation Results

The proposed multi-agent control schemes have been implemented in a MATLAB environment. Several simulation studies for different DCDS topologies have been carried out and tested to demonstrate the effectiveness of the proposed control schemes. A study period of 24 hours has been selected to test the continuous response of the proposed control scheme; the data for loads, PV and wind power profiles are provided in [12], [63] and illustrated in Appendix A.

3.5.1 Radial Test Network

The proposed control scheme is tested on the multi-feeder low voltage dc test system shown in Figure 3.6, [64], [65]. The data for the test system are similar to those of the ac system presented in [25], illustrated in Appendix A. **Error! Not a valid bookmark self-reference.** demonstrates the data of the generation and load in the test system. The system base voltage and power are 400V and 400KW, respectively. The revenue obtained due to the operation of each DG unit is calculated based on the DG type and its output power according to the microFIT price schedule applied in Ontario, Canada

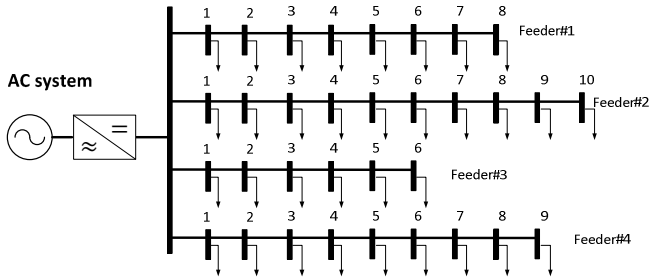

Figure 3.6: Four feeders test system

Table 3.1: DG data for case study 1

Feeder #	**Generation profile**			**Load profile**	
	Location	Type	Rating [p.u.]	Type	Total Peak [p.u.]
1	4,8	wind, wind	0.2,0.05	Com.	0.4
2	3,6,9	PV, DU*, DU	0.2,0.1,0.1	Res.	0.5
3	3,6	DU, Wind	0.2,0.1	Com.	0.3
4	5,8	PV, Wind	0.05,0.05	Res.	0.45

[66], while the operation cost of dispatchable units (DUs) is calculated using the following quadratic function [60]:

$$OC_i(p_i) = 8.7657 + 0.0656\, p_i + 0.0004\, {p_i}^2 \tag{3.47}$$

Since the system consists of four feeders, the communication layout is divided into four different sub-networks (i.e., each feeder is represented as a sub-network). In order to fulfill the communication network requirements, (2.1) is adopted to create the adjacency matrix. Consider feeder#2, for instance, in which there are three DG units representing three vertices: $\mathcal{V} = \{\mathcal{V}_1, \mathcal{V}_2, \mathcal{V}_3\}$. The set of directed edges in that graph is $\mathcal{E} = \{(\mathcal{V}_1, \mathcal{V}_2), (\mathcal{V}_2, \mathcal{V}_1), (\mathcal{V}_2, \mathcal{V}_3), (\mathcal{V}_3, \mathcal{V}_2)\}$, in which the agents are connected with the adjacency matrix, defined as:

$$\mathcal{W} = \begin{bmatrix} 2/3 & 1/3 & 0 \\ 1/3 & 1/3 & 1/3 \\ 0 & 1/3 & 2/3 \end{bmatrix} \tag{3.48}$$

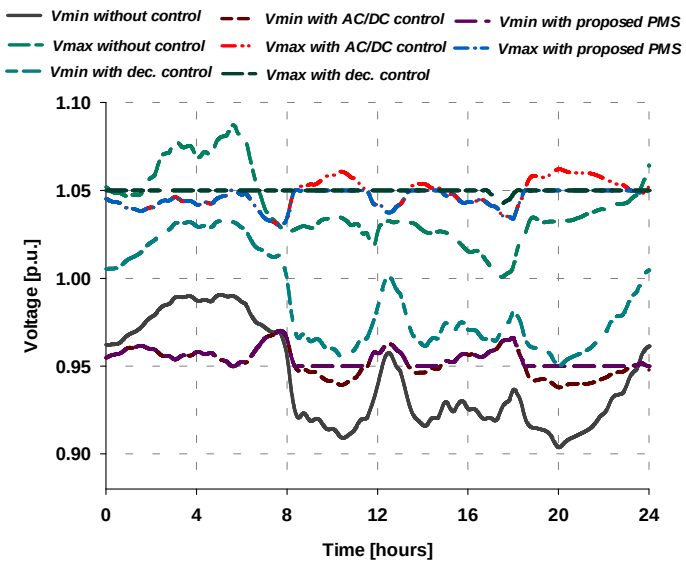

Figure 3.7: The system voltage profile according to different control schemes in the radial test system

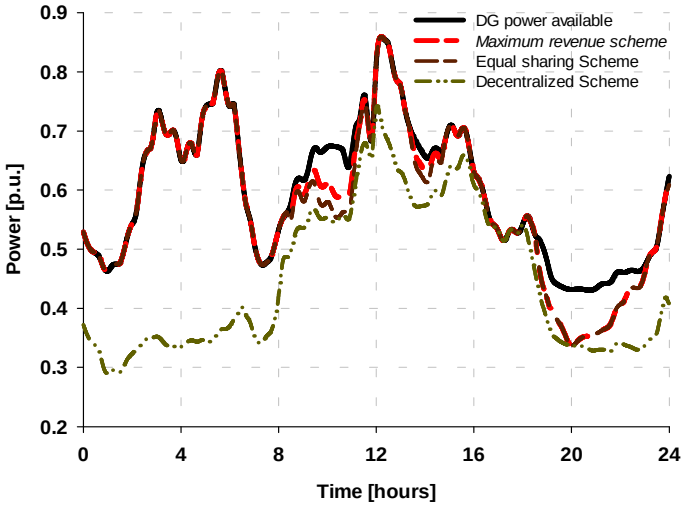

Figure 3.8: Total DG output power according to different control schemes in the radial test system

Four different types of control structures have been applied to illustrate the effectiveness of the proposed approach. In the first control structure, the ac/dc converter output voltage is set locally to a fixed value in all operating conditions. In the second control scheme, the ac/dc converter output voltage is controlled according to the first stage of the proposed control scheme. It is assumed, in the first and second control structures, that active power curtailment is not allowed. The third control structure is the same as the second control structure, but the second stage of the proposed control

schemes (i.e., the proposed active power curtailment strategies) are activated when needed. A decentralized (local) control is applied in the fourth control structure for both the ac/dc converter output voltage and active power curtailment simultaneously. In this type of control, the output voltage of the ac/dc converter is kept fixed, similar to the first control structure, and the DG units react according to the local voltage measurement. Based on this, the DG units have to curtail the output power until the local voltage equals the maximum permissible limit. Such a control scheme has been previously proposed for single-feeder ac distribution networks [28] and for small-scale DCDS [31].

Figure 3.7 shows the system minimum and maximum voltage for the period under study when the four control structures are applied. As shown in the figure, when the ac/dc converter output voltage is fixed and without any control over the DG output power, the system voltage constraints are frequently violated with high deviation in the system voltage beyond the permissible limits. The maximum and minimum system voltages approached 1.08 and 0.9 p.u., respectively. By the application of the first stage only of the proposed control scheme, appropriate control of the ac/dc output voltage drives the system voltage extremes – maximum and minimum values – to a symmetrical state of operation around the unity voltage. Therefore, it has a significant effect on reducing the fluctuation of the voltage profile and the deviation in the system voltage beyond the permissible limits (maximum recorded voltage is 1.065 p.u., while the minimum recorded voltage is 0.935 p.u.). Figure 3.7 also show that the proposed power management strategies restrict the system voltage to its permissible limits throughout the day (i.e., the maximum voltage is restricted to 1.05 p.u. and the minimum voltage to 0.95 p.u.). This occurs simultaneously due to the even voltage profile obtained by the first control stage. It is noteworthy that both equal curtailment and maximum revenue control schemes will result in the same voltage profile for the system around the day, since both strategies adopt the same first stage of voltage control via the ac/dc converter in normal conditions. In the presence of voltage violation, both strategies deal with the voltage limits as binding constraints, i.e., the system maximum and minimum voltages will be confined at the maximum and minimum permissible limits, respectively. Further, as shown in the figure, decentralized active power curtailment is also capable of maintaining the voltage profile within the specified limits. The symmetry in the voltage profile is absent in this control scheme, as there is no control over the ac/dc converter.

The aforementioned discussion showed that both the proposed control schemes and the decentralized control structure are capable of maintaining the system voltages within their permissible

level. However, the maximum power injected, which indicates the welfare and investors' satisfaction , is another essential aspect that needs further investigation for each scheme. Figure 3.8 shows the total output power of the DG units when the decentralized, equal curtailment, and maximum revenue control schemes are applied. As depicted in the figure, the total output power of the DG units is the lowest in the case of the decentralized approach, due to the output voltage inflexibility of the ac/dc converter. Both equal curtailment and maximum revenue have significantly higher capabilities to harvest more DG output power, with the difference of the injected DG power approaching 0.45 p.u. at 4:45 AM. The variances in the output power of the two proposed algorithms stem from their different objectives. In order to investigate this point, the system profile at 10:20 AM is studied as an example. At this instant, buses 6 and 9 at feeder #2 undergo overvoltage and bus 9 at feeder#4 undergoes undervoltage, without controlling the DG output powers.

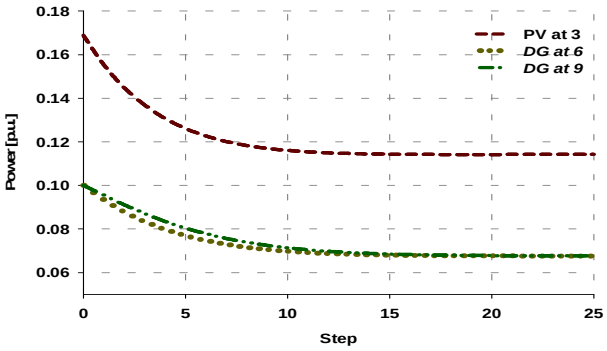

(a)

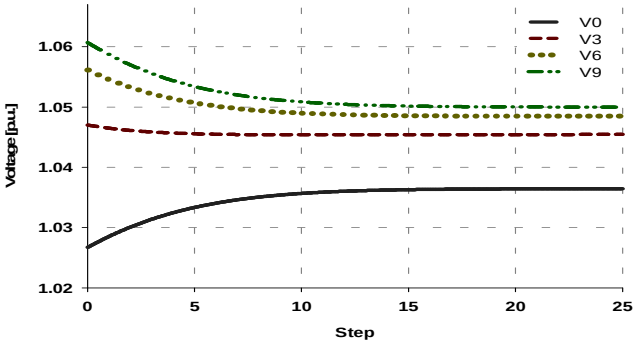

(b)

Figure 3.9: Four feeders test system Performance of the equal curtailment algorithm on radial system: (a) DG output power; and (b) DG voltage

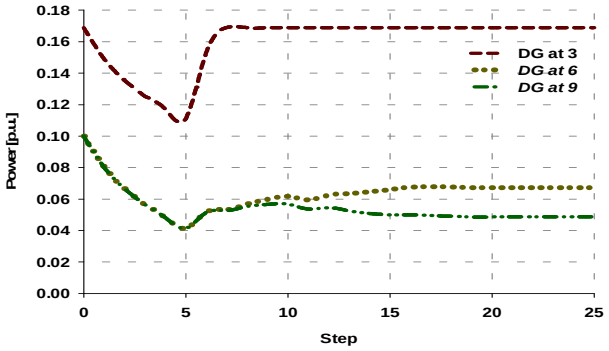

(a)

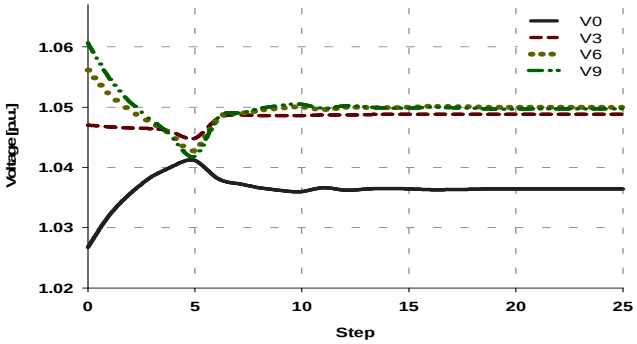

(b)

Figure 3.10: Four feeders test system Performance of the maximum revenue algorithm on radial system: (a) DG output power, and (b) DG voltage

Figure 3.9 and 3.10 illustrate DG output (power and voltage) during the activation of the equal curtailment and maximum revenue control schemes, respectively. The equal curtailment algorithm successfully regulates the system voltage and achieves the equal curtailment ratio among the DG units, regardless of their types and locations within 13 iterations. Similarly, the maximum revenue scheme confines the maximum voltage at the maximum permissible value (1.05 V) and achieves the global maximum revenue of the DG units within 17 iterations. In order to verify this claim, the output of the algorithm is compared with the solution offered by the general algebraic modeling system (GAMS®) software, as illustrated in Table 3.2. In the maximum revenue scheme, the dispatchable unit installed at bus 9 is subjected to higher power curtailment compared to the lower stream one because it is more sensitive to the maximum voltage nodes. In addition, since the PV unit is installed at a lower stream in the feeder and has higher revenue, it is not subjected to curtailment.

Table 3.2: Validation Results for Maximum Revenue Algorithm

Output	DLPDS	GAMS
DG at bus 3 (p.u.)	0.1689	0.1689
DG at bus 6 (p.u.)	0.0649	0.0643
DG at bus 9 (p.u.)	0.0487	0.0495
Total revenue ($/hr)	45.872	45.911

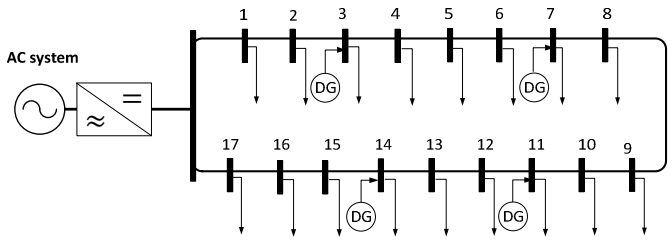

Figure 3.11: Meshed test system

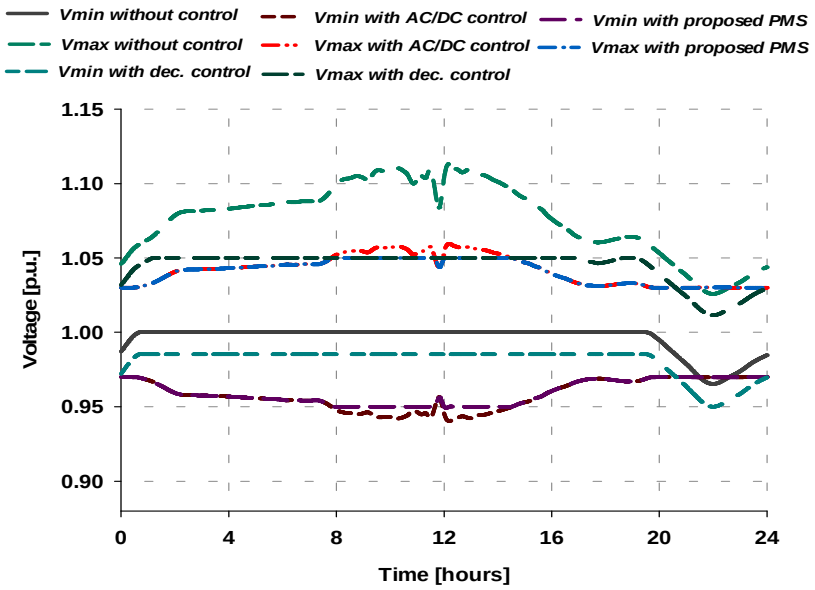

Figure 3.12: The system voltage profile according to different control schemes in the meshed test system

3.5.2 Meshed Test Network

In order to test the proposed algorithms in meshed networks, the 18-bus meshed DCDS illustrated in Figure 3.11 is considered in this study. The system loading is assumed residential, with a total loading of 0.9 p.u. For simplicity, the load distribution is considered uniform [25], [28]. Two dispatchable DG

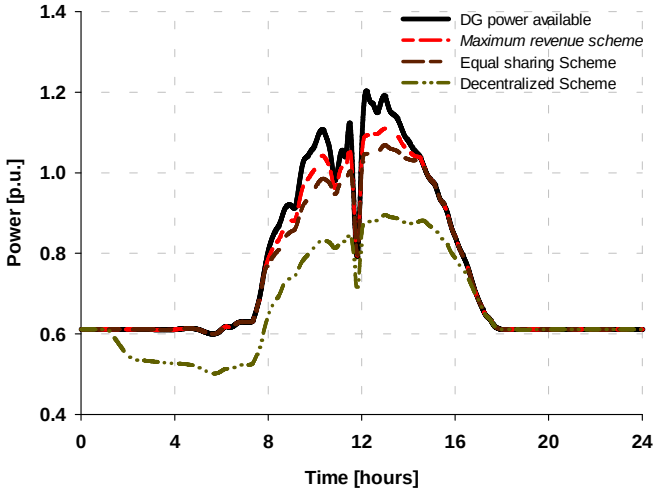

Figure 3.13: The total DG output power according to different control schemes in the meshed test system

units sized 0.2 and 0.4 p.u. are installed at buses 3 and 11, respectively. As well, two PV units sized 0.4 and 0.2 p.u. are installed at buses 7 and 14, respectively.

Similarly, the aforementioned four types of control schemes are applied in the test system. Figure 3.12 presents the minimum and maximum of the system voltage over 24 hours for the different control schemes. As shown in the figure, when the ac/dc converter output voltage is fixed and the active power curtailment is not allowed, the system maximum voltage undergoes high values (approaching 1.11 p.u.) beyond the permissible upper limit. When the ac/dc output voltage is controlled using the first stage of the proposed algorithm, the system maximum and minimum voltages appear in a symmetrical shape around the nominal system voltage (i.e., unity). The system voltage, however, still violates the permissible limits almost around noon. The implementation of either the proposed control strategies or the decentralized control scheme restricts the system voltage to its permissible limits all over the day. Only the proposed control schemes illustrate the coincidence of the maximum and minimum voltages at the same time in order to enable higher injection of the DG power. This is depicted in Figure 3.13, which presents the total power injection of the DG units under different control schemes – namely, decentralized, equal curtailment, and maximum revenue. Both proposed control algorithms outperform the decentralized approach in terms of the total power injection of the DG units. The figure shows that, in this case, the maximum revenue has a higher capability in injecting DG power than the equal curtailment scheme study.

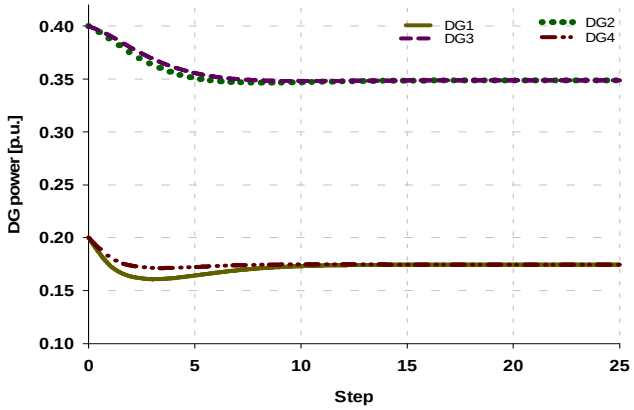

(a)

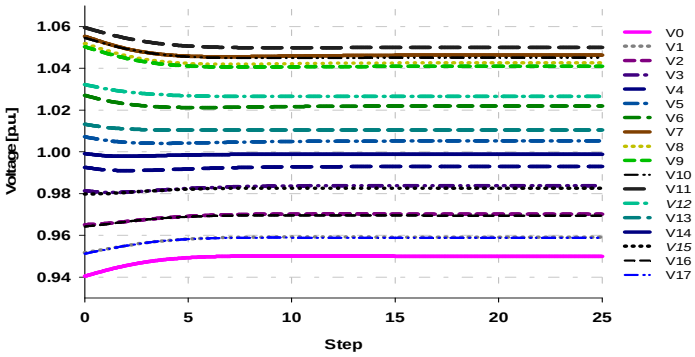

(b)

Figure 3.14: Performance of the equal curtailment algorithm on meshed test system: (a) DG output power, and (b) system voltage

In order to illustrate the performance of the equal curtailment and maximum revenue algorithms, the system states are observed at 12:10 PM. In this instant, the PV output=100% and the loading ratio=40%. This will lead to violations in the voltage constraints, as demonstrated previously in Figure 3.12. The activation of the equal curtailment and the maximum revenue schemes is illustrated in Figure 3.14 and 3.15, respectively. Both algorithms successfully regulate the system voltage and achieve the control objectives within 12 and 20 steps for the equal curtailment and the maximum revenue schemes, respectively. Unlike the equal curtailment scheme, a higher curtailment ratio is applied at the dispatchable DG unit at node 11 rather than the application of the same curtailment ratio over all DG units. Since the aforementioned DG has higher sensitivity to the maximum voltage at nodes 7 and 11. At the same time, the dispatchable DG unit presents less net revenue compared

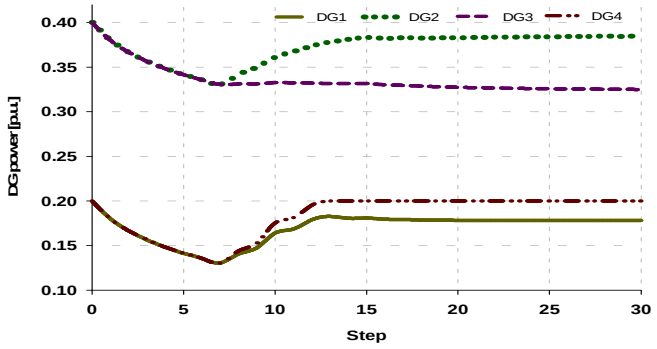

(a)

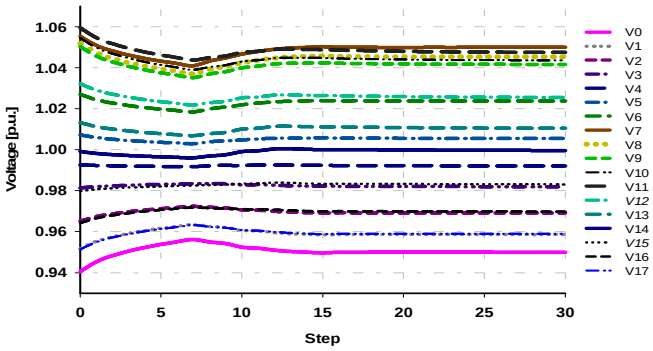

(b)

Figure 3.15: Performance of the maximum revenue algorithm on meshed test system: (a) DG output power, and (b) system voltage

with the PV installed at node 7. In addition, the voltage at node 11 is more sensitive to the change in the output power of the dispatchable unit installed at the same bus, compared to the one installed at node 3.

3.6 Discussion

This chapter has proposed a distributed multi-agent control scheme to mitigate the problem of voltage regulation in future dc distribution systems. The proposed scheme consists of two main stages. In the first stage, a distributed state estimation algorithm is implemented to provide the ac/dc converter with the required information for the voltage profile in the downstream dc network to make an appropriate decision. The second stage is a complementary stage activated when the ac/dc converter fails to individually provide appropriate voltage regulation. Two control strategies have been developed in

this work to determine the contribution of the different DG units in mitigating the problem of voltage regulation in the second stage. Several case studies for various topologies of dc networks were performed to test the effectiveness, robustness and convergence characteristics of the proposed multi-agent control scheme. The simulation results demonstrated that the control scheme proposed has appropriate convergence characteristics and are efficient in mitigating the problem of voltage regulation in dc distribution networks.

Chapter 4
Multi-Agent Supervisory Control for Power Management in DC Microgrids

4.1 Introduction

In chapter 3, different distributed power management schemes were proposed to manage the DG output power in dc microgrids operating in connected mode. Although the DG units could inject their maximum output power, since the main grid manipulates any difference between the microgrid generation and load, the high penetration of DG resources may deteriorate the system voltage profile due to its coupling with DG active powers. In islanded mode of operation, DG units are the main source of electrical power, since there in no main substain, and thus play more vital role within the dc microgrid. In addition to supplying the system loads, DG units are responsible for forming the network voltage. Therefore, an adequate power management scheme should be implemented for DG units in order to efficiently meet the load demands while maintaining an appropriate voltage profile.

In general, output DG power and voltage could be handled through equal power sharing algorithms which suit isolated microgrids dominated by renewable sources [34], [36], [67]. The main advantages of this approach are increasing life time of DG inverters, system adequacy and security. Based on the V/I droop characteristics, different DG units can operate to achieve power sharing. However, the presence of high resistance in the network links degrades sharing accuracy. Increasing the DG droop gain is one solution that overcomes such high resistance, yet it affects system stability margins and leads to high voltage deviations [26], [68]. On the other hand, economic performance is another important aspect of a successful isolated microgrid dominated by dispatchable nonrenewable sources. In that context, economic dispatch algorithms should be applied to optimize the total operating cost of DG units with different running costs and capacities [69], [70].

In this chapter, hierarchy control for dc microgrids is proposed to provide cooperative objectives within an isolated dc microgrid. The primary DG controller is the common V/I droop, which operates as an initial step toward maintaining a balance between the generation and loads. The proposed supervisory control is based on multi-agent algorithms that adapt the DG no-load voltage setting for

the achievement of either precise power sharing via a proposed distributed equal power sharing (DEPS) algorithm or economic dispatch via a proposed distributed equal incremental cost (DEIC) algorithm. Both algorithms rely on average consensus among agents and offer the further benefit of the potential to restore the system voltage to its nominal setting.

The remainder of the chapter is organized as follows. Section 4.2 provides a brief overview of the dc microgrid control hierarchy. In section 4.3, steady state analysis and the stability of the supervisory control algorithms are addressed. Details of the proposed supervisory control algorithms (DEPS and DEIC) are explained in section 4.4. Section 4.5 describes the verification of the effectiveness of the proposed algorithms through real-time case study simulations, and section 4.6 presents the conclusions.

4.2 Control Hierarchy Overview

4.2.1 Primary Control

The primary DG controller is based on current droop control, as shown in Figure 4.1. The main advantage of this scheme is the ability to enhance current sharing without communication. The droop characteristic can be expressed as

$$v = v^* - r\,i \tag{4.1}$$

where $v^*, v, i,$ and r are the DG no-load voltage setting, DG output voltage and current, and droop gain, respectively. It is noteworthy that the I-V droop characteristic is employed under the assumption

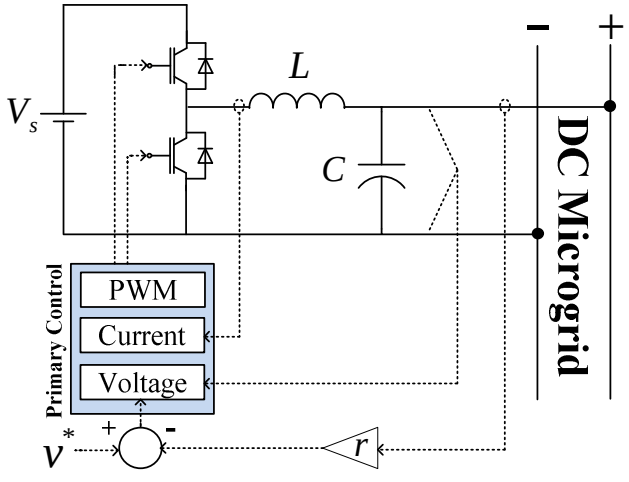

Figure 4.1: V/I droop control

of constant dc voltage node which is the input of the interfacing converter [71], [72]. This assumption can be realized through: 1) renewable DGs accompanied with energy storage units (Lead-Acid, Sodium, Zinc, Lithium-Ion, or Flow Battery), as assumed in [36]; and 2) dispatachable DGs. In the absence of system resistance, perfect sharing can be guaranteed. However, this is not the case in practical dc microgrids, in which feeder resistance is relatively high. The choice of different DG droop gains can compromise both perfect current sharing and system voltage regulation. Additional analyses of the choice of droop gain r for improving either sharing or the voltage profile are presented in [26], [34].

4.2.2 Supervisory Controller

The objectives of distributed supervisory control are to achieve precise equal power sharing (or economic dispatch) and to adjust the DG voltage levels for a variety of loading conditions by updating the no-load voltage of each DG. Without loss of generality, equal power sharing can be considered for equally rated DG units. For a system that includes N buses, the first N_g buses are assumed to be equipped with DG units, and the remaining buses, from $N_g + 1$ to N, are assigned for the system loads. The supervisory control should satisfy the power flow equations defined as

$$\begin{cases} p = v_j \sum_{k \in B} Y_{j,k}\, v_k \quad \forall \quad 1 \le j \le N_g \\ p_j = v_j \sum_{k \in B} Y_{j,k}\, v_k \quad \forall \quad N_g + 1 \le j \le N \end{cases} \tag{4.2}$$

$$mean\left(v_1 + \cdots + v_{N_g}\right) = v^{nom} \tag{4.3}$$

where p_j, v_j are the power and voltage at bus j, respectively; Y is the bus admittance matrix; B is a set of all the system buses; and v^{nom} is the nominal system voltage.

In (4.2), all DG power values are set as p in order to represent equal sharing. It should be noted that the set of equations defined by (4.2) cannot provide a unique solution due to the presence of $N + 1$ unknowns, i.e., $v_1, v_2, \ldots, v_N$ and p, and N equations. In other words, DG power sharing can take place at different DG voltage levels. Thus, (4.3) is introduced in order to provide a unique solution and to regulate the system voltage.

4.3 Steady-State Analyses

The following analyses relate the required change in the DG no-load voltage with the desired change in the DG output voltages and currents that achieve the supervisory control objectives. In addition, the stability of the supervisory control loop is investigated.

4.3.1 Droop Adjustment

The interaction between the DG output voltages and currents can be given by

$$V^* = V_g + RI_g \tag{4.4}$$

$$I = Y\,V \tag{4.5}$$

where V^*, V_g, and I_g are vectors of the DG no-load voltages, output voltages, and currents, respectively; R is a diagonal $N_g \times N_g$ matrix with element $R(j,j) = r_j$ (DGj droop gain); and I and V are vectors of the system currents and voltages at different buses, respectively.

This interaction can be represented in the following incremental form as a means of examining the system sensitivity:

$$\Delta V^* = \Delta V_g + R\,\Delta I_g \tag{4.6}$$

$$\Delta I = Y\,\Delta V \tag{4.7}$$

Eq. (4.7) can be written with partitioning system buses into DG buses and load buses as

$$\begin{bmatrix}\Delta I_g \\ \Delta I_l\end{bmatrix} = \begin{bmatrix}Y_{gg} & Y_{gl} \\ Y_{lg} & Y_{ll}\end{bmatrix}\begin{bmatrix}\Delta V_g \\ \Delta V_l\end{bmatrix} \tag{4.8}$$

where V_l , I_l are the vectors of load voltages and currents, respectively. Assuming no change in the load currents, i.e., $\Delta I_l = 0$, (4.8) can be rewritten as follows:

$$\Delta I_g = S\,\Delta V_g \tag{4.9}$$

with

$$S = Y_{gg} - Y_{gl}{Y_{ll}}^{-1}\,Y_{lg} \tag{4.10}$$

where S is a singular matrix of rank $N_g - 1$, since $\sum_g \Delta I_g = 0$, which makes the set of equations in (4.9) dependent. Hence, ΔV_g cannot be formulated as a function of ΔI_g. To convert (4.9) to an

independent set of equations, the average system voltage constraint, as defined by (4.3), should be incorporated into (4.9):

$$\begin{bmatrix}\Delta I_g \\ 0\end{bmatrix} = \begin{bmatrix} S \\ 1_{N_g}{}^T \end{bmatrix} \Delta V_g \tag{4.11}$$

where 1_{Ng} is a column vector of length N_g with all elements being ones. The objective of this constraint is to maintain a constant DG average voltage upon the reshaping of the DG output currents. The augmented matrix in (4.10) consists of $N_g + 1$ equations with one dependent equation, which can be eliminated by multiplying the average voltage constraint by a constant $\propto_i$ and adding the resultant row to i^{th} row of S, which then becomes

$$\Delta I_g = S_d \, \Delta V_g \tag{4.11}$$

$$S_d = S + \bar{\propto} \tag{4.12}$$

with

$$\bar{\propto} = (1_{Ng} \, [\propto_1 \quad \propto_2 \quad \cdots \quad \propto_N] \,)^T$$

where S_d is an $N_g \times N_g$ non-singular matrix. The ideal case for S_d is to be a diagonal matrix, resulting in decoupled agents. However, this cannot be realized in real networks. The off-diagonal elements of S_d can be minimized, via $\propto_i$, to reduce the DG coupling, as given by

$$\min_{\propto_i} \sum_{j \neq i} (S(i,j) + \propto_i)^2 \tag{4.13}$$

The solution of this minimization problem results is:

$$\propto_i = \frac{-\sum_{j \neq i} S(i,j)}{N_g - 1} = \frac{S(i,i)}{N_g - 1} \tag{4.14}$$

In the final step, the ΔV^* required for adjusting the DG output currents by ΔI_g^{req} without changing the average system voltage can be derived by substituting (4.11) in (4.6):

$$\Delta V^* = \left({S_d}^{-1} + R\right) \Delta I_g^{req} \tag{4.15}$$

It can be inferred from (4.15) that for a smaller system resistance (or relatively high droop gains), the updating of the DG no-load values ΔV^* is governed by the droop characteristic rather than by the system resistance values.

To restore the average system voltage by Δv^{req}, each DG no-load voltage v^* must be changed by the same value of Δv^{req}. Obtaining ΔV^* as a function of Δv^{req} by substituting (4.9) in (4.6) demonstrates the validity of this statement:

$$\Delta V^* = (E + R\,S)\Delta V_g = (E + R\,S)1_{N_g}\,\Delta v^{req} \tag{4.16}$$

where E is the identity matrix of size N_g, and $1_{N_g}\,\Delta v^{req}$ is the required change in DG output voltages ΔV_g. By definition, S is a symmetric matrix, with

$$\sum_j S(i,j) = 0 \quad \forall\, i \leq \quad N_g$$

Hence, (4.16) can be simplified as

$$\Delta V^* = 1_{N_g}\,\Delta v^{req} \tag{4.17}$$

The ΔV^* required for adjusting the DG output voltages and currents can then be formulated as

$$\Delta V^* = \left({S_d}^{-1} + R\right)\Delta I_g^{req} \;\; + 1_{N_g}\,\Delta v^{req} \tag{4.18}$$

Since each DG takes action locally, ΔV^* should be updated based on the diagonal elements of ${S_d}^{-1}$, as follows:

$$\Delta V^* = \theta S_I\,\Delta I_g^{req} \;\; + 1_{N_g}\,\Delta v^{req} \tag{4.19}$$

where $S_I = diag\left({S_d}^{-1}\right) + R$, and Θ is a design parameter. This relation is iteratively utilized for implementing the proposed distributed power management algorithms, as explained in section 2.3.

4.3.2 Stability of the Supervisor Control Loop

To address the stability of tracking any specific DG current reference, (4.19) can be restated for a supervisory control cycle (h), as

$$\Delta V^*(h) = \Theta S_I\,\left(I_g^{ref} - I_g(h-1)\right) + 1_{N_g}\left(v^{nom} - \frac{1}{N_g}{1_{N_g}}^T\,V_g(h-1)\right) \tag{4.20}$$

where I_g^{ref} is a vector of the DG reference currents that the DG units track to fulfil the control objective. Based on (4.16), the change in the DG voltages from iteration $(h-1)$ to iteration (h) after implementing $\Delta V^*(h)$ can be represented as

$$V_g(h) - V_g(h-1) \ = (E + R\ S)^{-1}\Delta V^*(h) \tag{4.21}$$

Substituting from (4.9) and (4.20) into (4.21) and rearranging the terms of the equation yields

$$V_g(h) = A\, V_g(h-1) + B\, I_g^{req} \ + C\, v^{nom} \tag{4.22}$$

with

$$A = E - (E + R\ S)^{-1}\left(\theta S_I S + \frac{1}{N_g}\, e\right)$$

$$B = \ \theta(E + R\ S)^{-1} S_I$$

$$C = (E + R\ S)^{-1} 1_{N_g}$$

where e is a $N_g \times N_g$ matrix with all elements equal to one.

Eq. (4.22) represents a multi-input multi-output (MIMO) digital system. A condition necessary for ensuring the stability of the supervisory MIMO system is that all eigenvalues of the matrix (A) be inside the unit circle. To fulfill this condition, Θ can be chosen such that

$$0 < \Theta < \Theta_c = \ \min_j \left(\frac{2\ \mathrm{Re}\{\sigma_j\}}{{\sigma_j}^2}\right)$$

where σ_j is the j^{th} nonzero eigenvalue of the matrix $((E + R\ S)^{-1} S_I S)$. In general, dc loads in distribution systems can be modelled as constant resistance, constant current, constant power loads (CPL), or any mix of these three types [73]. The proposed algorithms neglect the changes in the load currents Δi_l with respect to the changes in the DG currents Δi_g under the same change in the system voltage Δv, as given by (4.9). The current disturbance, i.e., Δi_l , is around 5% of Δi_g under the same change Δv, as illustrated in Appendix B. This assumption does not limit the application of the proposed algorithms in case of CPL and constant resistance loads; since the proposed algorithms implement integral actions, governed by (4.20) and (4.21), that are always triggered until achieving the control objectives while rejecting the current disturbances.

4.4 Proposed Multi-agent Supervisory Control Algorithms

The proposed supervisory algorithms have been defined based on a distributed control approach: DG units are considered as control agents that exchange information iteratively. As illustrated in Figure 4.2, the proposed multi-agent supervisory algorithm consists of three stages: I) DG data exchange, II)

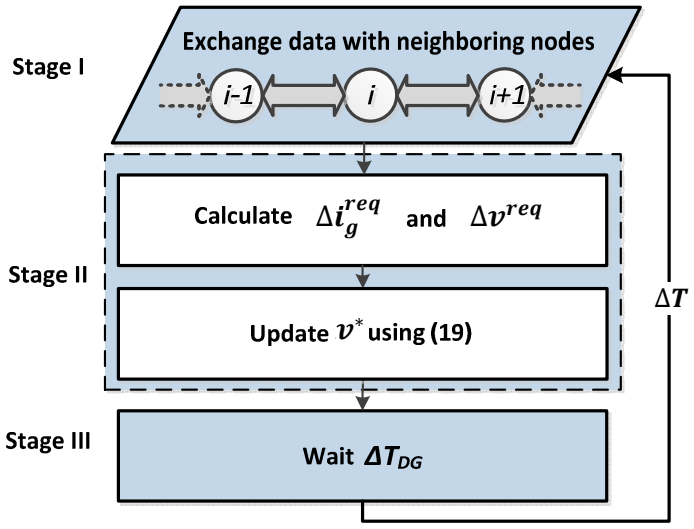

Figure 4.2: Supervisory control cycle

DG no-load voltage update, and III) waiting for the DG voltage settlement. In first stage, the proposed supervisory control relies on average consensus algorithms, as stated in section 2.3, wherein all DG units share the average values they have estimated for a specific variable. Accordingly, each DG could locally adapt its no-load voltage v^* in order to achieve either equal power sharing via the DEPS algorithm or economic dispatch via DEIC. These two power management algorithms are described in details hereunder. Finally, DG units must halt for a waiting time ΔT_{DG} that is essential for reaching steady state operating points, thereby avoiding data exchange during transients, which may lead to inappropriate decisions. ΔT_{DG} should be greater than the settling time of the DG primary control, which can be calculated based on DG transfer function analyses.

4.4.1 Proposed DEPS Algorithm

To operate in an equal power sharing mode, each agent must share a set of variables μ, Γ, and Ψ with its neighbors. The initial value of each parameter is defined as follows:

$$\begin{cases} \varkappa_u[0] = p_u \\ \Gamma_u[0] = p_u^r \\ \Psi_u[0] = v_u \end{cases} \tag{4.23}$$

where p_u, p_u^r, and v_u are the output and rated powers, and the voltage of DG_u, respectively.

These initial values are shared between neighboring agents and then updated based on (2.2) as illustrated earlier in section 2.3.2. The DG required power p_u^{req} can be estimated as

$$p_u^{req} = \lim_{k\to\infty} \frac{\varkappa_u[k]}{\Gamma_u[k]} \; \Gamma_u[0] \; = \frac{\sum_{t=1}^{N_g} p_t}{\sum_{t=1}^{N_g} p_t^r} \tag{4.24}$$

and the average system voltage v^{sys} can also be estimated as

$$v^{sys} = \lim_{k\to\infty} \Psi_u[k] = \frac{\sum_{t=1}^{N_g} v_t}{N_g} \tag{4.25}$$

The changes in the DG output current and voltage required for an effective solution of (4.24) and for restoring the average system voltage can be calculated by

$$\Delta i_u^{req} = \frac{\Delta\, p_u^{req}}{v_u + \Delta v^{req}} \tag{4.26}$$

$$\Delta v^{req} = v^{nom} - v^{sys} \tag{4.27}$$

where $\Delta\, p_u^{req} = p_u^{req} - p_u$.

The last step in implementing these changes ,i.e., Δi_u^{req} and Δv^{req},. to update the DG no-load voltages by substituting into (4.19).

It is noteworthy that the purpose of (4.27) is to minimize the sum of squared voltage deviations around the nominal value, i.e., $min_{\Delta v^{req}} \sum_u (v_u + v^{req} - v^{nom})^2$, which is the typical voltage regulation objective in ac distribution networks [25]. In order to consider the system upper and lower voltage bounds ($v_{per}^{min}, v_{per}^{max}$), additional variables (v^{min}, v^{max}) should be defined at each agent to represent the global upper and lower voltages of the system. Initially each agent could estimate those variables based on its measurement and then updated their values during the data exchange with its neighbors as discussed in [33]. Finally, Δv^{req} that considers the system upper and lower voltage limits can be given as

$$\Delta v^{req} = \begin{cases} v_{per}^{max} - v^{max} \;\; if \;\; v^{upp} + v^{nom} - v^{sys} > v_{per}^{max} \\ v_{per}^{min} - v^{min} \;\; if \;\; v^{low} + v^{nom} - v^{sys} < v_{per}^{min} \\ v^{nom} - v^{sys} \qquad\qquad\qquad\qquad otherwise \end{cases} \tag{4.28}$$

On the other hand, the proposed algorithm is flexible, i.e., can regulate the system voltage at its lower, nominal, and upper voltage levels according to the operator preference. For instance, v^{nom} in (4.27) can be replaced by the v_{per}^{min} or v_{per}^{max} to regulate the system voltage at its lower or upper bounds, respectively. When regulating the system voltage at the upper voltage bound, the system

losses and operational cost will be slightly decreased. However, this approach will reduce the system security because the system may violate the standard upper voltage bound with a sudden load reduction. Therefore, it may lead to faster equipment aging due to the higher electrical stress [74]. Such approach is avoided in the presented work.

4.4.2 Proposed DEIC Algorithm

The typical economic dispatch problem can be defined as

$$min \sum_{u \in G} OC_u(p_u) \tag{4.29a}$$

subject to the following:

A generation and loading equality constraint:

$$\sum_{u \in G} p_u = \sum_{d \in L} p_d + P_{loss} \tag{4.29b}$$

A DG minimum and maximum output power constraint:

$$p_u^{min} \leq p_u \leq p_u^{max} \ \forall\, u \in G \tag{4.29c}$$

where G and L are the sets of DG and load buses, respectively. OC_u, p_u^{min}, and p_u^{max} are DG_u operating cost, and DG_u minimum and maximum power limits, respectively. P_{loss} is the total system losses.

The DG operating costs are assumed to be quadratic, as is the common practice reported in the literature. The incremental cost thus becomes a linear function:

$$OC_u(p_u) = a_u + b_u P_u + c_u {P_u}^2 \tag{4.30}$$

$$\lambda_u = b_u + 2\, c_u\, P_u \tag{4.31}$$

where λ_u is the incremental cost for DG_u. It is noteworthy that when system losses are included in the economic dispatch, the formulation turns into an analytically intractable problem even with simplified representation for the generator cost functions[75], [76]. Without considering the system loss, problem (4.29) would be a well-known economic dispatch problem [77]. Since it becomes a quadratic convex problem, it has a unique optimal solution that satisfies the following relation:

$$\begin{cases} \lambda_u = \lambda^* & if \quad p_u^{min} < p_u < p_u^{max} \\ \lambda_u \geq \lambda^* & if \quad p_u = p_u^{min} \\ \lambda_u \leq \lambda^* & if \quad p_u = p_u^{max} \end{cases} \tag{4.32}$$

where λ^* is the optimal incremental cost for DG units that are not operating at their limit.

On the other hand, the implementation of droop characteristics implies that all DG units share the total system load and losses so that (4.29b) is always satisfied. The power limit constraint, as defined by (4.29c), is also guaranteed by the DG current control. Eq. (4.32) can be interpreted as a sufficient condition for a group of DG units to operate with optimal operating costs. In other words, by obtaining the average incremental cost (λ_{avg}) of all of the DG units that are not working at their limit, each DG can change its output power so that it operates at an incremental cost close to λ_{avg}.

As with DEPS, DEIC must produce an average consensus of a set of variables μ, Γ,and Ψ, which are defined initially as follows:

$$\varkappa_u[0] = \begin{cases} \lambda_u & if \quad u \in \rho \\ 0 & otherwise \end{cases} \tag{4.33a}$$

$$\Gamma_u[0] = \begin{cases} 1 & if \quad u \in \rho \\ 0 & otherwise \end{cases} \tag{4.33b}$$

$$\Psi_u[0] = v_u \tag{4.33c}$$

where ρ is a set of DG units that operate within their power limits; i.e., $DG_u \in \rho$ if $p_u^{min} < p_u < p_u^{max}$. The above initial $\varkappa, \Gamma,$ and Ψ values are updated based on (2.2). After sufficient iterations, the average incremental cost can be obtained:

$$\lambda_{avg} = \lim_{k \to \infty} \frac{\varkappa_u[k]}{\Gamma_u[k]} = \frac{\sum_{t \in \rho} \lambda_t}{|\rho|} \tag{4.34}$$

The average system voltage v^{sys} can be estimated using (4.25), as in the proposed DEPS algorithm. Based on (4.34), each agent can determine the appropriate change in its output power so that it approaches the desired λ_{avg}, as follows:

$$\Delta p_u^{req} = \frac{(\lambda_{avg} - \lambda_u)}{2\, c_{max}} \tag{4.35}$$

where c_{max} is a common constant for all DG units that satisfies

$$\frac{N_g}{N_g - 1} c_{max} \geq c_1, c_1, \ldots, c_{N_g} \tag{4.36}$$

This condition guarantees that all DG units converge to an optimal solution. The proof of this claim is provided in Appendix C. In the work presented in this work, c_{max} is chosen to be the largest DG quadratic coefficient of all of the OC functions. The changes in DG output currents and voltages required for guaranteeing equal incremental cost operation and for restoring the average system voltage can then be determined using (4.26) and (4.27). These changes can be realized through appropriate adjustments to all DG no-load voltages, using (4.19).

4.5 Real-Time Simulations

4.5.1 Load Variation

Real-time simulations were performed in order to demonstrate the effectiveness of the proposed consensus algorithms. A dc microgrid was modeled in an RT-LAB® simulator using a SimPowerSystems® blockset and an ARTEMiS® plug-in from OPAL-RT. The RT-LAB simulator provides parallel computation that permits the distribution of large and complex models over several processors for performing powerful computations with a high degree of accuracy and with low-cost real-time execution. The RT-LAB simulator was used to perform two main functions, the first of which is rapid control prototyping (RCP) realization, in which the proposed supervisory control is implemented to mimic actual DG supervisory controllers. RCP controllers are more flexible, easier to debug, and faster to implement than actual DG controllers. The second function is hardware-in-the-loop (HIL) realization, in which the proposed supervisory controllers, implemented as RCP, are connected to a virtual dc microgrid executed in real time.

The primary advantage of the HIL realization is the validation of the proposed algorithms as prototype controllers, an essential stage prior to practical implementation. Figure 4.3 shows the dc microgrid test system (with the hierarchy control), which mimics a typical dc shipboard system [7]. Table 4.1 lists the DG ratings [60] with the network link parameters illustrated in Table 4.2. As shown in Figure 4.3, the RT-LAB simulator consists of two processors (targets), each having 12 3.33 GHz cores dedicated to parallel computation. To achieve HIL realization, the network, DG converters, and DG primary controllers are implemented in target #1, using 5 cores, while the DG secondary controllers are implemented in Target # 2, using 4 cores that act as RCP controllers. The

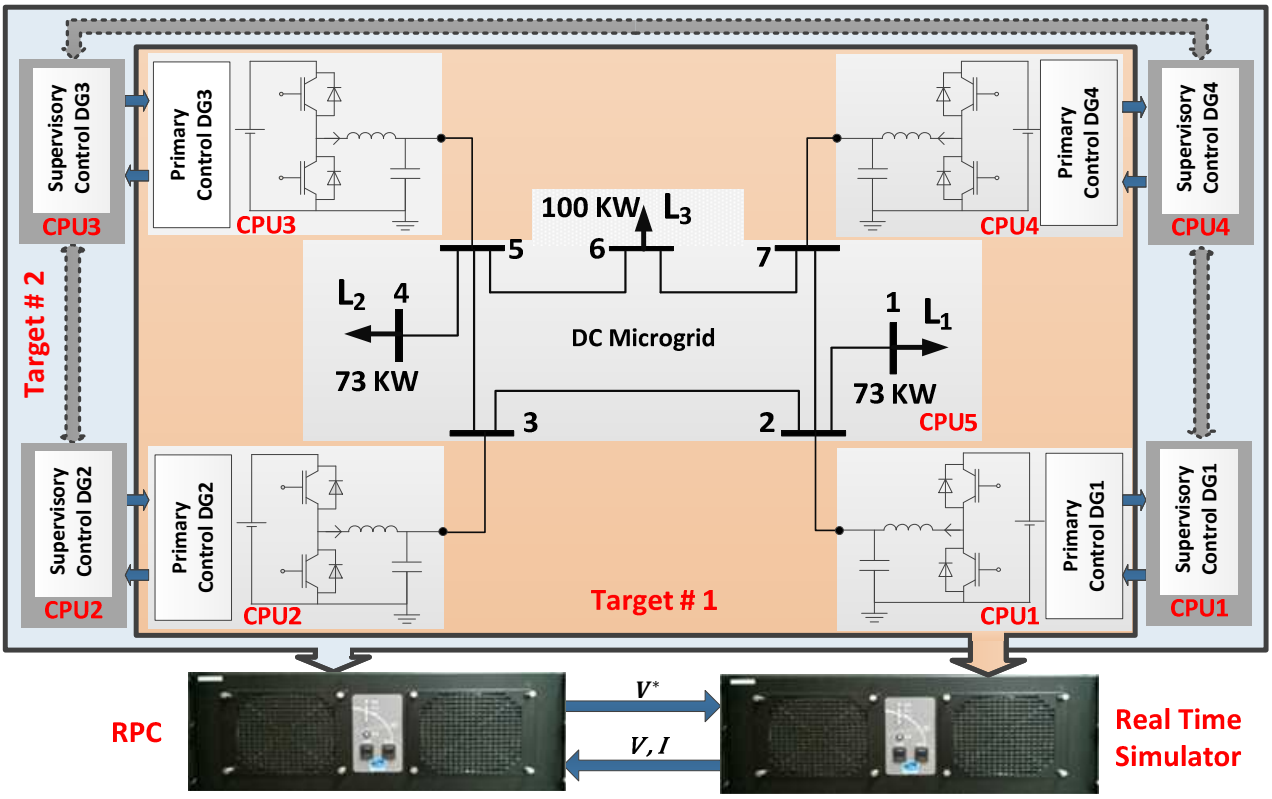

Figure 4.3: Schematic diagram for the test system implemented in the RTS system

interfacing between the targets is handled through fast I/O board. Each target has 32-analog and 64-digital I/O channels to exchange data in real time. The targets are equipped with Red Hat LINUX operating system and controlled via a Windows-based host PC using a TCP/IP connection. The developed MATLAB/Simulink models, for the virtual network and the supervisory controllers, are processed using RT-LAB interfacing software, runs on the host PC. This process consists of distributing the model subsystems between the target processors. Then, the models are compiled to a C-code generation uploaded on the target hardware to be run in real time. The proposed supervisory controllers read the DG output voltages and currents in order to generate the DG no-load voltages that are utilized by the DG primary controllers. For more details about RT-LAB and HIL applications, readers can refer to[78]–[80].

Based on the analysis provided in section 4.3, Θ must be less than 1.65 for supervisory control stability to be maintained. In this study, Θ is selected to be 0.6 such that all eigenvalues lie on the positive real side of the unit circle (i.e., $\sigma = [0, 0.54, 0.36, 0.27]^T$), which leads to an overdamped performance. The zero eigenvalue is affiliated with the system voltage restoration and is unaffected

Table 4.1: DG data

DG	Bus	a_u	b_u	c_u	p_u^r (kW)	Droop (Ω)
DG_1	2	4.0797	0.0792	0.0005	100	0.08
DG_2	3	0.8505	0.0689	0.0009	80	0.10
DG_3	5	2.0249	0.0301	0.0011	100	0.08
DG_4	7	3.5442	0.1189	0.0003	100	0.08

Table 4.2: System line parameters

From	To	R (Ω)	L (mH)
1	2	0.02	0.045
2	3	0.1	0.23
4	5	0.02	0.045
3	5	0.2	0.45
5	6	0.05	0.11
6	7	0.05	0.11
7	2	0.2	0.45

by Θ. This zero eigenvalue represents a deadbeat voltage restoration, since all of the DG units require one supervisory cycle in order to restore the average system voltage. In this work, the waiting time ΔT_{DG} is considered to be 250 ms, the data exchange cycle is considered to be 10 ms [81], and the total update time ΔT of the supervisory control cycle is considered to be 500 ms.

4.5.2 Load Variation

The initial DG no-load voltages are arbitrarily assigned for DG1, DG2, DG3, and DG4 as 413, 400, 407, and 400, respectively. Figure 4.4 illustrates the DG output powers and voltages for a variety of loading conditions when the DEPS is activated. At the beginning of the test, conventional droop-based control can neither provide accurate power sharing nor regulate the average system voltage. When the DEPS algorithm is activated at t = 5 s, all agents start implementing Stage (I) by exchanging information, reaching the average consensus about the control variables, i.e., μ, Γ, and Ψ. Then, the no-load voltages of the DG units are updated according to (4.19), i.e. Stage II. Lastly, the DG units apply the solution obtained from Stage (II) and wait for ΔT_{DG} to complete a supervisory

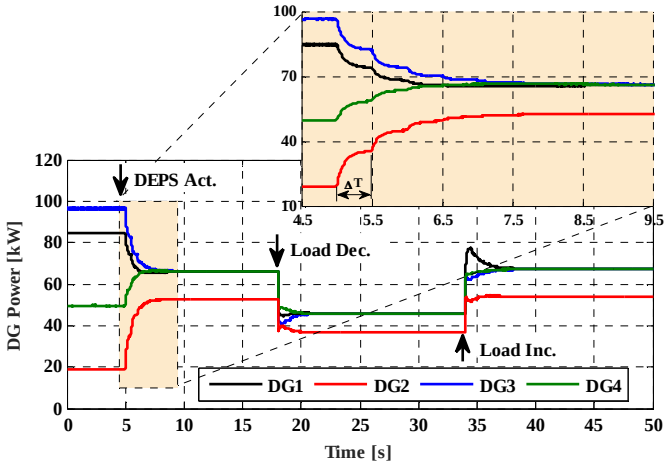

(a)

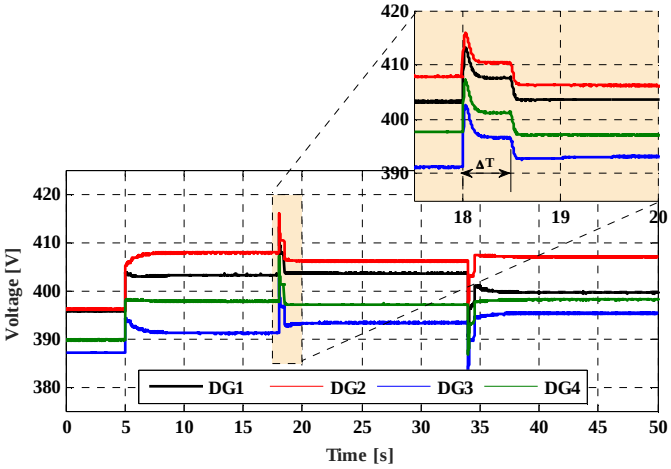

(b)

Figure 4.4: Performance of the DEPS algorithm: (a) DG output power; (b) DG output voltage

control cycle. During ΔT the system maintains its stability because the DG units still implement droop characteristic. Without the integrating the droop characteristics into the proposed supervisory controllers, the system need fast communication, i.e. high bandwidth, to ensure balanced load and generation. Approximately four supervisory control cycles are required such that all DG units can share the total load equally according to their ratings (i.e., 66.2 % for each DG). The DEPS algorithm is also able to restore the average system voltage to its nominal value of 400 V within one supervisory control cycle, see zoomed portion of Figure 4.4 (b). This performance is consistent with the deadbeat voltage response derived in section 4.3. After, restoring the average system voltage, the DG voltages

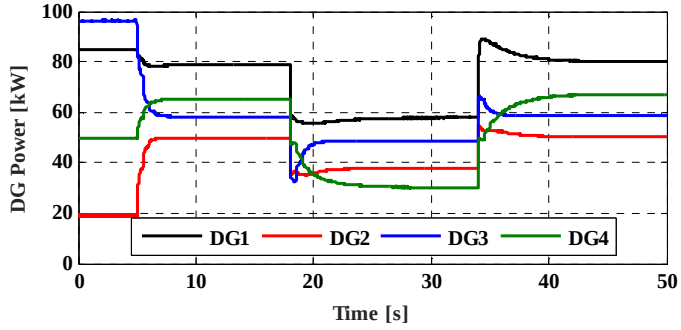

(a)

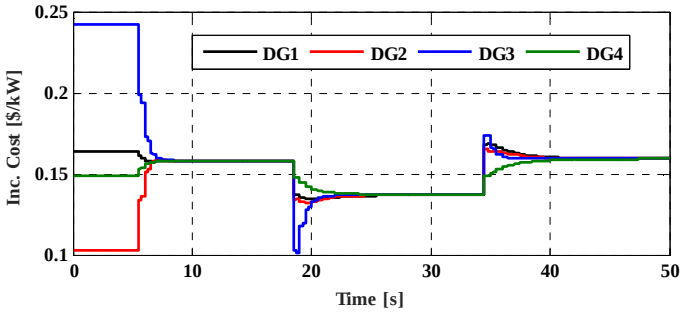

(b)

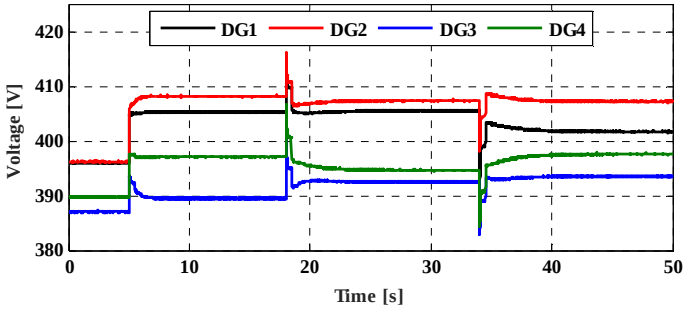

(c)

Figure 4.5: Performance of the DEIC algorithm: (a) DG output power; (b) incremental cost; (c) DG output voltage

are exponentially adapted to achieve the equal power sharing objective. This overdamped performance is guaranteed by the proper selection of θ.

To test the efficiency of the DEPS algorithm under loading variability, a load decrease and a subsequent load increase are introduced at t =18 s and t=34 s, respectively. First, the load decrease is applied by reducing the loads at buses 1, 4, and 6 by 30 kW, 30 kW, and 15 kW, respectively, i.e., a 30 % load reduction. DEPS drives the DG units to operate at equal power sharing and eliminates the increase in the average system voltage. The load increase is then applied by boosting the loads at

buses 1 and 6 by 50 kW and 30 kW, respectively. The DG1 output power has the greatest observable step change, at the beginning of the load increase, because it is adjacent to bus 1, which has the greatest load change. This case is considered dramatic for conventional droop control because it may result in highly unequal power sharing. However, the imprecise power sharing and the reduction in the average system voltage are mitigated by the DEPS algorithm. These results validate the robustness of the DEPS algorithm with respect to its ability to provide equal power sharing and to restore the average system voltage for a variety of loading conditions. DEPS also exhibits an overdamped performance, achievable by Θ, which is essential for avoiding overloading.

DEIC was tested by applying the same load variability employed in the DEPS validation. Figure 4.5 illustrates the DG output powers, incremental costs, and output voltages. In the initial stage of the test, conventional droop control results in uneconomic power dispatch accompanied by a deviation in the average system voltage. DEIC asymptotically drives the DG units to operate at equal incremental costs. The asymptotic convergence is governed by $C_{\max}$, which is considered to be 0.0011. The average system voltage is also maintained at its nominal value in all cases.

4.5.3 Response to High Resistive Network

In case of high resistive network, the power sharing accuracy becomes worse with higher voltage deviations [34]. In order to illustrate the robustness of the proposed algorithms under high resistive networks, the resistance and inductance of the network links are doubled. The system is tested for DEPS and DEIC algorithms under same loading level as stated in the subsection A. Figure 4.6 (a) and (c) verify the capability of the algorithms to attain equal power and equal incremental cost objectives, respectively. Figure 4.6 (b) and (d) illustrate that the average system voltage was restored around the nominal voltage, for both algorithms, but with higher diversity in the voltage profile compared with the previous case, which is an expected result due to the increase in the network link resistance.

4.5.4 Comparison with a Different Communication Architecture

In this subsection, the proposed DEPS is compared with the current sharing algorithm that is proposed in [14] and relies on common communication bus topology. Figure 4.7 (a) and (b) show the performance of the current sharing algorithm with 60 ms delay in the communication bus. Although the algorithm can successfully drive the DG units to share the load current, instability problem appears in the system voltage due to the communication time delay. Such a result matches the finding of the authors of [36]. In contrast, the proposed DEPS does not show such instability with the

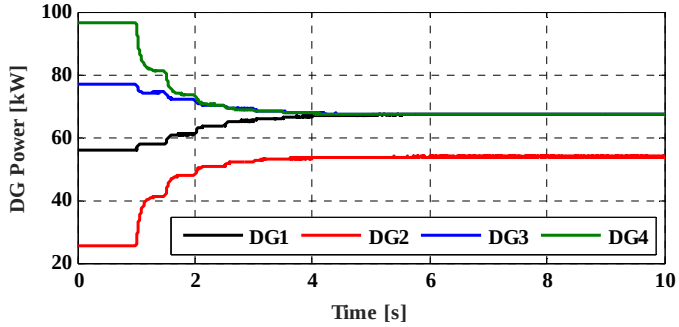

(a)

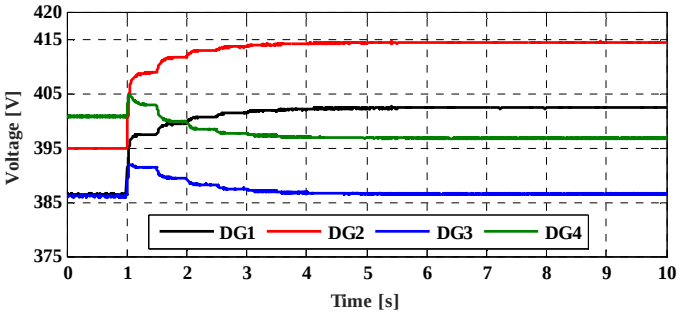

(b)

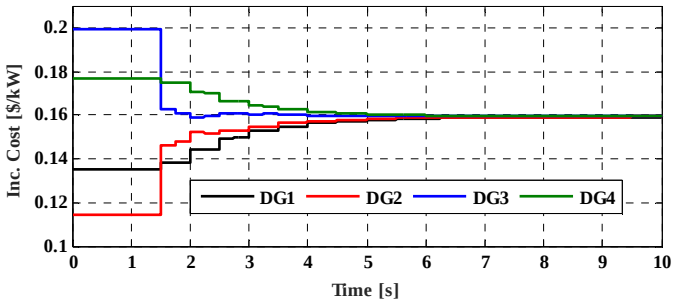

(c)

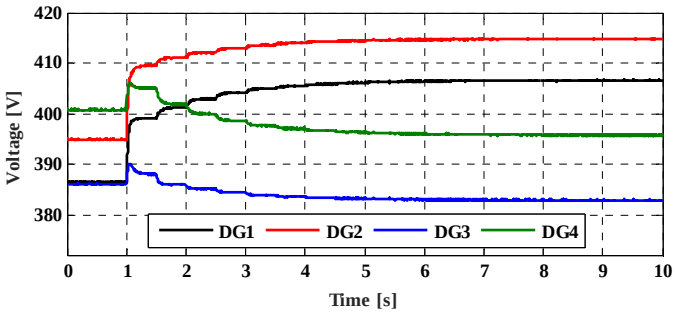

(d)

Figure 4.6: Algorithm performance in the case of high resistive network: (a)DG powers using DEPS (b)DG voltages using DEPS, (c) DG incremental costs using DEIC, (d) DG voltages using DEIC

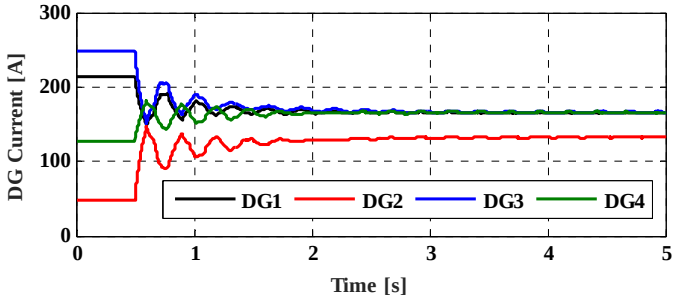

(a)

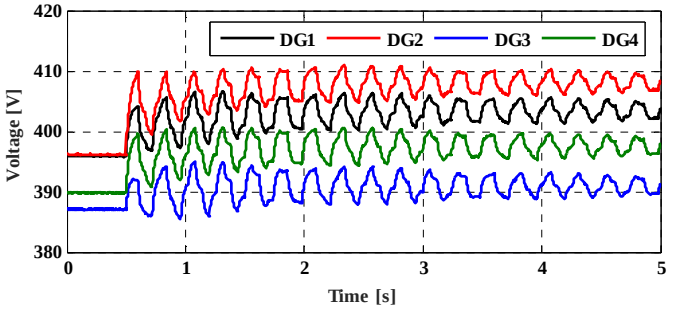

(b)

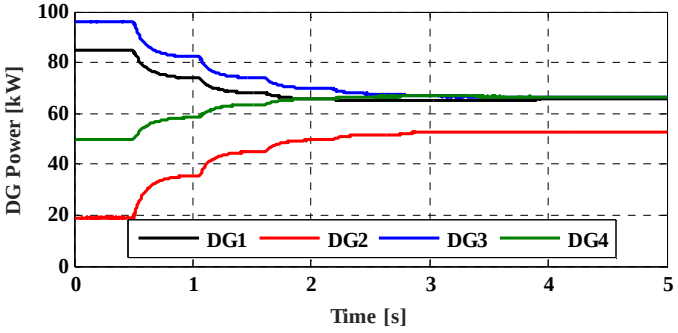

(c)

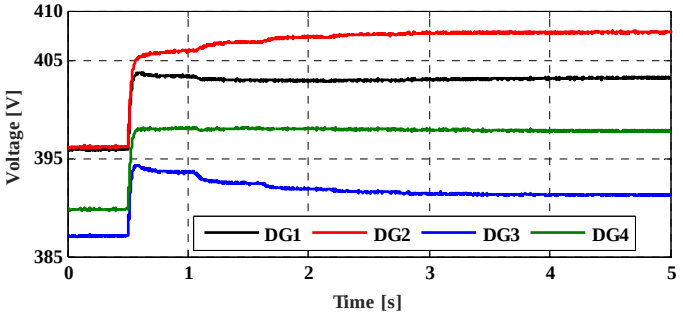

(d)

Figure 4.7: Performance with additional comm. delay: (a)DG output current using algorithm in [36]; (b)DG output voltage using algorithm in [36]; (c) DG output power using DEPS; (d)DG output voltage using DEPS

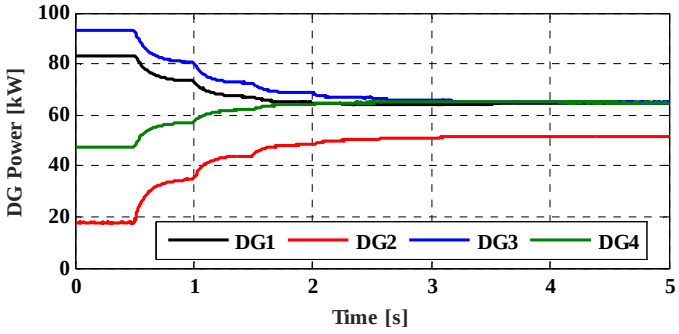

(a)

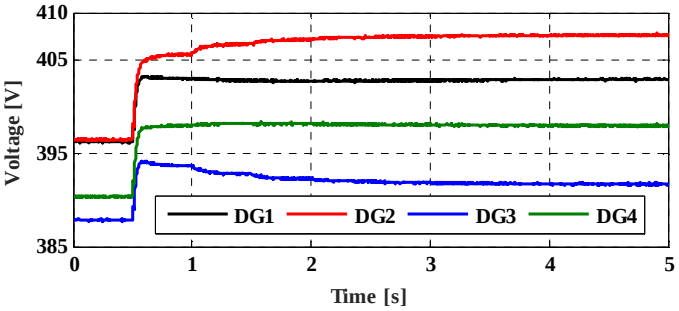

(b)

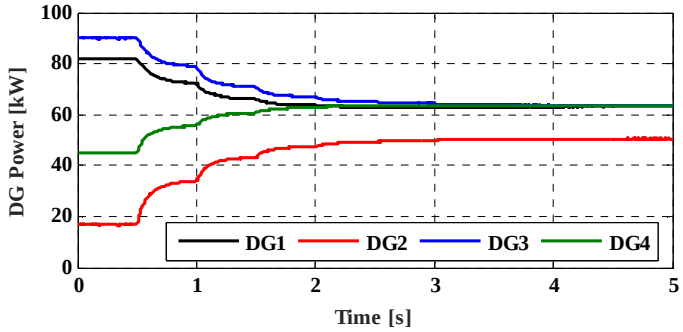

(c)

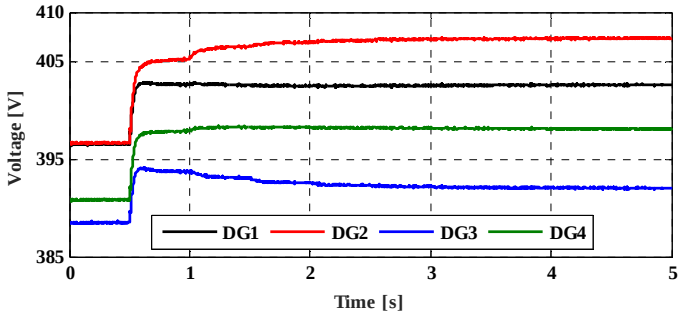

(d)

Figure 4.8: DEPS algorithm with different load types: (a)DG output power for constant current loads; (b)DG output voltage for constant current loads; c)DG output power for constant resistance loads; (b)DG output voltage for constant resistance loads

addition of the same 60 ms attributed to the communication delay as illustrated in Figure 4.7 (c) and (d). The communication time delay postpones the convergence of the DEPS without affecting the control objectives

4.5.5 Response to Different Load Types

In order to investigate the performance of the proposed DEPS under different loading conditions, the CPL loads, illustrated in Figure 4.3, are replaced by different load types with equivalent ratings. Figure 4.8 demonstrates the performance of the proposed DEPS under constant current and constant resistance loads. The proposed algorithm can result in equal power sharing and can restore the system voltage under different types of loads. These results confirm the effectiveness of the proposed algorithm in dealing with all types of load due to the integral actions governed by (4.20) and (4.21). Similar results are expected to be produced when the proposed DEIC is applied for different types of loads, because it depends on (4.20) and (4.21) as well.

4.6 Discussion

In this chapter, two supervisory control algorithms have been proposed for accurate power management in isolated dc microgrids. The proposed algorithms apply the average consensus theory to stimulate the DG units to exchange and thus update their information synchronously. The DG no-load voltages are adapted to provide equal power sharing and minimal operating costs. The proposed algorithms are also incorporated with DG droop-based primary controllers so that power balance is guaranteed, and assigning agents for the loads is unnecessary, an advantage that significantly reduces the number of agents required for achieving power management objectives. Supervisory control stability and incremental cost convergence have been proven mathematically. Real-time simulations using OPAL-RT have validated the practical implementation of the proposed algorithms in an HIL application. The results show that both algorithms provide precisely equal power sharing and minimal operating costs for a variety of loading conditions. The average system voltage is also maintained at its nominal value, an additional benefit of implementing the proposed algorithms. The simplicity of the new algorithms and the minimal associated implementation and communication requirements constitute key positive features that will facilitate practical implementation.

Chapter 5
A Sequential Power Flow Algorithm for Islanded Hybrid AC/DC Microgrids

5.1 Introduction

Chapters 3 and 4 address the power management schemes and main challenges that may arise in operating the dc microgrids as single entity in either islanded or grid-connected modes. However, in addition to these operational scenarios, the evolving dc network will most probably get integrated with the traditional ac network through ICs, accordingly forming a new hybrid distribution paradigm. If this hybrid ac/dc microgrid operates in grid connected mode, the operation of dc microgrids will be the same as the one addressed in chapter 3. If the connection with the main substation is lost, the hybrid distribution system forms an islanded microgrid that can partially or totally supply the local loads in the ac and dc subgrids. For higher system security, such islanded microgrids are characterized by droop control schemes that enable overall load sharing among the installed DGs [32]. For the ac subgrid, the frequency and voltage are adapted to govern the output active and reactive powers, respectively. Similarly in the dc subgrid, the output power is controlled by adjusting the DG voltage. To maintain a power balance between the ac and dc subgrids, the interlinking converter adopts an operational criterion that relates the ac frequency to the dc voltage [46]–[48].The accurate behavior of such sophisticated control scheme could be revealed through an appropriate power flow formulation takes into consideration: 1) the absence of a slack bus, 2) the frequency variation in the ac subgrid, and 3) the correlation between the frequency and dc voltage [82].

Accordingly, this chapter proposes a power flow for hybrid ac/dc microgrids operating in the islanded mode. The proposed algorithm adopts Newton-Raphson (NR) method to sequentially provide an accurate solution with low computational cost. Different operational modes for DGs, in both ac and dc subgrids, are considered with comprehensive loading models to render the algorithm generic. In addition, a model for the IC is proposed to permit solving the problem sequentially, thereby reducing the problem size in comparison with a unified one [52], [83]. The proposed

algorithm adapts first the common NR method to solve for islanded ac subgrid variables, including the frequency. Based on these variables and DG operational modes, the IC is modeled and the dc power flow variables are updated. The proposed algorithm has the advantage of less computational cost with respect to the Newton-trust region method (NTR) adopted in [49], since the latter entails calculation of Jacobian and Hessian matrices according to numerical bases.

The remainder of the work is organized as follows. Section 5.2 provides a brief overview of the control strategies applied in hybrid microgrids. The modeling of the ac and dc subgrids and the ICs are provided in sections 5.3, 5.4, and 5.5, respectively. In section 5.6, the proposed power flow algorithm is explained in detail. Section 5.7 describes the validation and computational efficiency of the proposed algorithm via several case studies, and section 5.8 concludes the work.

5.2 IC Operational Modes

In general, the hybrid microgrid consists of islanded ac and dc subgrids connected by an IC, as illustrated in Figure 5.1. The DGs within this microgrid operate according to different control strategies, mainly related to the IC functionality. As reviewed in the literature, the IC can achieve one of the following objectives:

a) providing a slack bus to the ac subgrid [44], in which the dc subgrid is assumed to be stiff because it has a higher power surplus. Thus, the ac-side DGs operate as PV/PQ buses. Any power mismatch in the ac subgrid, which is considered the weak system, will be compensated by the ac slack bus provided by the IC. To that end, the DG and storage units, installed in the dc subgrid, operate primarily based on P-V droop characteristics to maintain

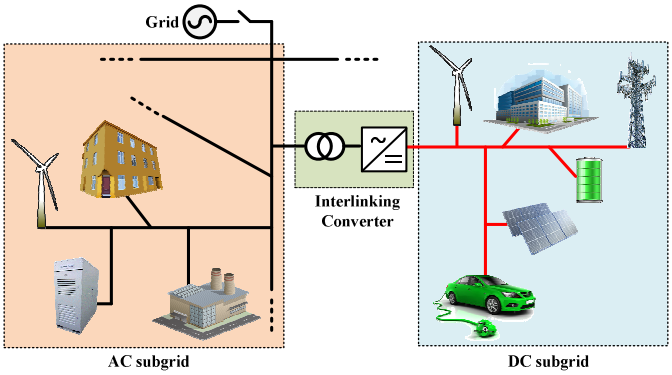

Figure 5.1: Schematic diagram of a hybrid microgrid

a power balance for the overall hybrid system.

b) providing a slack bus for the dc subgrid [45], [54] which is the opposite of the previous objective. The power capacity of the ac network is considered much higher, i.e., a stiff ac subgrid. The dc-side DGs are allowed to inject all the available power, while the ac-side DGs predominantly operate according to droop characteristics to achieve the overall loading and generation balance.

c) Sharing of source power, where the normalized frequency and dc voltage are intentionally equalized [46], [84]. Neither the ac nor dc subgrid dominates the other, none of them is stiff. In this mode, the DG loading in the ac and dc subgrids is interpreted via two different variables: the frequency and dc voltage. By measuring these two variables, the IC adapts the active power transfer between the two subgrids. Due to the absence of a stiff subgrid, the DGs mainly implement droop characteristics to fulfill the entire load demand of the hybrid system.

Typically, the hybrid system is divided into two subgrids to solve the power flow problem, assuming that they are decoupled. This assumption is valid in the case of the first and second objectives of the IC, because the weak subgrid can be mathematically decoupled from the stiff one. In such a case, the power flow is solved first for the weak subgrid which comprises a slack bus provided by the IC. The power transfer through the IC can then be calculated. Finally, the power flow problem can be solved for the stiff subgrid by modeling the interlinking bus as a constant power, with the value calculated in the previous step. However, the ac and dc subgrids cannot be mathematically decoupled in the third objective. The power flow algorithm should be solved for both subgrids iteratively, because the frequency and dc voltage are coupled. The main novelty of this work is the development of a power flow algorithm that can handle the third objective provided by the IC within islanded hybrid microgrids.

5.3 AC Microgrid Modeling

For an ac subgrid consisting of a set $\mathcal{J}_{ac}$ of buses, the active and reactive powers injected at any arbitrary bus $i \in \mathcal{J}_{ac}$ can be calculated as

$$P_{ac,i} = V_{ac,i} \sum_{j \in \mathcal{J}_{ac}} V_{ac,j}\, Y_{ij}\, cos(\delta_i - \delta_j - \theta_{ij}) \tag{5.1}$$

$$Q_i = V_{ac,i} \sum_{j \in \mathcal{J}_{ac}} V_{ac,j}\, Y_{ij}\, sin(\delta_i - \delta_j - \theta_{ij}) \tag{5.2}$$

where $P_{ac,i}$ and Q_i are the injected active and reactive powers, $V_{ac,i}$ and δ_i are the voltage magnitude and angle, Y_{ij} and θ_{ij} are the Y-bus admittance matrix magnitude and angle. Unlike in stiff ac systems, the admittance terms are not constant since they are function on the system frequency, which is variable in islanded microgrids:

$$Y_{ij} = \frac{1}{\sqrt{{R_{ij}}^2 + \omega^2\, {L_{ij}}^2}} \tag{5.3}$$

$$\theta_{ij} = \pi - \tan^{-1} \frac{\omega\, L_{ij}}{R_{ij}} \tag{5.4}$$

where R_{ij} and L_{ij} are the resistance and inductance between buses i and j, and ω is the frequency.

5.3.1 Load Modeling

Different ac loads can be modeled according to their behaviors with the changes in the applied voltage and frequency. To consider the voltage effect, the static load model can be represented by

$$P_{ac,Li} = P^o_{ac,i} \big(V_{ac,i}\big)^{\propto} \tag{5.5}$$

$$Q_{Li} = Q^o_i \big(V_{ac,i}\big)^{\beta} \tag{5.6}$$

where $P^o_{ac,i}$ and Q^o_i are the nominal values for the active and reactive powers, respectively; and $\propto$ and β are the active and reactive power exponents. The load model represented by (5.5) and (5.6) is generic and can represent the constant impedance, constant current, or constant power loads by assigning $\propto$ and β the value of two, one, or zero, respectively. In order to incorporate the frequency dependency in the load model, additional factors can be added:

$$P_{ac,Li} = P^o_{ac,i} \big(V_{ac,i}\big)^{\propto} (1 + K_{pf,i}\, \Delta\omega) \tag{5.7}$$

$$Q_{Li} = Q^o_i \big(V_{ac,i}\big)^{\beta} (1 + K_{qf,i}\, \Delta\omega) \tag{5.8}$$

where $\Delta\omega$ is the deviation of the frequency, i.e. $\Delta\omega = (\omega - \omega_0)$, K_{pf} and K_{qf} are two constants that range from 0 to 2 and from -2 to 0, respectively [85].

5.3.2 DG Modeling

In islanded ac microgrids, most of the DGs implement droop characteristics to share the system loading, while some DGs can operate in PV or PQ mode, such as renewable-based DGs. Both PV and PQ modes of operation are frequency independent, and thus, their incorporation in the power flow formulation is straightforward. For DG units operating according to droop characteristics, as depicted in Figure 5.2, the steady-state model can be given by

$$P_{ac,Gi} = \mu_i(\omega_i^* - \omega) \tag{5.9}$$

$$Q_{Gi} = \eta_i(V_{ac,i}^* - V_{ac,i}) \tag{5.10}$$

where $P_{ac,G}$ and Q_G are the DG output active and reactive powers, ω^* and V_{ac}^* are the no-load reference values for the DG output frequency and voltage, μ and η are the reciprocals of the DG droop gains. The droop characteristic in (5.9) implies an active power feedback that renders all DGs operating under a common frequency value, according to which the fractional contributions of active power are achieved as intended. Likewise, (5.10) implies a reactive power feedback to assist the reactive power sharing among the DGs. The droop gains of different DGs are tuned to maintain the system frequency and voltage within the permissible limits:

$$\mu_i = \frac{P_{ac,Gi}^{max}}{\omega_{max} - \omega_{min}} \tag{5.11}$$

$$\eta_i = \frac{Q_{Gi}^{max}}{V_{ac,max} - V_{ac,min}} \tag{5.12}$$

where $P_{ac,G}^{max}$ and Q_G^{max} are the maximum active and reactive powers of the DG unit, ω_{max} and ω_{min}

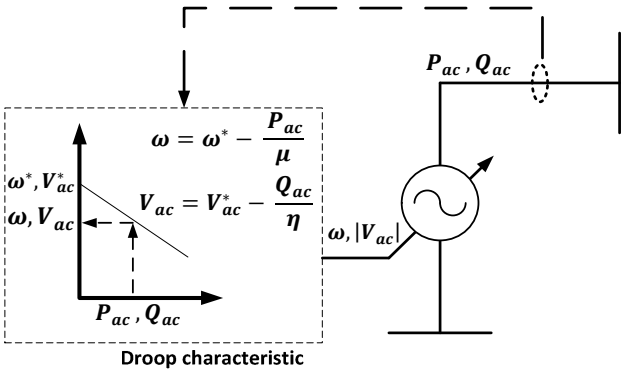

Figure 5.2: Steady-state model for a droop-based DG unit in the ac subgrid

are the maximum and minimum values for the system permissible frequency, $V_{ac,max}$ and $V_{ac,min}$ are the maximum and minimum allowable voltage magnitudes.

5.4 DC Microgrid Modeling

The power injected at any arbitrary bus i can be given by

$$P_{dc,i} = V_{dc,i} \sum_{j \in \mathcal{J}_{dc}} V_{dc,j} \, G_{ij} \quad \forall i \in \mathcal{J}_{dc} \tag{5.13}$$

where $P_{dc,i}$ is the injected power, $V_{dc,i}$ is the voltage of bus i, G is the conductance matrix , and $\mathcal{J}_{dc}$ is the set of dc buses.

5.4.1 Load Modeling

In dc distribution systems, different loads can be modeled as constant power, constant current, and constant resistance loads [73], [86]. Constant power loads are the most common type in dc distribution systems. dc motors, variable speed drives, and dc-dc power supplies are typical examples for this load category. Constant current modeling can provide more appropriate fitting for some motors that draw almost the same current for a wide range of input voltage. The constant resistance loads conform to various types of lamps, heaters, and relays. Only the constant resistance loads can be modeled implicitly within the system conductance matrix. Thus, an aggregated load connected at bus i can be generically modeled as

$$P_{dc,Li} = P^{o}_{dc,i} + V_{dc,i} \, I^{o}_{dc,i} \tag{5.14}$$

where $P^{o}_{dc,i}$ and $I^{o}_{dc,i}$ are the load constant power and constant current portions, respectively.

5.4.2 DG Modeling

The majority of the DGs follow a droop characteristic to share the system loading, whereas some DGs can inject constant powers. The integration of the constant power DGs in the power flow formulation is similar to the constant power loads but with opposite sign. On the other hand, droop characteristics can be realized via two main control structures, namely, I-V and P-V, demonstrated in Figure 5.3 and given by

$$P_{dc,Gi} = \vartheta_P (V^{*}_{dc,Pi} - V_{dc,i}) \tag{5.15}$$

$$I_{dc,Gi} = \vartheta_I (V^{*}_{dc,Ii} - V_{dc,i}) \tag{5.16}$$

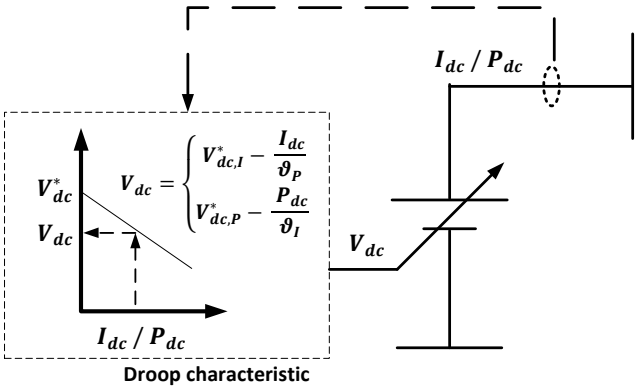

Figure 5.3: Steady-state model for a droop-based DG unit in the dc subgrid

where $P_{dc,Gi}$ and $I_{dc,Gi}$ are the DG out power and current, respectively; $V^*_{dc,P}$ and $V^*_{dc,I}$ are the DG no-load reference voltages; ϑ_P and ϑ_I are the reciprocals of the droop gains for the DG output power or current, respectively. To enhance the sharing among the DGs within an appropriate voltage level, the following formula is commonly adopted for choosing the DG droop gains:

$$\vartheta_{P,i} = \frac{P^{max}_{dc,Gi}}{V_{dc,max} - V_{dc,min}} \tag{5.17}$$

$$\vartheta_{I,i} = \frac{I^{max}_{dc,Gi}}{V_{dc,max} - V_{dc,min}} \tag{5.18}$$

where $P^{max}_{dc,Gi}$ and $I^{max}_{dc,Gi}$ are the maximum output power and current of the DG unit, $V_{dc,max}$ and $V_{dc,min}$ are the maximum and minimum allowable voltage levels for the dc subgrid, respectively.

5.5 IC Modeling

When neither the ac or dc subgrid is stiff, the main objective of the interlinking is to coordinate the two subgrids in order to achieve source power sharing. The main advantages of this operational mode can be summarized as follows [46]:

1) Increases system reliability by relieving overstressed sources, thus avoiding the chance of a single point failure;
2) distributes load transients among all DGs in the hybrid system, thereby keeping each individual DG power variation small;

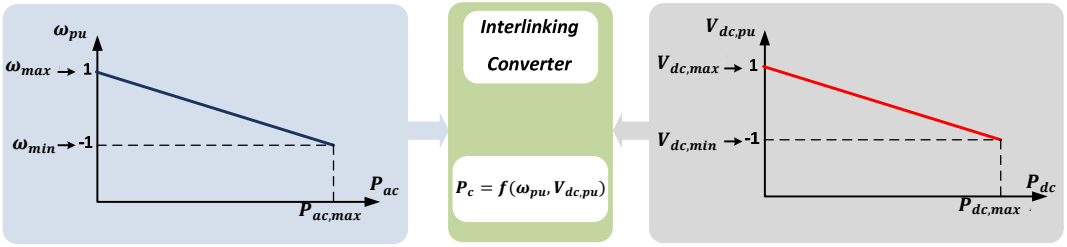

Figure 5.4: General steady-state model for the interlinking converter in source power sharing mode

3) considerably reduces the required back-up reserve within each subgrid, by sharing source capacities of the hybrid system.

To realize the above control objective, the IC measures the frequency and dc voltage as loading indicators for ac and dc subgrids, respectively. Then, the active power transfer between the two subgrids is controlled to equalize the normalized values of the frequency and dc voltage, as depicted in Figure 5.4:

$$\omega_{pu} = V_{pu,i} \quad \forall i \in \mathcal{I}_c \tag{5.19}$$

with,

$$\omega_{pu} = \frac{\omega - 0.5(\omega_{max} + \omega_{min})}{0.5(\omega_{max} - \omega_{min})} \tag{5.20}$$

$$V_{pu,i} = \frac{V_{dc,i} - 0.5(V_{dc,max} + V_{dc,min})}{0.5(V_{dc,max} - V_{dc,min})} \tag{5.21}$$

where $\mathcal{I}_c$ is the set of the ICs within the hybrid microgrid. By substituting from (5.20) and (5.21) into (19), the following relation can be obtained for the system frequency and dc bus voltage:

$$a_\omega\, \omega - a_V\, V_{dc,i} - a_{\omega V} = 0 \tag{5.22}$$

with,

$$a_\omega = \frac{2}{(\omega_{max} - \omega_{min})}$$

$$a_V = \frac{2}{(V_{dc,max} - V_{dc,min})}$$

$$a_{\omega V} = \frac{(\omega_{max} + \omega_{min})}{(\omega_{max} - \omega_{min})} - \frac{(V_{dc,max} + V_{dc,min})}{(V_{dc,max} - V_{dc,min})}$$

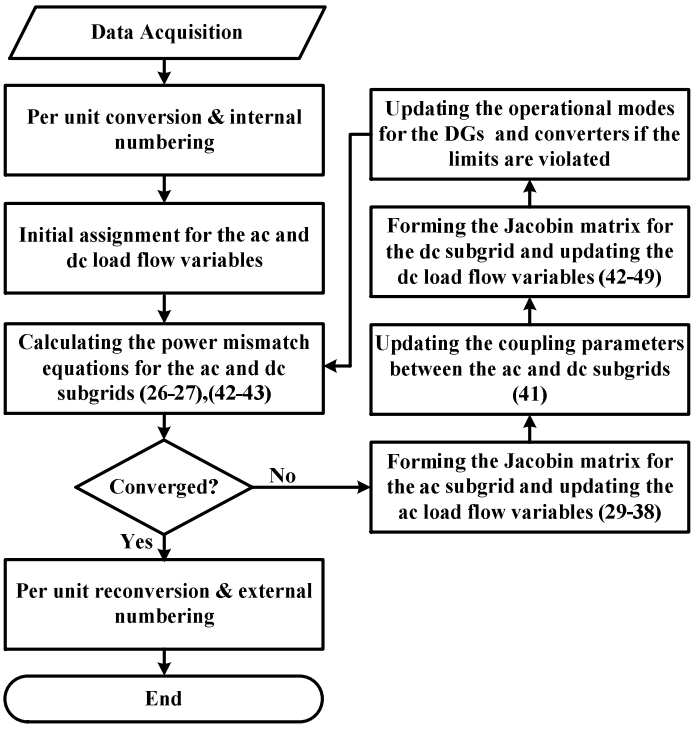

Figure 5.5: Proposed sequential power flow algorithm.

In addition to source active power sharing, the IC can support the reactive power at the ac side, given that the flow of the active power is from the dc to ac side [46], [48]. The reactive power support can be controlled via a droop characteristic unless the converter capacity is attained [47]. The reactive power of the IC $Q_{c,j}$, injected at the ac-side bus $j \in \mathcal{J}_{ac}$, can therefore be modelled as

$$Q_{c,j} = \begin{cases} \min\left(\eta_j (V_{ac,j}^{*} - V_{ac,j}), Q_{lim,j}\right) & if \quad P_{c,ac,j} > 0 \\ 0 & otherwise \end{cases} \tag{5.23}$$

with,

$$Q_{lim,j} = \sqrt{\left(S_{lim,i}\right)^2 - \left(P_{c,ac,j}\right)^2} \tag{5.24}$$

where $P_{c,ac}$ is the active power injected by the converter at the ac-side, S_{lim} and Q_{lim} are the apparent and reactive power limits of the IC. To enhance the calculations accuracy, the generic power losses formula for the IC is adopted in this work, [49], [87]:

$$P_{c,loss,j} = C_0 + C_1 \; I_{c,ac,j} + C_2 \; I_{c,ac,j}^2 \tag{5.25}$$

where $P_{c,loss,j}$ is the converter power loss, $I_{c,ac}$ is the injected current at the converter ac-side, and C_0, C_1 and C_2 are the quadratic function coefficients.

5.6 AC/DC Power Flow Procedure

The main challenge in solving the power flow of hybrid microgrids is the correlation between the ac and dc subgrids, which is triggered by equalizing the normalized values of the frequency and dc voltage. In this work, the NR method is accommodated to solve the power flow of hybrid microgrids sequentially, as depicted in Figure 5.5. The algorithm starts by acquiring the system data. Then, it applies a per unit conversion and internal bus numbering for the dc-side of the ICs. This internal numbering facilitates the incorporation of multiple dc subgrids into the power flow formulation [52], and is achieved by assigning the dc-side buses of the ICs their own converter numbers. Then, according to the initial guessing for the power flow variables, the mismatch equations are evaluated in the hybrid system. The remainder of this section provides more details regarding the power flow mismatch equations and the subroutines in the proposed algorithm.

5.6.1 AC Power Flow

The proposed power flow formulation for the ac subgrid defines generic expressions for the power mismatch equations and the associated Jacobian matrix. Each bus is assumed to have a generic load and DG in addition to a power injection due to an IC. The absence of any element, i.e. load, generation or IC, will be considered by replacing the corresponding element parameters with zeros in the power mismatch equations and the Jacobian matrix as well. The mismatch active and reactive power equations for any bus $i \in \mathcal{J}_{ac}$ are formulated by combining (5.1, 5.2) and (5.7-5.10):

$$F_{ac,Pi} = P_{ac,Gi} + P_{c,ac,i} - P_{ac,Li} - P_{ac,i} \tag{5.26}$$

$$F_{Qi} = Q_{Gi} + Q_{c,i} - Q_{Li} - Q_i \tag{5.27}$$

For an IC connecting buses $i \in \mathcal{J}_{ac}$ and $j \in \mathcal{J}_{dc}$, the active power injection at the ac side is modelled as a constant power, imitating a dummy constant power source:

$$P_{c,ac,i} = -P_{c,loss,i} - P_{c,dc,j} \tag{5.28}$$

where $P_{c,dc,j}$ is the power injected by the IC at the dc side. The value for $P_{c,dc,j}$ is initially assigned and then updated as explained in the following subsections. The reactive power of the IC $Q_{c,j}$ is consider as represented in (5.23).

For an ac subgrid of N_{ac} buses, including the ac-side buses of the IC, the number of the power mismatch equations is 2 N_{ac}. This set of equations will be solved for 2 N_{ac} unknowns: N_{ac} voltage magnitudes; the system frequency; and $N_{ac} - 1$ angles, since the first ac bus is chosen as a reference. Defining the Jacobian matrix for the ac subgrid as

$$J_{AC} = \begin{bmatrix} \frac{\partial F_{ac,P}}{\partial V_{ac}} & \frac{\partial F_{ac,P}}{\partial \omega} & \frac{\partial F_{ac,P}}{\partial \delta} \\ \frac{\partial F_{Q}}{\partial V_{ac}} & \frac{\partial F_{Q}}{\partial \omega} & \frac{\partial F_{Q}}{\partial \delta} \end{bmatrix} \tag{5.29}$$

with,

$$\begin{cases} \frac{\partial F_{ac,Pi}}{\partial V_{ac,i}} = -\propto P^{o}_{ac,i}(V_{ac,i})^{\propto -1}\left(1 + K_{pf,i}\,\Delta\omega\right) - V_{ac,i}Y_{ii}\cos(\theta_{ii}) - \sum_{j\in\mathcal{J}_{ac}} V_{ac,j}\,Y_{ij}\cos\left(\delta_i - \delta_j - \theta_{ij}\right) \\ \frac{\partial F_{ac,Pi}}{\partial V_{ac,j}} = -V_{ac,i}\,Y_{ij}\cos\left(\delta_i - \delta_j - \theta_{ij}\right) \qquad \forall\ j \neq i \end{cases} \tag{5.30}$$

$$\begin{cases} \frac{\partial F_{Qi}}{\partial V_{ac,i}} = -\eta_i - \beta Q^{o}_{i}(V_{ac,i})^{\beta-1}\left(1 + K_{qf,i}\,\Delta\omega\right) + V_{ac,i}\,Y_{ii}\sin(\theta_{ii}) - \sum_{j\in\mathcal{J}_{ac}} V_{ac,j}\,Y_{ij}\sin\left(\delta_i - \delta_j - \theta_{ij}\right) \\ \frac{\partial F_{Qi}}{\partial V_{ac,j}} = -V_{ac,i}\,Y_{ij}\ \sin\left(\delta_i - \delta_j - \theta_{ij}\right) \qquad \forall\ j \neq i \end{cases} \tag{5.31}$$

$$\begin{aligned} \frac{\partial F_{ac,Pi}}{\partial \omega} = &-\mu_i - P^{o}_{ac,i}(V_{ac,i})^{\propto} K_{pf,i} \\ &+ V_{ac,i}\left(V_{ac,i}\sum_{j\in\mathcal{J}_{ac}} \varrho_{ij} - \sum_{j\in\{\mathcal{J}_{ac}\setminus i\}} V_{ac,j}\ \left(\cos\left(\delta_i - \delta_j\right)\varrho_{ij} + \sin\left(\delta_i - \delta_j\right)\varpi_{ij}\right)\right) \end{aligned} \tag{5.32}$$

$$\begin{aligned} \frac{\partial F_{Qi}}{\partial \omega} = &-Q^{o}_{i}(V_{ac,i})^{\beta} K_{qf,i} \\ &+ V_{ac,i}\left(-V_{ac,i}\sum_{j\in\mathcal{J}_{ac}} \varpi_{ij} + \sum_{j\in\{\mathcal{J}_{ac}\setminus i\}} V_{ac,j}\ \left(\cos\left(\delta_i - \delta_j\right)\varpi_{ij} - \sin\left(\delta_i - \delta_j\right)\varrho_{ij}\right)\right) \end{aligned} \tag{5.33}$$

$$\begin{cases} \frac{\partial F_{ac,Pi}}{\partial \delta_i} = V_{ac,i}\sum_{j\neq i} V_{ac,j}\,Y_{ij}\sin(\delta_i - \delta_j - \theta_{ij}) \\ \frac{\partial F_{ac,Pi}}{\partial \delta_j} = -V_{ac,i}\,V_{ac,j}\,Y_{ij}\ \sin(\delta_i - \delta_j - \theta_{ij}) \quad \forall\ j \neq i \end{cases} \tag{5.34}$$

$$\begin{cases} \dfrac{\partial F_{Qi}}{\partial \delta_i} = -V_{ac,i} \sum_{j \neq i} V_{ac,j}\, Y_{ij}\, \cos(\delta_i - \delta_j - \theta_{ij}) \\ \dfrac{\partial F_{Qi}}{\partial \delta_j} = V_{ac,i}\, V_{ac,j}\, Y_{ij} \cos(\delta_i - \delta_j - \theta_{ij}) \quad \forall\ j \neq i \end{cases} \tag{5.35}$$

The rest of the Jacobian matrix elements are given at the end of the next page, where $i, j \in \mathcal{J}_{ac}$, and ϱ_{ij} and ϖ_{ij} are defined as:

$$\varrho_{ij} = \begin{cases} \dfrac{2R_{ij}\omega L_{ij}^2}{(R_{ij}^2 + \omega^2 L_{ij}^2)^2} & if\ |y_{ij}| > 0 \\ 0 & if\ |y_{ij}| = 0 \end{cases} \tag{5.36}$$

$$\varpi_{ij} = \begin{cases} \dfrac{(R_{ij} - \omega^2 L_{ij}^2) L_{ij}}{(R_{ij}^2 + \omega^2 L_{ij}^2)^2} & if\ |y_{ij}| > 0 \\ 0 & if\ |y_{ij}| = 0 \end{cases} \tag{5.37}$$

y_{ij} is the admittance between buses i and j. The ac power flow variables are then updated as follows:

$$\begin{bmatrix} V_{ac}^{(k+1)} \\ \omega^{(k+1)} \\ \delta^{(k+1)} \end{bmatrix} = \begin{bmatrix} V_{ac}^{(k)} \\ \omega^{(k)} \\ \delta^{(k)} \end{bmatrix} - {J_{AC}}^{-1} \begin{bmatrix} F_{ac,P}^{(k)} \\ F_Q^{(k)} \end{bmatrix} \tag{5.38}$$

where $V_{ac}^{(k)}$ and $V_{ac}^{(k+1)}$ indicate the system voltage values at iterations k and $k+1$, respectively.

5.6.2 Representation of AC and DC Coupling

To solve the problem sequentially, the mutual coupling between the frequency and dc voltages of multiple ICs should be defined. The total power transfer $P_{c,tot}$ from the ac to dc subgrids can be formulated in terms of the mismatch between the power generation, and loading and losses $P_{ac,Loss}$ in the ac subgrid:

$$P_{c,tot} = \left(\sum_{i \in \mathcal{J}_{ac}} P_{ac,Gi} - P_{ac,Li} \right) - P_{ac,Loss} \tag{5.39}$$

Neglecting the change in the system losses [47], [85], the overall change in the total power transfer $P_{c,tot}$ with respect to the change in the ac subgrid frequency can be expressed as:

$$\frac{\partial P_{c,tot}}{\partial \omega} = -\sum_{i \in \mathcal{J}_{ac}} \left(\mu_j + P_{ac,oj} \left(V_{ac,j} \right)^{\propto} K_{pf,j} \right) \tag{5.40}$$

Based on (5.40), the sensitivity of the total power transfer with respect to the frequency has a negative value. Thus, the ac subgrid can be represented as a dummy large droop-based DG with a droop characteristic defined as

$$P_{c,tot} = \mu_{ac} (\omega_{ac}^{*} - \omega) \tag{5.41}$$

with

$$\mu_{ac} = -\frac{\partial P_{c,tot}}{\partial \omega} \quad , \quad \omega_{ac}^{*} = \omega + \frac{P_{con,tot}}{\mu_{ac}}$$

where μ_{ac} and ω_{ac}^{*} are the virtual reciprocal droop gain and no-load frequency for the dummy DG, respectively. The values of μ_{ac} and ω_{ac}^{*} are updated during the algorithm iterations. Eq. (5.41) represents the relation between the system frequency and the power transfer from the ac to dc subgrids, and hence is essential for solving the dc power flow.

5.6.3 DC Power Flow

In this step, the voltages of dc subgrids and the power of the ICs are updated. Each bus in these subgrids is assumed to have a generic load, power injection via an IC, and P-V and I-V droop-based DGs. Similar to the approach followed in the ac subgrid, the parameters of any absent element will be replaced by a zero value. The power mismatch equation at any bus $i \in \mathcal{J}_{dc}$ is formulated by combing (5.13-5.16):

$$F_{dc,Pi} = P_{dc,Gi} + V_{dc,i}\, I_{dc,Gi} + P_{c,dc,i} - P_{dc,Li} - P_{dc,i} \tag{5.42}$$

The power injections of the ICs at the dc-side buses represent additional power flow variables to be solved in this step. Substituting from (5.41) into (5.22) leads to an additional set of equations for the dc-side interfacing buses:

$$F_{c,i} = P_{c,tot} + \bar{a}_{V,i}\, V_{dc,i} + a_{PV,i} \tag{5.43}$$

where

$$\bar{a}_{V,i} = \frac{\mu_{ac}\, a_{V,i}}{a_{\omega,i}} \quad , \quad a_{PV,i} = \frac{\mu_{ac} (a_{\omega V,i} - a_{\omega,i}\, \omega_{ac}^{*})}{a_{\omega,i}}$$

According to (5.43), the frequency is replaced by dc variables; the power flow could thus be solved for the dc subgrids as a separate problem. For dc subgrids with a total number of N_{dc} buses, including N_c of the ICs' buses, there are $N_{dc} + N_c$ power mismatch equations. This set of equations matches the total number of dc unknown variables, i.e., bus voltages and interlinking power injections. Defining the Jacobian matrix for the dc subgrid as

$$J_{DC} = \begin{bmatrix} \dfrac{\partial F_{dc,P}}{\partial V_{dc}} & \dfrac{\partial F_{dc,P}}{\partial P_{c,dc}} \\ \dfrac{\partial F_c}{\partial V_{dc}} & \dfrac{\partial F_c}{\partial P_{c,dc}} \end{bmatrix} \tag{5.44}$$

with,

$$\begin{cases} \dfrac{\partial F_{dc,Pi}}{\partial V_{dc,i}} = -\vartheta_{P,i} + \vartheta_{I,i}\left(V^*_{dc,Ii} - 2\,V_{dc,i}\right) - I^o_{dc,i} - V_{dc,i}G_{ii} - \displaystyle\sum_{j\in\mathcal{J}_{dc}} V_{dc,j}\,G_{ij} \\ \dfrac{\partial F_{dc,Pi}}{\partial V_{dc,j}} = -V_{dc,i}G_{ij} \qquad\qquad \forall\ j \neq i \end{cases} \tag{5.45}$$

$$\frac{\partial F_{dc,Pi}}{\partial P_{c,dc,j}} = \begin{cases} 1 & if \quad j = i \\ 0 & if \quad j \neq i \end{cases} \tag{5.46}$$

$$\frac{\partial F_{c,i}}{\partial V_{dc,j}} = \begin{cases} \bar{a}_{V,i} & if \quad j = i \\ 0 & if \quad j \neq i \end{cases} \tag{5.47}$$

$$\frac{\partial F_{c,i}}{\partial P_{c,dc,j}} = 1 \tag{5.48}$$

The last element of the Jacobian matrix is given at the end of this page. The dc voltages and the power injected via the ICs are updated as follows:

$$\begin{bmatrix} V_{dc}^{(k+1)} \\ P_{ac,dc}^{(k+1)} \end{bmatrix} = \begin{bmatrix} V_{dc}^{(k)} \\ P_{ac,dc}^{(k)} \end{bmatrix} - {J_{DC}}^{-1} \begin{bmatrix} F_{dc,P}^{(k)} \\ F_c^{(k)} \end{bmatrix} \tag{5.49}$$

After updating both ac and dc power flow variables, the operational limits of the DGs and ICs are checked. If some converters violate their corresponding limits, they will switch to the constant power mode as a protective precaution. Finally, the maximum power mismatch is checked all over the hybrid system to guarantee the algorithm convergence. If the algorithm is not converged, the aforementioned steps will be sequentially iterated.

It is noteworthy that if a slack bus exists, formed by a large generation unit or by a connection to the main grid, the system frequency and dc voltage of the IC will be constant and regulated. In other words, the ac frequency and dc voltage will be decoupled, i.e., $\partial F_{ac,P}/\partial\omega$ and $\partial F_Q/\partial\omega$ terms will be eliminated from (5.29) as well as the DG droop constants in (5.31). For the dc subgrid, the Jacobian matrix will contain only the $\partial F_{dc,P}/\partial V_{dc}$ term, because the IC is just a slack bus. Hence, the power flow will be similar to the problem introduced in [52].

5.7 Case Studies

5.7.1 Algorithm Validation

To prove the accuracy and validity of the proposed algorithm, the output results of the algorithm are contrasted against the steady-state results of a detailed time-domain simulation created in a PSCAD/EMTDC environment. In general, time-domain software (such as PSCAD/EMTDC or Simulink/Matlab) employs a set of differential equations for each system component to capture the overall system dynamic behavior. Such software is avoided in steady-state analyses due to its extremely high computational time compared with algebraically developed power flow algorithms.

5.7.1.1 Algorithm Performance in the Droop-Based Control Strategy

The hybrid system under study, presented in Figure 5.6, is a combination of the islanded ac and dc systems presented in [71], [88]. The selected subgrids are relatively small, and thus appropriate for the time-domain simulations. The ac subgrid consists of 6 buses in which two DGs operate according to droop characteristics. The dc subgrid consists of 5 buses, with two droop-based DGs installed at buses 1 and 3, and a constant power DG installed at bus 5. An IC is placed between bus 5 and 2 in the ac and dc subgrids, respectively.

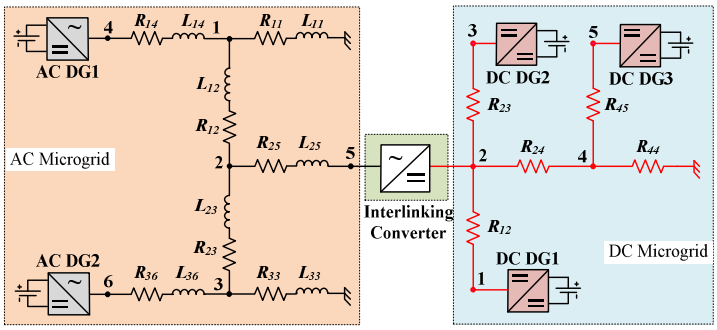

Figure 5.6: Test system #1

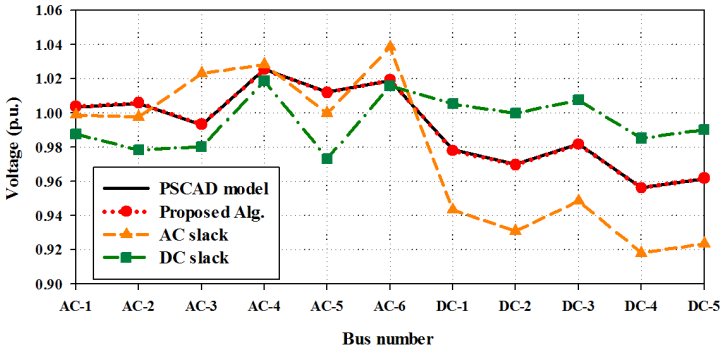

Figure 5.7: System voltage profile using different power flow algorithms

Table 5.1: Validation results of test system#1(decentralized mode)

Bus#	PSCAD/EMTDC			Proposed Algorithm		
	V_{ac} (p.u.)	δ (deg.)	V_{dc} (p.u.)	V_{ac} (p.u.)	δ (deg.)	V_{dc} (p.u.)
1	1.0034	0	0.9786	1.0039	0	0.9781
2	1.0058	-0.1643	0.9703	1.006	-0.1641	0.9699
3	0.9931	-3.0283	0.9822	0.9934	-3.0447	0.9818
4	1.0256	1.5946	0.9564	1.0255	1.5908	0.9563
5	1.0122	0.0901	0.9616	1.0121	0.0903	0.9620
6	1.0190	-3.2756	-	1.0194	-3.2821	-
$P_{c,ac}$(p.u.)	0.2128			0.2131		

To highlight the limitation of the conventional power flow in hybrid systems with the frequency and dc voltage coupling, a comparison between the proposed algorithm and the conventional power flow is conducted [49], [51]. It is worth mentioning that the conventional power flow algorithm

requires a slack bus in either the ac or dc subgrid. Hence, for the conventional power flow, two objectives are assumed to be provided by the IC: ac slack bus or dc slack bus. Figure 5.7 illustrates the bus voltages attained by the proposed algorithm, conventional power flow, and detailed time-domain PSCAD-EMTDC simulation. Unlike the proposed algorithm, none of the approaches solved by the conventional power flow coincide with the solution provided by the detailed time-domain model. Table 5.1 indicates the detailed power flow variables attained from the proposed algorithm and from the detailed time-domain simulation. Both results show high matching with 0.55% maximum phase error and 0.052% maximum voltage magnitude error. These results indicate the accuracy of the proposed power flow algorithm in hybrid systems with frequency and dc voltage coupling.

5.7.1.2 Power Sharing between Subgrids

The proposed algorithm is then used to demonstrate the power transfer between the ac and dc subgrids when the IC equalizes the normalized frequency and dc voltage. The dc load is kept constant while increasing the loads in the ac side. Figure 5.8 illustrates: a) DG active powers, b) DG reactive powers, c) active and reactive powers of the IC, and d) the normalized frequency and dc voltage.

The operational modes of the hybrid system can be divided into five regions. In regions II, III, and IV, all DGs operate approximately at the same active power to share the overall loading, as depicted in Figure 5.8 (a). This is not the case for regions I and V, in which the DGs cannot show such cooperation, having reached the IC's power limit. As shown in Figure 5.8 (b), the reactive power sharing between the ac DGs is not as accurate as the active power, because it relies on local voltage measurements rather than the system frequency.

In regions I and II, the dc subgrid is highly loaded compared with the ac subgrid, and thus, the IC transfers power from the ac to dc subgrid as shown in Figure 5.8 (c). Accordingly, the IC is not allowed to support the ac side with a reactive power. Conversely, the IC transfers power from the dc to ac side in regions III, IV, and V, when the ac subgrid is highly loaded with respect to the dc subgrid. Hence, the IC is enabled to supply reactive power. In region IV, the IC supports the ac subgrid with reactive power up to the converter power limit, while the converter can only transfers active power in region V. As illustrated in Figure 5.8 (d), the IC attempts to equalize the normalized frequency and dc voltage in all regions. However, this objective it is not feasible in regions I and V due to the converter's power limit.

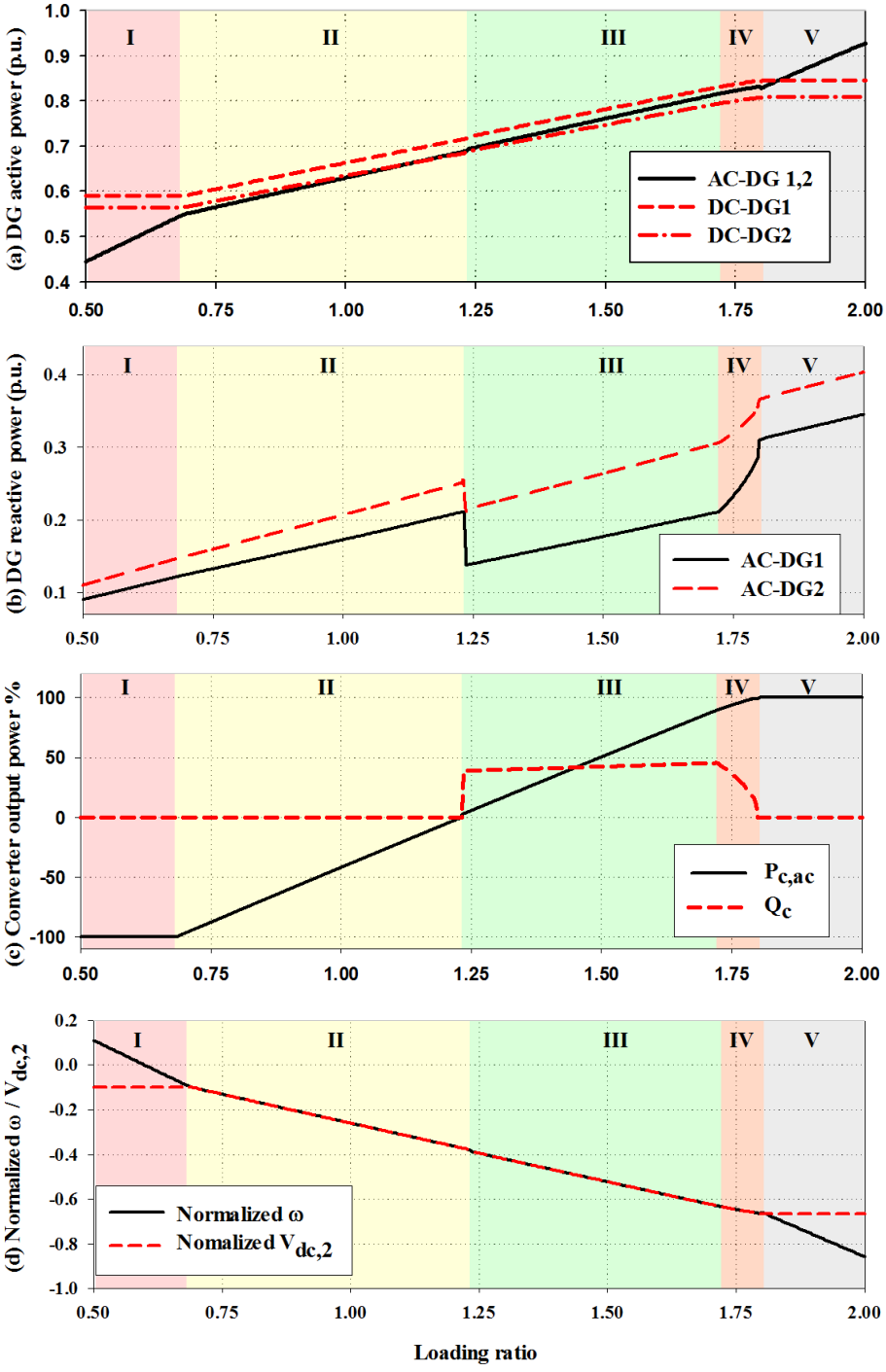

Figure 5.8: The behavior of the hybrid microgrid with the IC operates to achieve source power sharing

Table 5.2: Validation results of test system#1(dispatchable mode)

Bus#	PSCAD/EMTDC			Proposed Algorithm		
	V_{ac} (p.u.)	δ (deg.)	V_{dc} (p.u.)	V_{ac} (p.u.)	δ (deg.)	V_{dc} (p.u.)
1	0.9739	-1.6079	1.0077	0.9737	-1.6045	1.0079
2	0.9710	-1.7252	1.0000	0.9708	-1.7213	1.0000
3	0.9643	-4.0344	1.0087	0.9645	-4.0173	1.0089
4	1.0000	0.0000	0.9872	1.0000	0.0000	0.9873
5	0.9723	-1.5331	0.9945	0.9722	-1.5337	0.9943
6	0.9909	-4.2995	-	0.9913	-4.2945	-
$P_{c,ac}$(p.u.)	0.1057			0.1058		

5.7.1.3 Algorithm Performance in the existence of a slack DG unit

The proposed algorithm is tested when all DG units are switched to the dispatchable mode except a single DG unit providing the system slack bus, i.e., DG1 of the ac subgrid. The remaining DG units are diapatched by the distribution network operator (DNO). DG2 of the ac subgrid is assigned to deliver active and reactive powers of 0.8 and 0.3 p.u, respectively. The IC regulates its dc-link voltage at 1.0 p.u.. In the dc subgrid, the output powers of DG1, DG2 and DG3 are 0.8, 0.6, and 0.7 p.u., respectivley. Table 5.2 shows the results of the detailed time-domain simulation in contrast with the proposed algorithm, in the light of the discusstion provided at the end of section 5.6. The maximum percentage errors are less than 0.04% and 0.43% for the voltage magnitudes and phases, respectively. These results verify the wide capability of the proposed approach in solving the power flow problem under different control paradigms.

5.7.2 AC System Extension with Multiple DC Subgrids

The following study is carried out to check the performance of the proposed algorithm when solving the power flow of an ac distribution system extended by multiple dc subgrids. For that purpose, the 38-bus ac distribution system [89] is extended by connecting two dc subgrids, with the topology given in [7] at buses 34 and 38. Both ac and dc subgrids are equipped with droop-based DGs at locations illustrated in Figure 5.9. For robustness validation, the dc microgrids are assigned different

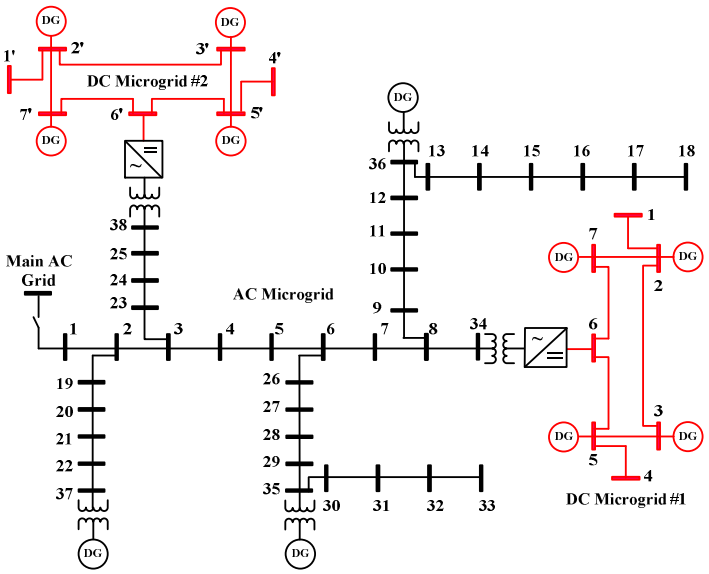

Figure 5.9: Test system #2

loading factors, i.e., 100% and 50% for dc microgrids #1 and #2, respectively. Table 5.3 shows the voltage profile, load and power generation at each bus of the hybrid system. The dc voltages at buses 6 and 6' are equal, since their normalized values are forced to track the normalized frequency. This is physically achieved by transferring less power from dc microgrid #1 to the ac microgrid, rather than more power from lightly loaded dc microgrid #2. Meeting the equal normalized frequency and dc voltage criterion leads to proper power coordination between the ac and dc microgrids. In other words, all DGs have a very similar loading ratio, despite the loading condition of each individual subgrid.

In order to evaluate the computational cost of the proposed NR technique, its computational time is compared with the unified NTR method, which is proposed for ac microgrids in [49]. For more details about NTR, reader could refer to Appendix D. Figure 5.10 demonstrates the computational time versus the summation of squared errors (SSE), for both NTR and NR techniques, using the same computer, with a Core i5 processor (3 GHz) and 4 GB of RAM. The proposed algorithm can approach 10^{-15} SSE in 0.268 s, compared to 7.140 s using the NTR method. The results reflect the computational efficiency of the NR algorithm, which depends only on algebraically formulated Jacobian matrices to solve the problem with a quadratic rate of convergence. This approach contrasts with the NTR technique, which entails numerically calculated Jacobian and Hessian matrices with higher computational effort [90]..

Table 5.3: Power flow results for test system#2, $\omega = 0.9888\, p.u$

Bus	Voltage (p.u., deg.)		Load (p.u.)		Gen. (p.u.)		Bus	Voltage (p.u., deg.)		Load (p.u.)		Gen. (p.u.)	
	V_{ac}	δ	P	Q	P	Q	P	V_{ac}	δ	P	Q	P	Q
1	0.9885	0	-	-	-	-	20	0.9979	0.1997	0.0887	0.0402	-	-
2	0.9885	0	0.0978	0.0579	-	-	21	1.0008	0.2840	0.0890	0.0406	-	-
3	0.9867	-0.0137	0.0888	0.0373	-	-	22	1.0066	0.4771	0.1094	0.0935	-	-
4	0.9864	0.0155	0.1162	0.0764	-	-	23	0.9857	-0.0728	0.0871	0.0481	-	-
5	0.9866	0.0435	0.0586	0.0287	-	-	24	0.9844	-0.1983	0.4056	0.1917	-	-
6	0.9871	0.1232	0.0592	0.0187	-	-	25	0.9863	-0.2824	0.4068	0.1930	-	-
7	0.9880	0.1512	0.1942	0.0970	-	-	26	0.9870	0.1458	0.0582	0.0242	-	-
8	0.9901	0.1102	0.1948	0.0978	-	-	27	0.9869	0.1780	0.0592	0.0234	-	-
9	0.9920	0.1848	0.0592	0.0193	-	-	28	0.9868	0.3261	0.0582	0.0193	-	-
10	0.9945	0.2675	0.0588	0.0198	-	-	29	0.9871	0.4471	0.1164	0.0677	-	-
11	0.9950	0.2736	0.0442	0.0298	-	-	30	0.9840	0.5345	0.1930	0.5743	-	-
12	0.9962	0.2830	0.0591	0.0348	-	-	31	0.9803	0.4618	0.1456	0.0653	-	-
13	0.9904	0.2292	0.0487	0.0342	-	-	32	0.9794	0.4422	0.2037	0.0930	-	-
14	0.9881	0.1693	0.1174	0.0771	-	-	33	0.9792	0.4357	0.0575	0.0377	-	-
15	0.9867	0.1451	0.0581	0.0097	-	-	34	0.9981	0.0411	-	-	**0.2786**	0.3712
16	0.9852	0.1352	0.0592	0.0185	-	-	35	1.0072	0.6715	-	-	0.9762	0.6525
17	0.9829	0.0850	0.0578	0.0191	-	-	36	1.0127	0.7022	-	-	0.9762	0.3725
18	0.9821	0.0864	0.0986	0.0817	-	-	37	1.0110	0.5663	-	-	0.9762	0.4562
19	0.9893	0.0195	0.0881	0.0387	-	-	38	0.9895	-0.2875	-	-	**0.4952**	0.5175

Bus	Voltage (p.u.)	Load (p.u)	Gen.(p.u.)	Bus	Voltage (p.u.)	Load (p.u)	Gen.(p.u.)
1	0.9681	0.1000	-	1'	0.9719	0.0500	-
2	0.9691	-	0.1813	2'	0.9724	-	0.1764
3	0.9708	-	0.1789	3'	0.9732	-	0.1752
4	0.9560	0.1100	-	4'	0.9579	0.0550	-
5	0.9571	-	0.1993	5'	0.9585	-	0.1973
6	**0.9522**	0.2500	-	6'	**0.9522**	0.1250	-
7	0.9587	-	0.1970	7'	0.9592	-	0.1962

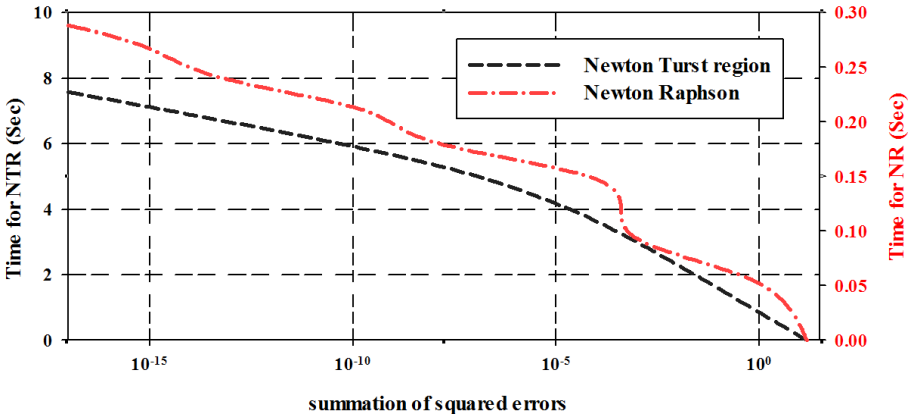

Figure 5.10: Computational cost for NTR algorithm [49] and the proposed NR algorithm

5.8 Discussion

This chapter proposes a novel power flow algorithm for hybrid islanded microgrids. In these systems, droop-based DG units are employed to maintain the generation and loading balance, while the ICs manage the power flows among the subgrids according to the changes in the frequency and dc

voltages. The proposed algorithm sequentially adopts the NR method to handle the unique features of the islanded hybrid systems: coupling between the variable frequency and dc voltages, and the absence of a slack bus. To validate the proposed algorithm's accuracy, its output results are contrasted against the results of a detailed PSCAD/EMTDC simulation and conventional power flow algorithms. The results confirm the proposed algorithm's precision in solving the power flow of hybrid islanded microgrids, with computational time significantly lower than that of the NTR technique. Accordingly, the proposed power flow algorithm can be considered a convenient tool in operational and planning studies of hybrid islanded microgrids.

Chapter 6
Optimum Network Configuration for Maximizing System Loadability

6.1 Introduction

In chapter 5, different components of the hybrid ac/dc microgrids are extensively modelled in the islanded mode of operation. The application of droop characteristics proves to provide a suitable means for sharing the overall system loading among all DG units installed within the hybrid ac/dc microgrids. However, other operational objectives could be achieved through the installation of a supervisory control layer in a hierarchal control scheme [91]. The communication of this supervisory control will not be critical, and thus entails minimum requirements, since the balancing between loads and DG units is always maintained by the droop characteristics implemented in the primary control level. This chapter broadly aims at investigating the improvement in the hybrid ac/dc microgrids performance through the deployment of a supervisory control level that manages the system configuration. For that purpose, an optimum power flow (OPF) problem is formulated and executed by the supervisory control to enhance the system behavior through changing the DG droop settings and system topological structure. As a case study, the system loadability is considered as the primary measure of the system performance in this analysis.

The remainder of this chapter is organized as follows: section 6.2 presents the modeling approach for droop-based DG units and ICs in the proposed OPF problem. Section 6.3 demonstrates the complete OPF formulation for increasing system loadability through droop setting adjustment. In section 6.5, the proposed OPF formulation is extended by including the possibility of system reconfiguration, and section 6.6 highlights the numerical results for the different approaches. Finally, section 6.7 discusses the main findings in the chapter.

6.2 Droop-controlled DG units and ICs modelling for OPF studies of islanded hybrid microgrids

6.2.1 Control parameters

In chapter 5, it was demonstrated that the power sharing behavior could be achieved through following droop characteristics in both ac and dc microgrids as modelled in (5.9-5.10) and (5.15-5.16), respectively. These operational scheme is the main pillar for achieving the sharing process among the DG units within an individual microgrid, either ac or dc. At the same time, the sharing process between the subgrids is achieved via ICs that transfer active power between the ac and dc subgrids based on the frequency and dc voltage values (5.22). In addition, the ICs could provide a reactive power support for the ac side as illustrated in (5.23). It is noteworthy that all the stated equations only comprise the static droop settings which affect the system steady-state behaviour. The practical control loops nonetheless imply additional dynamic settings that influence only the system transit performance, and thus not shown in these analysis. Hereby, the static droop settings are the control variables of interest that are gathered in a control parameter vector x:

$$x = \left\{ x_i \middle| \forall\, i \epsilon\, B_{ac,droop} \cup\ B_{dc,droop} \cup \mathcal{I}_c \ \right\} \tag{6.1}$$

given that

$$x_{i\epsilon\, B_{ac,droop}} = \left\lfloor \omega_i^* , \mu_i, V_{ac,i}^* , \eta_i \right\rceil$$

$$x_{i\epsilon\, B_{dc,droop}} = \left\lfloor V_{dc,Pi}^* , \vartheta_P, V_{dc,Ii}^*, \vartheta_I \right\rceil$$

$$x_{i\epsilon\, \mathcal{I}_c} = \left\lfloor a_{\omega i} , a_{Vi}, a_{\omega Vi} \right\rceil$$

where $B_{ac,droop}$ and $B_{dc,droop}$ are the set of buses that contain droop-based DG units in the ac and dc subgrids, respectively.

6.2.2 DG Capacity

Typically the DG units in both ac and dc subgrids are equipped with a current limiter that prevent any current violation behind the ratings of the power electronic components of each DG unit. In other words, the units installed in the ac subgrid follow the droop characterises (5.9-5.10) up to their maximum active and reactive power limits, $P_{ac,Gi}^{max}$ and $Q_{ac,Gi}^{max}$, respectively. On the other hand, if the droop characteristics result in ratings violation, a DG unit is switched to constant active and reactive

power source. In islanded microgrid, the DG active power is given higher priority to serve the load. Thus, $P_{ac,Gi}^{max}$ could be allowed to approach $S_{ac,Gi}^{max}$ while $Q_{ac,Gi}^{max}$ is dynamically changed to not violating the DG maximum capacity:

$$P_{ac,Gi}^{max} = S_{ac,Gi}^{max} \tag{6.2}$$

$$Q_{ac,Gi}^{max} = \sqrt{{S_{ac,Gi}^{max}}^2 - {P_{ac,Gi}}^2} \tag{6.3}$$

The behavior of a DG unit in the ac subgrid could be inclusively represented using the complementary constraints for an appropriate modeling in the OPF problem. As defined in [92], the complementary constraint problem is to obtain the vector $\sigma \in \Re^n$ such that for the given mappings $F_1(\sigma) \in \Re^n \longrightarrow \Re^n$ and , $F_2(\sigma) \in \Re^n \longrightarrow \Re^n$,

$$F_1(\sigma) \geq 0, \qquad F_2(\sigma) \geq 0, \qquad F_1(\sigma) \times F_1(\sigma) = 0 \tag{6.4}$$

Using the notation "⊥" which represents complement, (6.4) can be rewritten as

$$0 \leq F_1(\sigma) \perp F_1(\sigma) \geq 0 \tag{6.5}$$

Following this definition, the constraints in (6.6) - (6.7) ensures that the active and reactive power generation of the DG unit is either following the droop characteristics given by (5.9) and (5.10) or set at the DG limits, $P_{ac,Gi}^{max}$ and $Q_{ac,Gi}^{max}$, given by (6.2) and (6.3).

$$0 \leq S_{ac,Gi}^{max} - P_{ac,Gi} \perp \mu_i(\omega_i^* - \omega) - P_{ac,Gi} \geq 0 \tag{6.6}$$

$$0 \leq \sqrt{{S_{ac,Gi}^{max}}^2 - {P_{ac,Gi}}^2} - Q_{ac,Gi} \perp \eta_i\left(V_{ac,i}^* - V_{ac,i}\right) - Q_{ac,Gi} \geq 0 \tag{6.7}$$

Likewise, the operational limits for droop-based DG units in dc subgrids could be represented in the OPF as:

$$0 \leq P_{dc,Gi}^{max} - P_{dc,Gi} \perp \vartheta_P(V_{dc,Pi}^* - V_{dc,i}) - P_{dc,Gi} \geq 0 \tag{6.7}$$

$$0 \leq I_{dc,Gi}^{max} - I_{dc,Gi} \perp \vartheta_I\left(V_{dc,Ii}^* - V_{dc,i}\right) - I_{dc,Gi} \geq 0 \tag{6.9}$$

The representation of an IC operation is not straightforward as the DG units, since the active power transfer between the subgrids could hold either positive or negative values based on the loading condition of each subgrid. This fact could be modelled by employing the complementary constraints for the squared value of the active power injection at the ac side, $P_{c,ac,j}$, while checking its polarity if the IC hits the maximum power capacity:

$$0 \leq \left(S_{lim,i}\right)^2 - \left(P_{c,ac,j}\right)^2 \perp (a_\omega\, \omega - a_V\, V_{dc,i} - a_{\omega V})^2 - {P_{c,ac,j}}^2 \geq 0 \tag{6.10}$$

$$(a_\omega\, \omega - a_V\, V_{dc,i} - a_{\omega V}) \times P_{c,ac,j} \leq 0 \tag{6.11}$$

The IC reactive power injection at the ac side still could be modelled using the complementary constraints representation as

$$0 \leq \sqrt{\left(S_{lim,i}\right)^2 - \left(P_{c,ac,j}\right)^2} - Q_{c,j} \perp \eta_j (V^*_{ac,j} - V_{ac,j}) - Q_{c,j} \geq 0 \tag{6.12}$$

6.3 Maximizing System Loadability through Adjustment of DG Droop Characteristics

The loadability concept in islanded microgrid is very similar to the one defined for conventional power system [92], [93]; it is related to the maximum load that could be severed within the grid according to a specific system configuration. Beyond this maximum load value, the power-flow problem will not converge as there is no feasible solution of the system. If the system is not solvable due to attaining a voltage collapse condition, the last solvable operating condition is defined as a static bifurcation point. How far a specific operating point is from the static bifurcation point indicates the voltage stability margin of the system at this operating point. To this point, two types of bifurcation should be distinguished. The first bifurcation type is associated with the singularity condition of the system Jacobian matrix with linear increase in load. This bifurcation type is defined as saddle node bifurcation (SNB). The second type is known as limit induced bifurcation (LIB) since it is related to reaching the maximum generation capacity of the installed units. In islanded microgrid, the system is vulnerable to LIB due to the system limited resources, and hence a careful attention should be given for the system configuration to increase the voltage stability margin at different operating conditions.

It is important to recall that the main power sources in the islanded microgrids are DG units that are responsible for feeding both active of reactive powers based on their droop characteristics. However, on one hand manipulating the droop characteristics will define the active and reactive power share from each DG unit to cover the system load. On the other hand, the active and reactive power of each DG unit is governed by the maximum capacity of the unit. Accordingly, based on the DG droop settings, the system LIB is defined and hence the static stability margin.

In the proposed OPF formulation, the optimum droop settings that maximize the system loadbility level are investigated. The objective function of the problem could represented as

$$Min - \ LF \tag{6.13}$$

where LF is the loading factor beyond which there will be no feasible solution for the load flow problem. In addition to this objective function, there are a set of constraints:

1) DG and IC constraints as demonstrated in (6.6)-(6.12):
2) Power flow constraints as demonstrated in chapter 5.
3) The voltage magnitude bounds for the ac and dc subgrids:

$$V_{ac,min} \leq V_{ac,i} \leq V_{ac,max} \tag{6.14}$$

$$V_{dc,min} \leq V_{dc,i} \leq V_{dc,max} \tag{6.15}$$

4) System frequency limits:

$$\omega_{min} \leq \omega \leq \omega_{max} \tag{6.16}$$

5) Droop settings constraints could be defined as

$$x^{min} \leq x \leq x^{max} \tag{6.16}$$

where x^{min} and $x^{max}$are the lower and upper bounds of the droop parameters of the DG units and ICs. These bounds are assigned according to the minimum and maximum permissible deviations in the system voltages and frequency at the PCC for zero to maximum output power produced by DG units.

6.4 Maximizing System Loadability through Network Reconfiguration

Smart distribution systems provide numerous features that could guarantee higher reliable service and more efficient power management. The reconfiguration capability could be considered as one of the most salient features. The reconfiguration process implies changing the system topological structure, changing feeder connections, through manipulating the system tie switches. This process could contribute in system electrical performance by selecting the optimum system structure that could add the system functional objective while meeting the system operational constraints [94]. The reconfiguration feature has been extensively investigated for conventional distribution systems. No study has been, however, conducted to accommodate the coexistence of dc and ac subgrids in an

islanded hybrid ac/dc paradigm, which is the main focus in this part. Although the main objective in this analysis is still maximizing the system loadability, the system reconfiguration is considered as additional degree of freedom in the optimization problem. Hence, the objective function and constraints in the aforementioned formulation, section 6.3, are not changed while the change of system topological structure is considered by introducing switches states, $sw_{(i,j)}$, as additional integer control variables. The presence of the system switches poses new constraints that guarantee the radiality of the resultant network configuration.

In comparison with meshed ac distribution topology which is employed in a very limited rural areas, radial topology constitutes the common practice in the design of ac distribution networks at different levels due to several economical and technical factors: 1) easier coordination between the protection components, 2) less short circuit current level, and 3) cheaper construction requirements. In accordance with radiality condition, the ac subgrid must not contain any closed loop with all nodes energized. In order to maintain this condition in the proposed OPF problem, the ac subgrid within the hybrid paradigm is represented as a tree graph. As stated in [14], Eq. (6.17) represents a necessary but not sufficient condition to have a tree graph.

$$\sum_{i} sw_{(i,j)} = N_{ac} - 1 \quad \forall \quad i,j \in \mathcal{J}_{ac} \tag{6.17}$$

Along with (6.17), the system topology must be strongly connected, i.e., there is a path between any two nodes in the system, to ensure power supply for all system buses. This connectivity condition is guaranteed through the following rules [94]:

- Switches that do are not reside within any loop must be closed.
- For a set of switches that always belong to the same two loops, defined as a common branch vector, only one switch could be open.
- For a set of switches that are not within other loops, defined as a non-common branch vector, only one switch could be open.
- Switches within common branch vectors but incident to common interior nodes cannot be simultaneously opened.

6.5 Numerical Results

In order to highlight the importance of the droop settings adjustment, the 33-bus test ac system is employed and extended with two dc distribution systems as illustrated in Figure 6.1. The default conventional droop settings for the ac units are demonstrated in Table 6.1, while the eight dc units, as illustrated in Figure 6.1, are assigned same capacity of 0.15 p.u. with droop settings as 1.05 and 1.5 for $V^*_{dc,P}$ and ϑ_{Pi}, respectively. The system performance is tested with increasing the system loading factor. As shown in Figure 6.2, the DG units are capable to feed system demand up to loading factor of 1.3. Through investigating the DG output active and reactive powers, we could elicit valuable

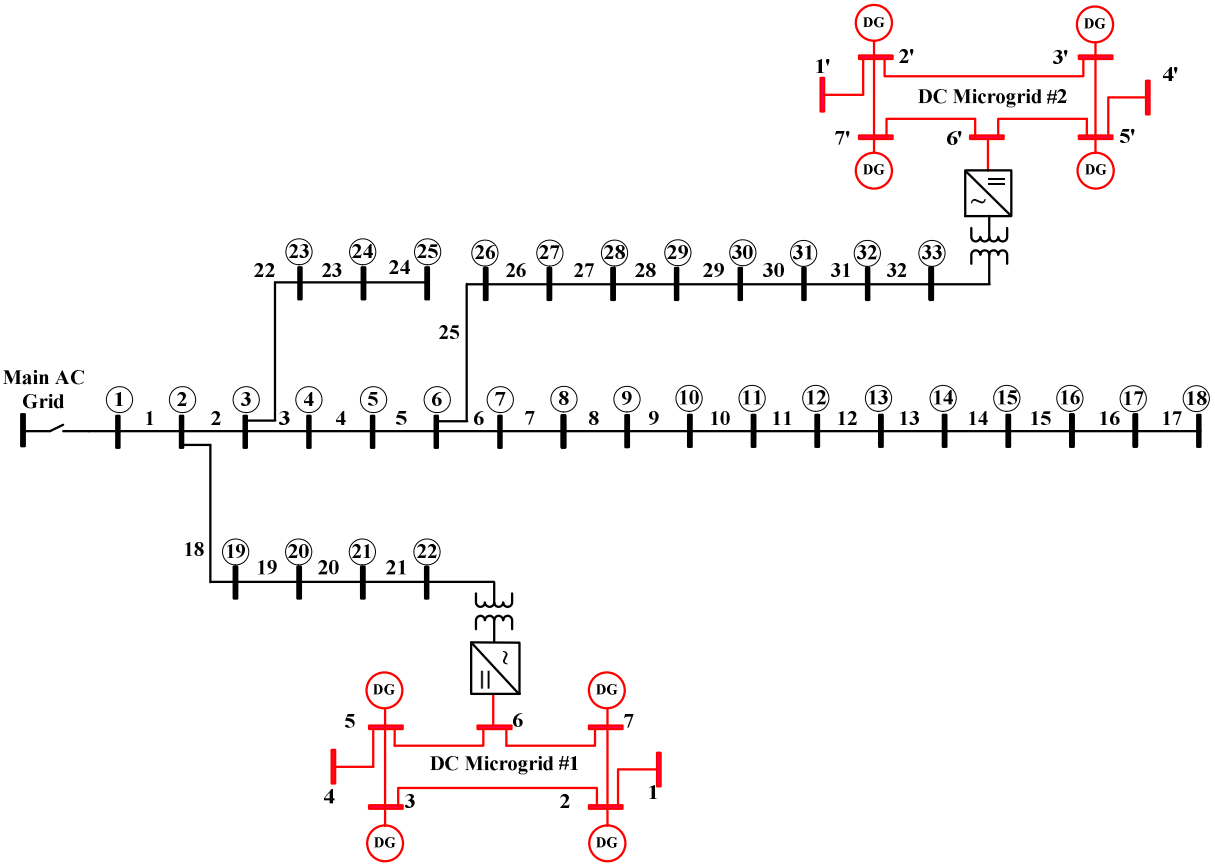

Figure 6.1: 33-bus distribution test system

Table 6.1: Conventional DG settings in p.u

DG #	Bus #	$S^{max}_{ac,Gi}$	ω^*_i	μ_i,	$V^*_{ac,i}$	η_i
1	9	0.6	1.0083	30	1.4849	0.045
2	19	0.5	1.0083	25	1.4849	0.23
3	25	0.5	1.0083	25	1.4849	0.045

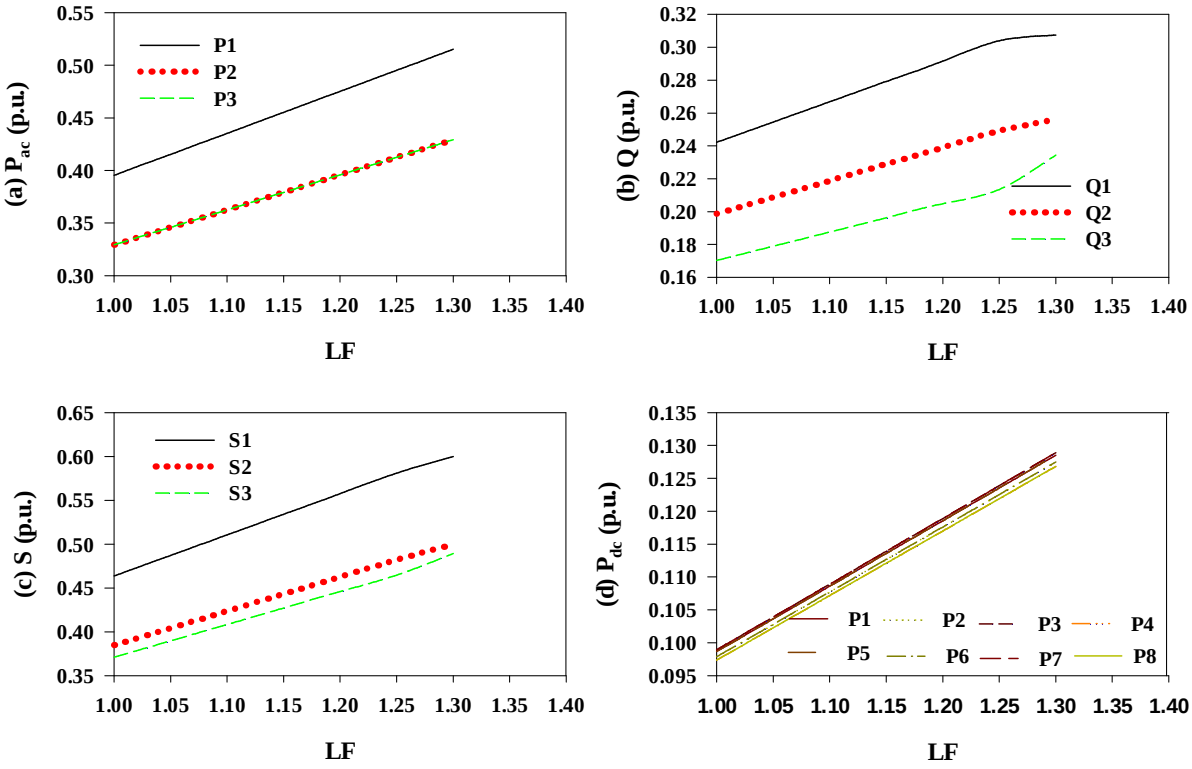

Figure 6.2: DG output with default droop settings: (a) AC-DG active power, (b) AC-DG reactive power, AC-DG apparent power and (b) DC-DG active power

information that interprets the limitation of system loadability. The DG units at the ac subgrids start to approach their maximum capacity at 1.300 loading factor, as demonstrated in Figure 6.2 (c), while the DGs in the dc side still have available active power capacity, as shown in Figure 6.2 (d). Thus, the system loadability is mainly limited by the availability of the reactive power produced by the ac units since the system still capable of providing an active power support through the dc ones. It is important to recall that this type of loadability is associated with the LIB of the DG units due to an improper management of the DG powers.

On the other hand, the proposed OPF could be utilized to obtain the optimum droop settings as shown in Table 6.2. These adjustments of the droop settings could increase the system loadability by additional 8%. This increase is affiliated to a better power management of the system resources. As illustrated in Figure 6.3 (d and c), both ac and dc units simultaneously approach their maximum capacity limits at 1.380 LF. In other words, the adjustment of the DG droop settings enables an optimum utilization of the units through an efficient dispatching of the available system resources.

Table 6.2: DG optimum settings (p.u.).

DG #	ω_i^*	$V_{ac,i}^*$
1	1.0149	1.4835
2	1.0150	1.4854
7	1.0150	1.4959

DG #	$V_{dc,Pi}^*$	DG #	$V_{dc,Pi}^*$
1	1.1226	5	1.1225
2	1.1232	6	1.1285
3	1.1217	7	1.1234
4	1.1242	8	1.1238

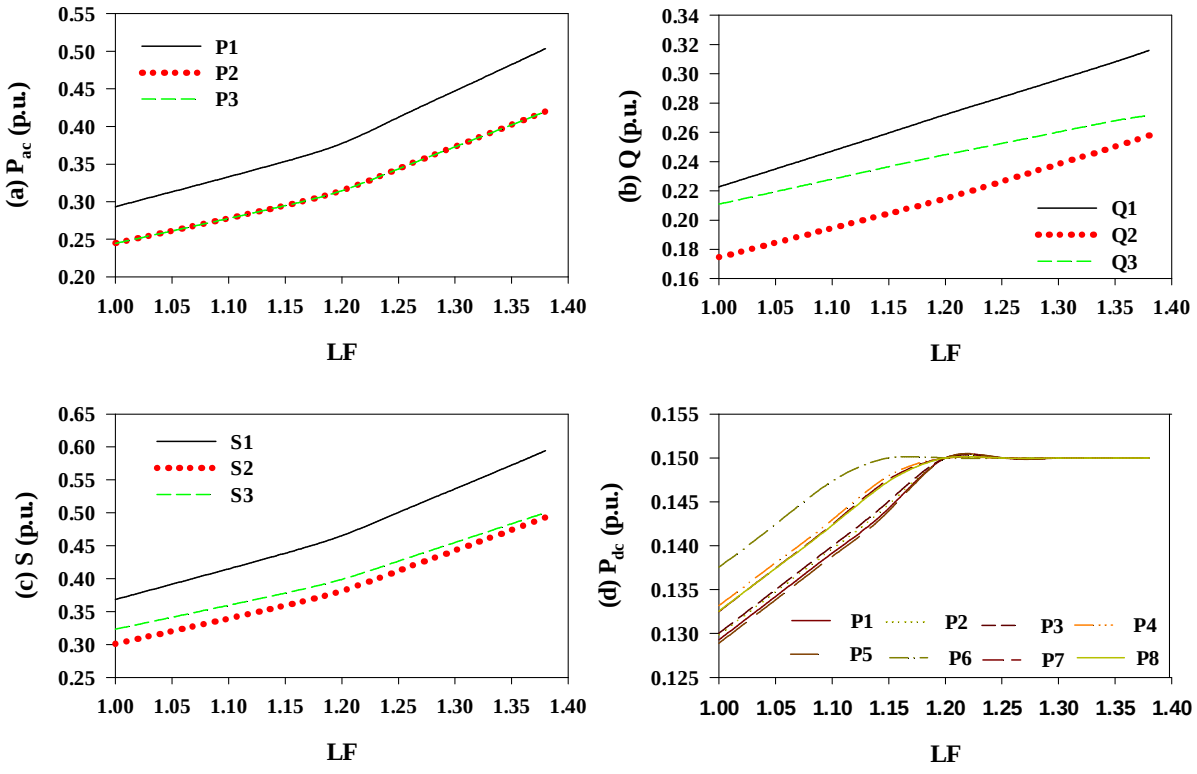

Figure 6.3: DG output with droop adjustment: (a) AC-DG active power, (b) AC-DG reactive power, AC-DG apparent power and (b) DC-DG active power

The effect of the system reconfiguration on the system loadability is addressed through considering additional tie lines as shown in Figure 6.4. The assumption of maintaining all the system switching closed, albeit theoretical, indicates the maximum system loadibility level. This assumption is followed in this analysis and the optimum DG droop settings are recalculated according to the proposed OPF formulation. By testing the resultant droop settings, Table 6.3, we could notice that the system loadability could be increased by only 1.4 %, i.e. maximum LF = 1.394. This minimum influence on the system loadability complies with the fact that the loadability level of ADNs is governed by the availability of the system resources (LIB). This situation is different in the bulk power system, in which the reconfiguration strategy is much more effective in the system loadability level, since the system loadability is determined based on the system capability in transmitting power through its structural topology (SNB).

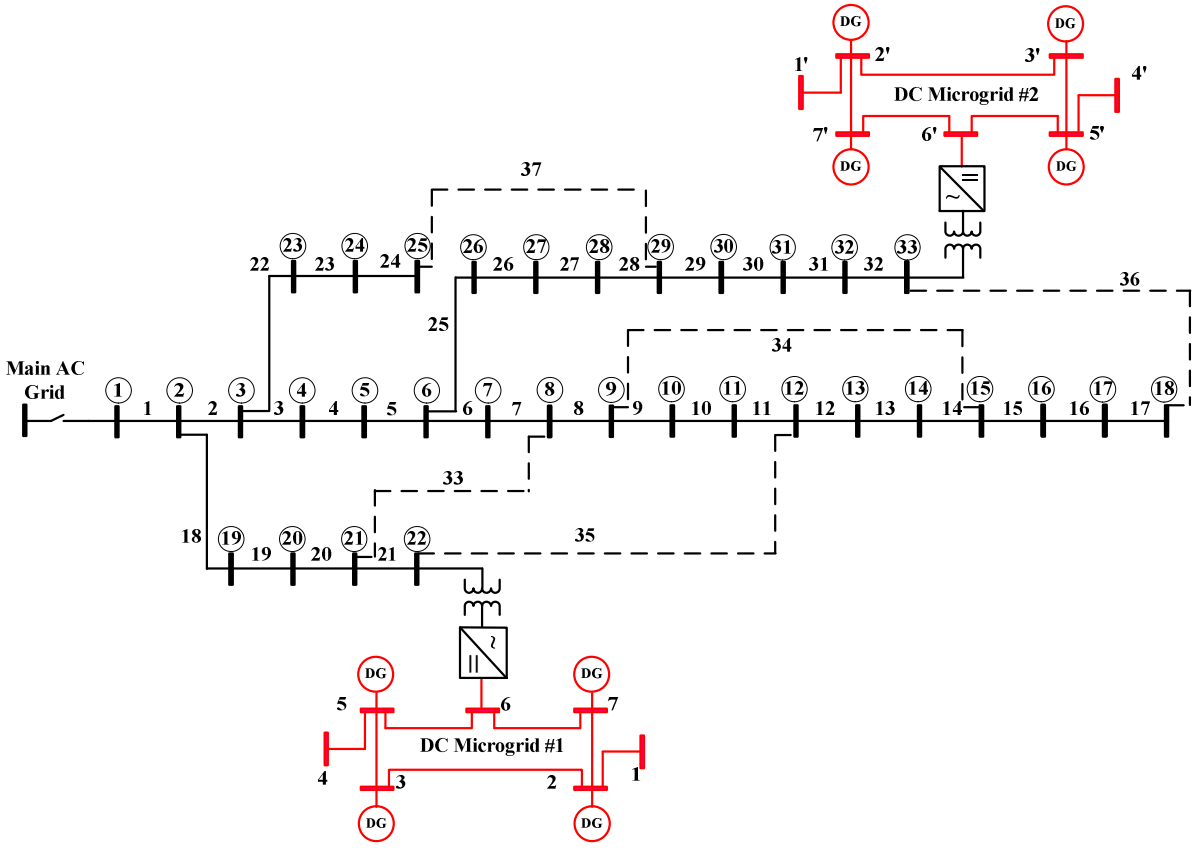

Figure 6.4: 33-bus distribution test system with additional tie switches

Table 6.3: DG settings in p.u. with all the system switches are close

DG #	ω_i^*	$V_{ac,i}^*$
1	1.0152	1.5322
2	1.0152	1.5495
7	1.0152	1.5075

DG #	$V_{dc,Pi}^*$	DG #	$V_{dc,Pi}^*$
1	1.1236	5	1.1235
2	1.1246	6	1.1246
3	1.1229	7	1.1228
4	1.1240	8	1.1240

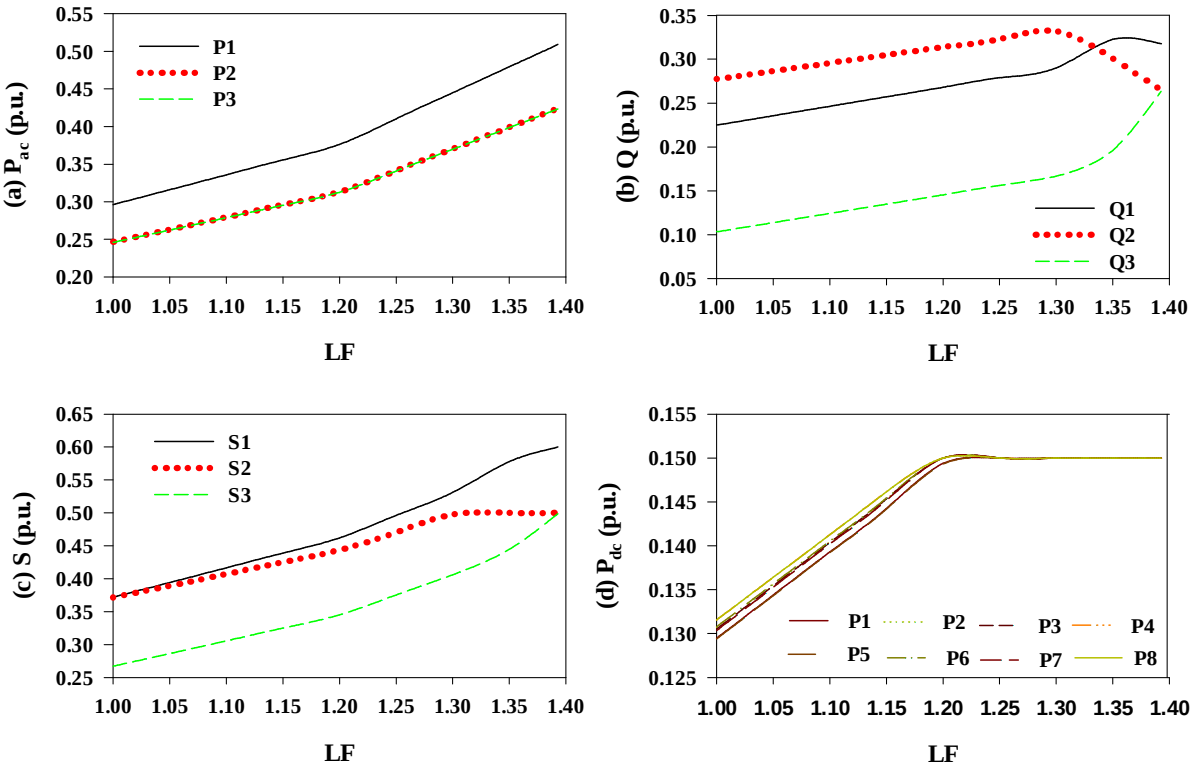

Figure 6.5: DG output with system reconfiguration: (a) AC-DG active power, (b) AC-DG reactive power, AC-DG apparent power and (b) DC-DG active power

6.6 Discussion

In this chapter the steady-state modeling of the DG units is employed to investigate the effect of DG settings and system reconfiguration on the overall system loadability level. The results demonstrate that adjusting the DG settings could increase the system loadability by 8%, while augmenting the microgrid with the reconfiguring capability could add further increase by 1.4% to the system loadability. These results comply with the effectiveness of both approaches on the LIB of ADNs.

Chapter 7
Summary, Contributions, and Future Work

7.1 Summary and Conclusions

The primary goal of the work presented in this thesis was to establish a discipline framework that would allow the seamless integration of dc microgrids into an ADN paradigm. To this end, numerous technical challenges associated with dc microgrids have been addressed and novel control algorithms and steady-state analysis tools have been developed. A detailed summary of the main studies conducted in this research are highlighted below.

Based on the review contained in chapter 2, the work published in the literature has fallen short with respect to addressing the voltage regulation issues inherent in grid-connected DCDSs. A comprehensive study was therefore conducted in chapter 3 to highlight the critical role of IC voltage and DG power in shaping the voltage profile of a system. A distributed control algorithm has been developed that can dynamically adjust the IC voltage setting. The proposed algorithm has been extended with the addition of a second stage that optimally curtails the DG output power if the IC fails to maintain the entire system voltage within permissible limits. To enable consideration of different DCDS operational perspectives, two curtailment strategies have been devised. The first results in an equal curtailment ratio of DG units, a non-cooperative strategy appropriate for a discrete ownership scenario, whereas the second maximizes overall revenue, a cooperative strategy suitable for a single ownership scenario. The convergence characteristics of both strategies have been verified mathematically, and their effectiveness and robustness have been validated through their application in several case studies.

Chapter 4 has provided a discussion of a number of power management studies previously proposed for islanded dc microgrids; however, the work performed was based on either centralized control algorithms, which entail an expensive communication infrastructure, or distributed control algorithms, which are applicable only for very limited situations. Two new distributed power management schemes have therefore been introduced, which are based on consensus theory and are compatible with different operational strategies in the context of islanded dc microgrids. The first

scheme is directed at increasing system reliability through precise sharing of equal power among the DG units. The second scheme minimizes operational costs through the optimal dispatch of the units. As a byproduct improvement in the power quality of the system, the proposed schemes provide additional enhancement of the system voltage profile. Since the schemes rely on mathematical approaches, their stability and convergence was proven analytically, and their efficacy was successfully demonstrated through real-time OPAL-RT simulations in a hardware-in-the-loop (HIL) application.

As explained in chapter 5, the operational philosophy for islanded hybrid ac/dc microgrids entails a convenient steady-state tool for analyzing such an evolving paradigm. Unlike conditions in grid-connected networks, in a islanded hybrid microgrid, the ac frequency and the dc voltage are variables that are coupled through ICs. This operational feature imposes further complexity that adds to that created by the absence of a slack bus within the entire network. A novel power flow algorithm was therefore developed in order to incorporate different DG unit and IC operating modes. To reduce problem complexity, the algorithm has been designed to be sequential, i.e., to solve separately for each ac and dc subgrid. However, the coupling between the ac frequency and dc voltage is considered by means of the adaptation of the IC model during the algorithm iterations. The proposed algorithm relies on the Newton-Raphson method, which solves the load flow problem for the ac and dc subgrids accurately but with a reduced computational cost. The accuracy of the algorithm has been validated with the use of detailed time-domain simulations using PSCAD/EMTDC. Its robustness and high rate of convergence compare favourably with those of conventional and unified power flow algorithms.

Finally, the proposed steady-state modeling approach of the ac/dc microgrids was employed in optimum configuration analysis in chapter 6. The study has highlighted the effect of DG droop adjustment and topological structure reconfiguration in the system loadability margin.

7.2 Contributions

The primary contributions of the work presented in this thesis can be summarized as follows:

1. DCDS voltage regulation problems have been demonstrated and established, and effective voltage control algorithms have accordingly been introduced as a means of enhancing the system voltage profile through the optimal adjustment of both the IC voltage setting and the DG output power.

2. Distributed and robust power management algorithms have been developed in order to increase the reliability, reduce the operational cost, and improve the voltage profile of islanded dc microgrids.

3. Conventional power flow algorithms have been examined and proven to be unsuitable for performing steady-state analysis in the context of islanded hybrid ac/dc microgrids. An efficient power flow algorithm that provides precise modelling of hybrid distribution networks operating in islanded mode has therefore been developed.

4. The optimum configuration of hybrid ac/dc microgrids has been investigated through formulating an OPF problem. Two configuration approaches have been considered, namely, DG droop settings and system structural topology, in order to serve maximum load demand in the islanded mode of operation.

7.3 Direction of Future Work

Building on the results presented in this thesis, the following areas are suggested for future exploration:

1. Development of a generic planning formulation for new distribution systems: Based on such a planning model, ac and dc subgrids could be defined within a hybrid ac/dc paradigm. The size of the distributed generation and the energy storage systems could also be allocated for each zone along with the capacity of the ICs between zones of different types.

2. Investigation of optimum droop settings that achieve optimal load flow criteria in islanded hybrid ac/dc microgrids: In that context, numerous studies could be conducted with a view to increasing system reliability by enhancing system fault rejection capability, or with the goal of reducing the operational cost of the system through the optimal dispatch of the DG units.

3. Studies for identifying the optimum reconfiguration of islanded hybrid ac/dc microgrids: Such work could examine a variety of operational perspectives that include minimizing switching and fuel costs and enhancing the system voltage profile.

Bibliography

[1] T.-F. Wu, C.-H. Chang, L.-C. Lin, G.-R. Yu, and Y.-R. Chang, "DC-Bus Voltage Control With a Three-Phase Bidirectional Inverter for DC Distribution Systems," *IEEE Trans. Power Electron.*, vol. 28, no. 4, pp. 1890–1899, Apr. 2013.

[2] "Biomass-to-Fuel-Cell Power For Renewable Distributed Power Generation," 2013. [Online]. Available: http://www.ballard.com/files/PDF/White_Papers/Biomass_to_FC_Power_-_White_Paper_-_Feb_2013.pdf.

[3] E. Jung, H. Yoo, S.-K. Sul, H.-S. Choi, and Y.-Y. Choi, "A Nine-Phase Permanent-Magnet Motor Drive System for an Ultrahigh-Speed Elevator," *IEEE Trans. Ind. Appl.*, vol. 48, no. 3, pp. 987–995, May 2012.

[4] X. She, A. Q. Huang, S. Lukic, and M. E. Baran, "On Integration of Solid-State Transformer With Zonal DC Microgrid," *IEEE Trans. Smart Grid*, vol. 3, no. 2, pp. 975–985, Jun. 2012.

[5] Y. Liu, A. Pratt, P. Kumar, M. Xu, and F. C. Lee, "390V Input VRM for High Efficiency Server Power Architecture," in *APEC 07 - Twenty-Second Annual IEEE Applied Power Electronics Conference and Exposition*, 2007, pp. 1619–1624.

[6] G. AlLee and W. Tschudi, "Edison Redux: 380 Vdc Brings Reliability and Efficiency to Sustainable Data Centers," *IEEE Power Energy Mag.*, vol. 10, no. 6, pp. 50–59, Nov. 2012.

[7] P. Kankanala, S. C. Srivastava, A. K. Srivastava, and N. N. Schulz, "Optimal Control of Voltage and Power in a Multi-Zonal MVDC Shipboard Power System," *IEEE Trans. Power Syst.*, vol. 27, no. 2, pp. 642–650, May 2012.

[8] W. Jiang, S. Member, B. Fahimi, and S. Member, "Active Current Sharing and Source Management in Fuel Cell – Battery Hybrid Power System," vol. 57, no. 2, pp. 752–761, 2010.

[9] M. E. Baran and I. M. El-Markabi, "A Multiagent-Based Dispatching Scheme for Distributed Generators for Voltage Support on Distribution Feeders," *IEEE Trans. Power Syst.*, vol. 22, no. 1, pp. 52–59, Feb. 2007.

[10] B. A. Robbins, C. N. Hadjicostis, and A. D. Dominguez-Garcia, "A Two-Stage Distributed Architecture for Voltage Control in Power Distribution Systems," *IEEE Trans. Power Syst.*, vol. 28, no. 2, pp. 1–13, 2013.

[11] H. E. Farag, E. F. El-Saadany, and R. Seethapathy, "A Two Ways Communication-Based Distributed Control for Voltage Regulation in Smart Distribution Feeders," *IEEE Trans. Smart Grid*, vol. 3, no. 1, pp. 271–281, Mar. 2012.

[12] H. E. Z. Farag and E. F. El-Saadany, "A Novel Cooperative Protocol for Distributed Voltage Control in Active Distribution Systems," *IEEE Trans. Power Syst.*, vol. 28, no. 2, pp. 1–1, May 2013.

[13] M. E. Elkhatib, R. El Shatshat, and M. M. A. Salama, "Decentralized Reactive Power Control for Advanced Distribution Automation Systems," *IEEE Trans. Smart Grid*, vol. 3, no. 3, pp. 1482–1490, Sep. 2012.

[14] A. Zidan and E. F. El-Saadany, "A Cooperative Multiagent Framework for Self-Healing Mechanisms in Distribution Systems," *IEEE Trans. Smart Grid*, vol. 3, no. 3, pp. 1525–1539, Sep. 2012.

[15] T. Logenthiran, D. Srinivasan, A. M. Khambadkone, and H. N. Aung, "Multiagent System for Real-Time Operation of a Microgrid in Real-Time Digital Simulator," *IEEE Trans. Smart Grid*, vol. 3, no. 2, pp. 925–933, Jun. 2012.

[16] H. Liang, B. J. Choi, A. Abdrabou, W. Zhuang, and X. S. Shen, “Decentralized Economic Dispatch in Microgrids via Heterogeneous Wireless Networks,” *IEEE J. Sel. Areas Commun.*, vol. 30, no. 6, pp. 1061–1074, Jul. 2012.

[17] S. Martinez, “On Distributed Convex Optimization Under Inequality and Equality Constraints,” *IEEE Trans. Automat. Contr.*, vol. 57, no. 1, pp. 151–164, Jan. 2012.

[18] E. Seneta, *Non-negative Matrices and Markov Chains*. New York, NY: Springer New York, 1981.

[19] C. Godsil and G. F. Royle, *Algebraic Graph Theory*. Springer, 2001.

[20] A. Nedic, A. Olshevsky, A. Ozdaglar, and J. N. Tsitsiklis, “On Distributed Averaging Algorithms and Quantization Effects,” *IEEE Trans. Automat. Contr.*, vol. 54, no. 11, pp. 2506–2517, Nov. 2009.

[21] A. Nedic, A. Ozdaglar, and P. A. Parrilo, “Constrained Consensus and Optimization in Multi-Agent Networks,” *IEEE Trans. Automat. Contr.*, vol. 55, no. 4, pp. 922–938, Apr. 2010.

[22] H. Yang, D. Yi, J. Zhao, and Z. Dong, “Distributed Optimal Dispatch of Virtual Power Plant via Limited Communication,” *IEEE Trans. Power Syst.*, vol. 28, no. 3, pp. 3511–3512, Aug. 2013.

[23] S. Bolognani and S. Zampieri, “A Distributed Control Strategy for Reactive Power Compensation in Smart Microgrids,” *IEEE Trans. Automat. Contr.*, vol. PP, no. 11, pp. 1–1, Nov. 2013.

[24] J.-H. Choi and J.-C. Kim, “The online voltage control of ULTC transformer for distribution voltage regulation,” *Int. J. Electr. Power Energy Syst.*, vol. 23, no. 2, pp. 91–98, Feb. 2001.

[25] M. E. Elkhatib, R. El Shatshat, and M. M. A. Salama, “Optimal Control of Voltage Regulators for Multiple Feeders,” *IEEE Trans. Power Deliv.*, vol. 25, no. 4, pp. 2670–2675, Oct. 2010.

[26] J. Beerten and R. Belmans, “Analysis of Power Sharing and Voltage Deviations in Droop-Controlled DC Grids,” *IEEE Trans. Power Syst.*, vol. PP, no. 99, pp. 1–10, 2013.

[27] L. Yu, D. Czarkowski, and F. de Leon, “Optimal Distributed Voltage Regulation for Secondary Networks With DGs,” *IEEE Trans. Smart Grid*, vol. 3, no. 2, pp. 959–967, Jun. 2012.

[28] R. Tonkoski, L. A. C. Lopes, and T. H. M. El-Fouly, “Coordinated Active Power Curtailment of Grid Connected PV Inverters for Overvoltage Prevention,” *IEEE Trans. Sustain. Energy*, vol. 2, no. 2, pp. 139–147, Apr. 2011.

[29] G. W. Ault, R. A. F. Currie, and J. R. McDonald, “Active power flow management solutions for maximising DG connection capacity,” in *2006 IEEE Power Engineering Society General Meeting*, 2006, p. 5 pp.

[30] S. Gill, I. Kockar, and G. W. Ault, “Dynamic Optimal Power Flow for Active Distribution Networks,” *IEEE Trans. Power Syst.*, vol. PP, no. 99, pp. 1–11, 2013.

[31] D. Chen, L. Xu, and L. Yao, “DC Voltage Variation Based Autonomous Control of DC Microgrids,” *IEEE Trans. Power Deliv.*, vol. 28, no. 2, pp. 637–648, Apr. 2013.

[32] J. M. Guerrero, J. C. Vasquez, J. Matas, L. G. de Vicuna, and M. Castilla, “Hierarchical Control of Droop-Controlled AC and DC Microgrids—A General Approach Toward Standardization,” *IEEE Trans. Ind. Electron.*, vol. 58, no. 1, pp. 158–172, Jan. 2011.

[33] M. E. Elkhatib, R. El-Shatshat, and M. M. A. Salama, “Novel Coordinated Voltage Control for Smart Distribution Networks With DG,” *IEEE Trans. Smart Grid*, vol. 2, no. 4, pp. 598–605, Dec. 2011.

[34] S. Anand, B. G. Fernandes, and J. Guerrero, “Distributed Control to Ensure Proportional Load Sharing and Improve Voltage Regulation in Low-Voltage DC Microgrids,” *IEEE Trans. Power Electron.*, vol. 28, no. 4, pp. 1900–1913, Apr. 2013.

[35] T. M. Haileselassie and K. Uhlen, “Impact of DC Line Voltage Drops on Power Flow of MTDC Using Droop Control,” *IEEE Trans. Power Syst.*, vol. 27, no. 3, pp. 1441–1449, Aug. 2012.

[36] X. Lu, J. Guerrero, K. Sun, and J. Vasquez, “An Improved Control Method for DC Microgrids Based on Low Bandwidth Communication with DC Bus Voltage Restoration and Enhanced Current Sharing Accuracy,” *IEEE Trans. Power Electron.*, vol. PP, no. 99, pp. 1–1, 2013.

[37] W. J. Dally and B. P. Towles, *Principles and Practices of Interconnection Networks (The Morgan Kaufmann Series in Computer Architecture and Design)*. Morgan Kaufmann, 2004.

[38] X. Yu, X. She, X. Zhou, and A. Q. Huang, “Power Management for DC Microgrid Enabled by Solid-State Transformer,” *IEEE Trans. Smart Grid*, vol. PP, no. 99, pp. 1–12, 2013.

[39] C. Jin, P. Wang, J. Xiao, Y. Tang, and F. H. CHOO, “Implementation of Hierarchical Control in DC Microgrids,” *IEEE Trans. Ind. Electron.*, vol. PP, no. 99, pp. 1–1, 2013.

[40] T. Dragicevic, J. M. Guerrero, J. C. Vasquez, and D. Skrlec, “Supervisory Control of an Adaptive-Droop Regulated DC Microgrid With Battery Management Capability,” *IEEE Trans. Power Electron.*, vol. 29, no. 2, pp. 695–706, Feb. 2014.

[41] X. Yu, X. She, X. Ni, and A. Q. Huang, “System Integration and Hierarchical Power Management Strategy for a Solid-State Transformer Interfaced Microgrid System,” *IEEE Trans. Power Electron.*, vol. PP, no. 99, pp. 1–1, Aug. 2013.

[42] S. Jung, H. Lee, C. S. Song, J.-H. Han, W.-K. Han, and G. Jang, “Optimal Operation Plan of the Online Electric Vehicle System Through Establishment of a DC Distribution System,” *IEEE Trans. Power Electron.*, vol. 28, no. 12, pp. 5878–5889, Dec. 2013.

[43] X. Li, C. Wang, L. Guo, and Y. Li, “A nonlinear disturbance observer based DC bus voltage control for a hybrid AC/DC microgrid,” in *2013 IEEE Energy Conversion Congress and Exposition*, 2013, pp. 1655–1662.

[44] X. Liu, P. Wang, and P. C. Loh, “A Hybrid AC/DC Microgrid and Its Coordination Control,” *IEEE Trans. Smart Grid*, vol. 2, no. 2, pp. 278–286, Jun. 2011.

[45] X. Lu, J. M. Guerrero, K. Sun, J. C. Vasquez, R. Teodorescu, and L. Huang, “Hierarchical Control of Parallel AC-DC Converter Interfaces for Hybrid Microgrids,” *IEEE Trans. Smart Grid*, vol. PP, no. 99, pp. 1–10, 2013.

[46] P. C. Loh, D. Li, Y. K. Chai, and F. Blaabjerg, “Autonomous Operation of Hybrid Microgrid With AC and DC Subgrids,” *IEEE Trans. Power Electron.*, vol. 28, no. 5, pp. 2214–2223, May 2013.

[47] N. Eghtedarpour and E. Farjah, “Power Control and Management in a Hybrid AC/DC Microgrid,” *IEEE Trans. Smart Grid*, vol. 5, no. 3, pp. 1494–1505, May 2014.

[48] P. C. Loh, D. Li, Y. K. Chai, and F. Blaabjerg, “Autonomous Control of Interlinking Converter With Energy Storage in Hybrid AC–DC Microgrid,” *IEEE Trans. Ind. Appl.*, vol. 49, no. 3, pp. 1374–1382, May 2013.

[49] M. M. A. Abdelaziz, H. E. Farag, E. F. El-Saadany, and Y. A.-R. I. Mohamed, “A Novel and Generalized Three-Phase Power Flow Algorithm for Islanded Microgrids Using a Newton Trust Region Method,” *IEEE Trans. Power Syst.*, vol. 28, no. 1, pp. 190–201, Feb. 2013.

[50] A. Elrayyah, Y. Sozer, and M. E. Elbuluk, “A Novel Load-Flow Analysis for Stable and Optimized Microgrid Operation,” *IEEE Trans. Power Deliv.*, vol. 29, no. 4, pp. 1709–1717, Aug. 2014.

[51] W. Wang and M. Barnes, “Power Flow Algorithms for Multi-Terminal VSC-HVDC With Droop Control,” *IEEE Trans. Power Syst.*, vol. 29, no. 4, pp. 1721–1730, Jul. 2014.

[52] J. Beerten, S. Cole, and R. Belmans, “Generalized Steady-State VSC MTDC Model for Sequential AC/DC Power Flow Algorithms,” *IEEE Trans. Power Syst.*, vol. 27, no. 2, pp. 821–829, May 2012.

[53] C. Li, S. K. Chaudhary, J. C. Vasquez, and J. M. Guerrero, “Power flow analysis for droop controlled LV hybrid AC-DC microgrids with virtual impedance,” in *2014 IEEE PES General Meeting* |

Conference & Exposition, 2014, pp. 1–4.

[54] A. A. Hamad, H. E. Farag, and E. F. El-Saadany, "A Novel Multiagent Control Scheme for Voltage Regulation in DC Distribution Systems," *IEEE Trans. Sustain. Energy*, vol. 6, no. 2, pp. 534–545, Apr. 2015.

[55] A. I. Hamad, H. E. Farag, and E. F. El-Saadany, "A distributed control scheme for voltage regulation in DC distribution systems," in *2014 IEEE PES General Meeting | Conference & Exposition*, 2014, pp. 1–5.

[56] S. X. Chen, H. B. Gooi, and M. Q. Wang, "Sizing of Energy Storage for Microgrids," *IEEE Trans. Smart Grid*, vol. 3, no. 1, pp. 142–151, Mar. 2012.

[57] J. Grainger and J. . W. Stevenson, *Power System Analysis*. McGraw-Hill Science/Engineering/Math, 1994.

[58] Z. Hu and F. Li, "Cost-Benefit Analyses of Active Distribution Network Management, Part I: Annual Benefit Analysis," *IEEE Trans. Smart Grid*, vol. 3, no. 3, pp. 1067–1074, Sep. 2012.

[59] Y. Ueda, K. Kurokawa, T. Tanabe, K. Kitamura, and H. Sugihara, "Analysis Results of Output Power Loss Due to the Grid Voltage Rise in Grid-Connected Photovoltaic Power Generation Systems," *IEEE Trans. Ind. Electron.*, vol. 55, no. 7, pp. 2744–2751, Jul. 2008.

[60] S.-J. Ahn, S.-R. Nam, J.-H. Choi, and S.-I. Moon, "Power Scheduling of Distributed Generators for Economic and Stable Operation of a Microgrid," *IEEE Trans. Smart Grid*, vol. 4, no. 1, pp. 398–405, Mar. 2013.

[61] S. P. Boyd and L. Vandenberghe, *Convex Optimization*. Cambridge University Press, 2004.

[62] R. G. Bartle and D. R. Sherbert, *Introduction to Real Analysis, 4th Edition*. John Wiley & Sons, 2011.

[63] J. A. Jardini, C. M. V. Tahan, M. R. Gouvea, S. U. Ahn, and F. M. Figueiredo, "Daily load profiles for residential, commercial and industrial low voltage consumers," *IEEE Trans. Power Deliv.*, vol. 15, no. 1, pp. 375–380, 2000.

[64] P. Nuutinen, P. Peltoniemi, and P. Silventoinen, "Short-Circuit Protection in a Converter-Fed Low-Voltage Distribution Network," *IEEE Trans. Power Electron.*, vol. 28, no. 4, pp. 1587–1597, Apr. 2013.

[65] M. Shahidehpour, "DC Microgrids: Economic Operation and Enhancement of Resilience by Hierarchical Control," *IEEE Trans. Smart Grid*, vol. 5, no. 5, pp. 2517–2526, Sep. 2014.

[66] "FIT/microFIT PRICE SCHEDULE (August 26, 2013)." [Online]. Available: http://microfit.powerauthority.on.ca/sites/default/files/2013-FIT-Price-Schedule-Tables.pdf.

[67] Y. Xu, W. Zhang, W. Liu, X. Wang, F. Ferrese, C. Zang, and H. Yu, "Distributed Subgradient-Based Coordination of Multiple Renewable Generators in a Microgrid," *IEEE Trans. Power Syst.*, vol. 29, no. 1, pp. 23–33, Jan. 2014.

[68] S. Anand and B. G. Fernandes, "Reduced-Order Model and Stability Analysis of Low-Voltage DC Microgrid," *IEEE Trans. Ind. Electron.*, vol. 60, no. 11, pp. 5040–5049, Nov. 2013.

[69] A. A. Hamad, M. A. Azzouz, and E. F. El-Saadany, "Multiagent Supervisory Control for Power Management in DC Microgrids," *IEEE Trans. Smart Grid*, vol. 7, no. 2, pp. 1057–1068, 2016.

[70] A. A. Hamad and E. F. El-Saadany, "Multi-agent supervisory control for optimal economic dispatch in DC microgrids," *Sustain. Cities Soc.*, Mar. 2016.

[71] N. Pogaku, M. Prodanovic, and T. C. Green, "Modeling, Analysis and Testing of Autonomous Operation of an Inverter-Based Microgrid," *IEEE Trans. Power Electron.*, vol. 22, no. 2, pp. 613–625, Mar. 2007.

[72] Y. Mohamed and E. F. El-Saadany, "Adaptive Decentralized Droop Controller to Preserve Power Sharing Stability of Paralleled Inverters in Distributed Generation Microgrids," *IEEE Trans. Power Electron.*, vol. 23, no. 6, pp. 2806–2816, Nov. 2008.

[73] K. Fleischer and R. S. Munnings, "Power systems analysis for direct current (DC) distribution systems," *IEEE Trans. Ind. Appl.*, vol. 32, no. 5, pp. 982–989, 1996.

[74] Y. Kako, "Multi-Factor Aging of Insulation Systems - Infinite Sequential Stressing Method -," *IEEE Trans. Electr. Insul.*, vol. EI-21, no. 6, pp. 913–917, Dec. 1986.

[75] R. Mudumbai, S. Dasgupta, and B. B. Cho, "Distributed Control for Optimal Economic Dispatch of a Network of Heterogeneous Power Generators," *IEEE Trans. Power Syst.*, vol. 27, no. 4, pp. 1750–1760, Nov. 2012.

[76] G. Binetti, A. Davoudi, F. L. Lewis, D. Naso, and B. Turchiano, "Distributed Consensus-Based Economic Dispatch With Transmission Losses," *IEEE Trans. Power Syst.*, vol. 29, no. 4, pp. 1711–1720, Jul. 2014.

[77] J. Zhu, *Optimization of Power System Operation (IEEE Press Series on Power Engineering)*. Wiley-IEEE Press, 2009.

[78] A. Yamane, J. Belanger, T. Ise, I. Iyoda, T. Aizono, and C. Dufour, "A Smart Distribution Grid Laboratory," in *IECON 2011 - 37th Annual Conference of the IEEE Industrial Electronics Society*, 2011, pp. 3708–3712.

[79] O. Crăciun, A. Florescu, I. Munteanu, A. I. Bratcu, S. Bacha, and D. Radu, "Hardware-in-the-loop simulation applied to protection devices testing," *Int. J. Electr. Power Energy Syst.*, vol. 54, pp. 55–64, Jan. 2014.

[80] C. Dufour and J. Belanger, "On the Use of Real-Time Simulation Technology in Smart Grid Research and Development," *IEEE Trans. Ind. Appl.*, vol. PP, no. 99, pp. 1–1, 2014.

[81] S. T. Cady, A. D. Dominguez-Garcia, and C. N. Hadjicostis, "Robust implementation of distributed algorithms for control of distributed energy resources," in *2011 North American Power Symposium*, 2011, pp. 1–5.

[82] A. A. Hamad, M. A. Azzouz, and E. F. El Saadany, "A Sequential Power Flow Algorithm for Islanded Hybrid AC/DC Microgrids," *IEEE Trans. Power Syst.*, vol. PP, no. 99, pp. 1–10, 2015.

[83] M. El-marsafawy and R. Mathur, "A New, Fast Technique for Load-Flow Solution of Integrated Multi-Terminal DC/AC Systems," *IEEE Trans. Power Appar. Syst.*, vol. PAS-99, no. 1, pp. 246–255, Jan. 1980.

[84] P. C. Loh, D. Li, Y. K. Chai, and F. Blaabjerg, "Hybrid AC–DC Microgrids With Energy Storages and Progressive Energy Flow Tuning," *IEEE Trans. Power Electron.*, vol. 28, no. 4, pp. 1533–1543, Apr. 2013.

[85] Kundur, *Power System Stability And Control*. 1994.

[86] D. Salomonsson and A. Sannino, "Load modelling for steady-state and transient analysis of low-voltage DC systems," *IET Electr. Power Appl.*, vol. 1, no. 5, p. 690, 2007.

[87] G. Daelemans, "VSC HVDC in meshed networks," Katholieke Universiteit Leuven, Leuven, Belgium, 2008.

[88] H. Mohsenian-Rad and A. Davoudi, "Towards Building an Optimal Demand Response Framework for DC Distribution Networks," *IEEE Trans. Smart Grid*, vol. 5, no. 5, pp. 2626–2634, Sep. 2014.

[89] D. Singh, R. K. Misra, and D. Singh, "Effect of Load Models in Distributed Generation Planning," *IEEE Trans. Power Syst.*, vol. 22, no. 4, pp. 2204–2212, Nov. 2007.

[90] A. Messac, *Optimization in Practice with MATLAB*. Cambridge University Press, 2015.

[91] M. M. A. Abdelaziz, M. F. Shaaban, H. E. Farag, and E. F. El-Saadany, "A Multistage Centralized Control Scheme for Islanded Microgrids With PEVs," *IEEE Trans. Sustain. Energy*, vol. 5, no. 3, pp. 927–937, Jul. 2014.

[92] W. Rosehart, C. Roman, and A. Schellenberg, "Optimal Power Flow With Complementarity Constraints," *IEEE Trans. Power Syst.*, vol. 20, no. 2, pp. 813–822, May 2005.

[93] R. S. Al Abri, E. F. El-Saadany, and Y. M. Atwa, "Optimal Placement and Sizing Method to Improve the Voltage Stability Margin in a Distribution System Using Distributed Generation," *IEEE Trans. Power Syst.*, vol. 28, no. 1, pp. 326–334, Feb. 2013.

[94] M. M. A. Abdelaziz, H. E. Farag, and E. F. El-Saadany, "Optimum Reconfiguration of Droop-Controlled Islanded Microgrids," *IEEE Trans. Power Syst.*, vol. 31, no. 3, pp. 2144–2153, May 2016.

[95] J. J. Moré and D. C. Sorensen, "Computing a Trust Region Step," *SIAM J. Sci. Stat. Comput.*, vol. 4, no. 3, pp. 553–572, Sep. 1983.

[96] J. Nocedal and S. J. Wright, Eds., *Numerical Optimization*. New York: Springer-Verlag, 1999.

Appendix A

Data of Test Networks

The per unit data for commercial and residential loads, PV and wind power profiles are illustrated as follows:

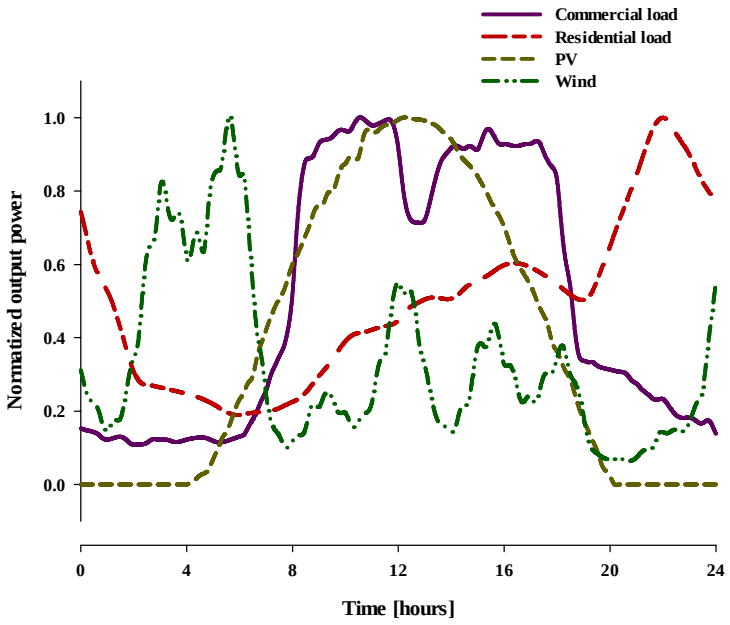

Figure A. 1: Load and generation profiles

The data of the test system shown in Figure 3.6 are given as follows:

Table A 1: Four feed test system data

Feeder	Total resistance R_{Line} [p.u.]	Total load P [p.u.]
#1	0.1080	0.4
#2	0.0880	0.5
#3	0.1374	0.3
#4	0.0945	0.45

Appendix B

Relation between Load and Generation Current Change with System Voltage Variation

The constant power load (CPL) can be modeled by current source (i_{cpl}) in parallel with negative resistance (r_{cpl}) that depend on the load power and terminal voltage (v) [40], [68]. The current source and resistance model can be converted to the equivalent voltage source and resistance model, as shown in Figure B. 1. The constant power model is similar to the very common DG model shown in Figure B. 2, in which the DG droop gain (r) is represented in terms of its per unit value ($r_{p.u.}$).

Considering same rating DG unit and CPL load operating at the nominal voltage:

$$p^r = p_{cpl} \qquad for \qquad v = v^{nom} \tag{B.1}$$

Under the same change in the terminal voltage (Δv), the change in the CPL current relative to that in the DG can be given by

$$\Delta i_L = r_{p.u.} \Delta i_g \tag{B.2}$$

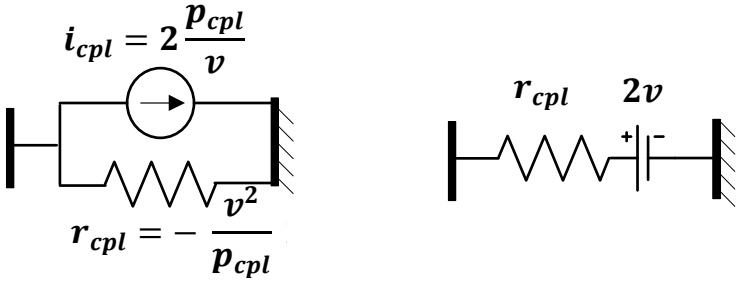

Figure B. 1: Linearized mode of CPL load

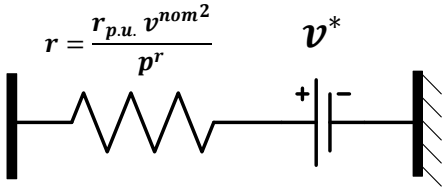

Figure B. 2: DG model

Typically $r_{p.u.}$ is small and around (%5) [35], thus the change in the load current with respect to the change in the DG current can be neglected. Similar analysis can be carried out in case of constant resistance loads.

Appendix C
Convergence of DEIC Algorithm

For a set of DG units that update their output power based on (4.35), the condition expressed in (4.36) must be satisfied, guaranteeing the convergence to λ_{avg} after a sufficient number of supervisory iterations. According to (4.31) and (4.35), λ_u and λ_{avg} can be determined after the first supervisory control cycle as

$$\lambda_u[1] = \lambda_u[0] + \frac{c_u\,(\lambda_{avg}[0] - \lambda_u[0])}{c_{max}} \tag{C.1}$$

$$\lambda_{avg}[1] = \lambda_{avg}[0] + \frac{\sum_{j\in\rho} c_j(\lambda_{avg}[0] - \lambda_j[0])}{|\rho|\,c_{max}} \tag{C.2}$$

Let d_u be defined for each agent, which represents the difference between λ_{avg} and λ_u, as follows:

$$d_u[0] = \lambda_{avg}[0] - \lambda_u[0] \tag{C.3}$$

After the first supervisory cycle, d_u can thus be given by

$$d_u[1] = d_u[0] + \frac{\sum_{j\in\rho} c_j\, d_j[0]}{|\rho| c_{max}} - \frac{c_u\, d_u[0]}{c_{max}} \tag{C.4}$$

For all agents $u \in \rho$, (B.4) can be generalized in a matrix form as

$$D[1] = A\,D[0] \tag{C.5}$$

where

$$D = [d_1 \quad d_2 \quad \cdots \quad d_{|\rho|}]^T \tag{C.6}$$

$$A = \begin{bmatrix} \left(1 - \frac{(|\rho|-1)c_1}{|\rho|\,c_{max}}\right) & \frac{c_2}{|\rho|\,c_{max}} & \cdots & \frac{c_{|\rho|}}{|\rho|\,c_{max}} \\ \frac{c_1}{|\rho|\,c_{max}} & \left(1 - \frac{(|\rho|-1)c_2}{|\rho|\,c_{max}}\right) & \cdots & \frac{c_{|\rho|}}{|\rho|\,c_{max}} \\ \vdots & \vdots & \ddots & \vdots \\ \frac{c_1}{|\rho|\,c_{max}} & \frac{c_2}{|\rho|\,c_{max}} & \cdots & \left(1 - \frac{(|\rho|-1)c_{|\rho|}}{|\rho|\,c_{max}}\right) \end{bmatrix} \tag{C.7}$$

After h supervisory cycles:

$$D[h] = A^h \, D[0] \tag{C.8}$$

Matrix A is primitive and column stochastic. The permittivity is directly inferred since all elements are strictly positive, which is governed by (4.36). The column stochastic property is fulfilled since the summation of any of its columns equals one. These two characteristics lead to

$$\lim_{h \to \infty} d_u[h] = o_u \sum_j d_j[0] = 0 \tag{C.9}$$

where o_u is constant, which implies that, after sufficient h supervisory cycles, all DG units will have the same $\lambda_u[h] = \lambda_{avg}$, provided that (4.36) is fulfilled.

Appendix D
Unified Newton Trust Region

Newton trust region method is a general mathematical tool, belonging to the gradient descent family, for solving a set of nonlinear equations. According to this method, a set of nonlinear equations, modelling the steady-state behavior of different component of islanded hybrid microgrid in our case, are formulated as an minimization problem:

$$min \begin{cases} F_1(X) = f_1(X) - A_1 = 0 \\ F_2(X) = f_2(X) - A_2 = 0 \\ \vdots \\ F_i(X) = f_i(X) - A_i = 0 \\ \vdots \\ F_n(X) = f_n(X) - A_n = 0 \end{cases} \quad \text{(D.1)}$$

where $F_i(X)(i = 1,2, \dots, n)$ is the set of the nonlinear functions describing the system; $f_i(X)$ and A_i are the variable dependent and independent terms, respectively; and n is the number of power flow unknowns. The system power flow variables are presented based on an initial guess X_0. After each iteration, the system variables are updated by Δ_k that guarantees $F_i(X_k + \Delta_k) < F_i(X_k)$. In order to calculate Δ_k, the original function $F_i(X_k)$.is represented by a simpler quadratic model $\tilde{F}_{i|k}(X_k)$ that has a similar behavior around X_k:

$$\tilde{F}_{i|k}(\Delta_k). = F_i(X_k) + \Delta_k^T \nabla F_i(X_k) + \frac{1}{2} \Delta_k^T \nabla^2 F_i(X_k) \Delta_k \quad \text{(D.2)}$$

where $\nabla F_i(X_k)$ and $\nabla^2 F_i(X_k)$ are the gradient and Hessian of F_i at X_k . The behavior of the model function $\tilde{F}_{i|k}(\Delta_k)$ is only trusted to match the original function $F_i(X_k)$ in a region r_k around X_k. Thus, the step Δ_k can be calculated as the minimizer of $\tilde{F}_{i|k}$ within the region r_k:

$$min\, \tilde{F}_{i|k}(\Delta_k) \quad \text{(D.3a)}$$

$$subject\ to\ \|\Delta_k\| < \varsigma_k \quad \text{(D.3b)}$$

The trust region radius ς_k is a flexible boundary which is updated after each iteration according to the behavior of the model function $\tilde{F}_{i|k}$. The update is evaluated by calculating a comparison ratio γ_k defined as

$$\gamma_k = \frac{F_i(X_k) - F_i(X_k + \Delta_k)}{\tilde{F}_{i|k}(0) - \tilde{F}_{i|k}(\Delta_k)} \tag{D.4}$$

If γ_k is high enough, $\gamma_k \geq 0.09$, $\tilde{F}_{i|k}$ is considered a very successful model for representing $F_i(X_k)$. The solution is thus updated ($X_{k+1} = X_k + \Delta_k$) and the trust region is expanded ($\varsigma_{k+1} = 2\,\varsigma_k$). If $\gamma_k \in [0.01, 0.09[$, $\tilde{F}_{i|k}$ gives a satisfactory behavior; the solution is updated with the computed step ($X_{k+1} = X_k + \Delta_k$) without changing the trust region boundaries ($\varsigma_{k+1} = \varsigma_k$). On the other hand, $\tilde{F}_{i|k}$ demonstrates a poor performance for small values of $\gamma_k < 0.01$. In this case, the obtained solution is rejected with shrinking the trust-region boundary ($\varsigma_{k+1} = \varsigma_k/2$). According to the trust region algorithm, step Δ_k is calculated in each iteration by solving the problem presented in (C.3). The well-known formula for the problem solution is given in [95]:

$$(\nabla^2 F_i(X_k) + \lambda I)\Delta_k^* = -\nabla F_i(X_k) \tag{D.5}$$

where λ is the Lagrangian multiplier satisfying $\lambda \geq 0$. If ς_k is big enough, the problem turns into unconstrained minimization of $\tilde{F}_{i|k}$ with $\lambda = 0$:

$$\Delta_k^* = -\left(\nabla^2 F_i(X_k)\right)^{-1} - \nabla F_i(X_k) \tag{D.6}$$

Otherwise, if $\Delta_k^* > \varsigma_k$the optimum solution is expressed as

$$\Delta_k^* = -(\nabla^2 F_i(X_k) + \lambda I)^{-1} - \nabla F_i(X_k) \tag{D.7}$$

For a certain value of $\lambda > 0$ that grantees $\|\Delta_k\| < \varsigma_k$. The Dogleg method is one of the most effective techniques that are commonly utilized to estimate λ. In this method, the function $\Delta_k(\lambda)$ is approximated by a piecewise linear polygon $\tilde{\Delta}(\tau)$*:*

$$\tilde{\Delta}(\tau) = \begin{cases} \tau\,\Delta^u & 0 \leq \tau < 1 \\ \Delta^u + (\tau - 1)(\Delta^* - \Delta^u) & 1 \leq \tau \leq 2 \end{cases} \tag{D.8}$$

where Δ^u is the solution of $\tilde{F}_{i|k}$ in (C.2), i.e., the Cauchy point [96]. The problem is then solved at $\left\|\tilde{\Delta}(\tau)\right\| = \varsigma_k$. The flow chart presented in Figure D. 1 summaries the main steps of Newton-trust region method for solving the power flow problem.

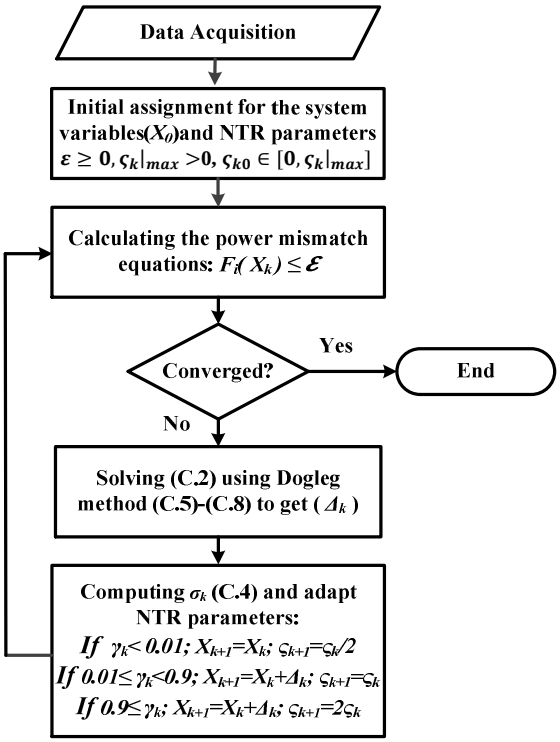

Figure D. 1: the power flow algorithm using NTR